Geochemical criteria for reservoir quality variations in chalk from the North Sea

Kunzendorf, Helmar; Sørensen, P.

Publication date:
1990

Document Version
Publisher's PDF, also known as Version of record

Link back to DTU Orbit

Citation (APA):
Kunzendorf, H., & Sørensen, P. (1990). Geochemical criteria for reservoir quality variations in chalk from the North Sea. (Risø-M; No. 2779).

RISØ

Risø-M-2779

Geochemical Criteria for Reservoir Quality Variations in Chalk from The North Sea

H. Kunzendorf and P. Sørensen

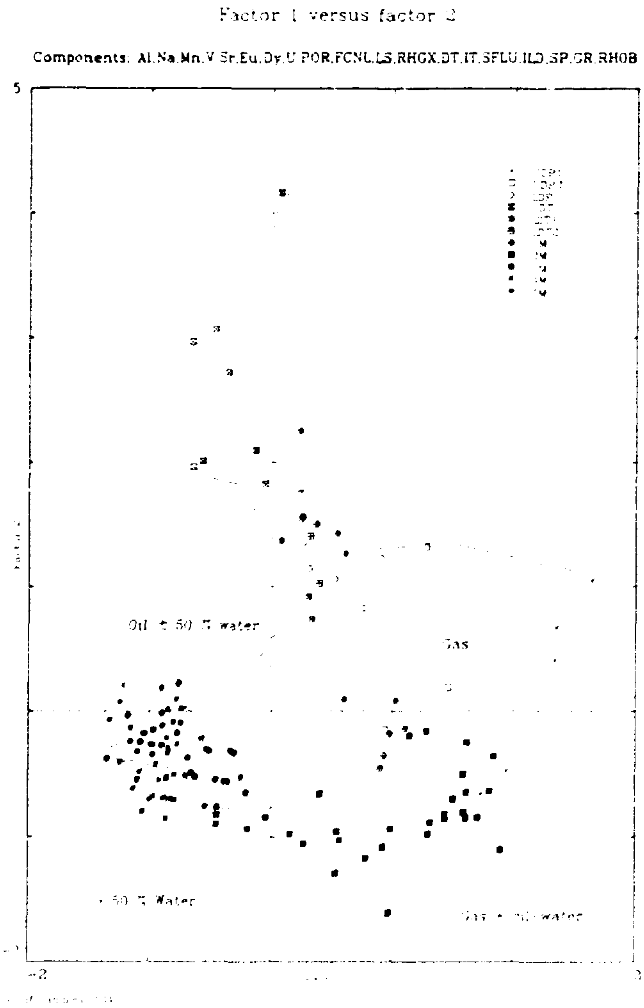

Risø National Laboratory, DK-4000 Roskilde, Denmark
December 1989

Geochemical Criteria for Reservoir Qaulity Variations in Chalk from The North Sea

Risø-M-2779

H. Kunzendorf and P. Sørensen

Chemistry Department

Risø National Laboratory, DK-4000 Roskilde, Denmark
December 1989

Abstract. The research project (EFP-86) systematically investigates the influence of chalk geochemistry on petrophysical parameters determining hydrocarbon reservoir quality, i.e. porosity and permeability.

Two wells of the North Sea Tyra gas field were chosen for the present investigation: the central well TWB-8 and eastern marginal well E-1x. Geophysical logging data with interpretations exist for both wells.

Drill core sections of Upper Maastrichtian and Danian chalk were selected for the geochemical investigations. Chemical data on chalk samples were gathered by using both conventional (X-ray fluorescence) and special instrumental analytical techniques (instrumental neutron activation). The geochemical data are compared with the well-logging results.

Geophysical logging suggests that there is reduced porosity in the Danian reservoir units LDP and UDT in both the central and marginal wells.

The chalk drill core samples from the section with reduced porosity also show a lower Ca content. At the same time, a high Si content is observed in these samples and a number of trace elements in chalk show a similar distribution with depth. Silicon diagenesis is therefore regarded as being responsible for reservoir quality variations in Tyra rocks.

A linear dependence is observed between chalk porosity and silicon content of chalk, i.e. reservoir porosity may be estimated from the Si content of chalk. Chalk permeability may also be determined by Si content but the linear dependency is less significant.

Geochemically, depth distributions of elements Al, Fe and Sc show the same trends as that for Si. Therefore, diagenetic changes in chalk also include clay minerals.

Other features of the Tyra gas reservoir are displayed through the chemical data.

The gas zone in TWB-8 is characterized by low contents of Na and Cl, i.e. lower water saturation is indicated.

Low concentrations of rare earths in all chalk samples show a shale-normalized pattern that is characteristic of marine sediments laid down under oxic conditions. Some changes that occur with depth in the Ce anomaly probably indicates a slight change in the depositional environment.

A most pronounced feature of the Tyra chalk is the depth distribution of manganese: the content continuously decreases with depth, i.e. from Danian (about 2000 ppm) to Maastrichtian strata (less than 200 ppm). In this respect, no other chemical element in chalk correlates with Mn. At present, there is no indication as to which mineral or mineral phase one is likely to find the element.

This work has been carried out under the Danish Ministry of Energy's Energy Research Program, EFP-86 (EM-Journal no. 1313/86-5).

ISBN 87-550-1511-5
ISSN 0418-6435

Grafisk Service, Risø 1990

Geokemiske kriterier for reservoirkvaliteters variation i Nordsøkalk

Dansk Resumé

Til den foreliggende undersøgelse udvalgtes to af Tyra strukturens borehuller, den centrale boring TWB-8 og den marginale boring E-lx. For begge borehuller eksisterer borehuls-logging data med delvis interpretation. Til geokemiske studier blev der udtaget prøver fra kalk borekernesektioner, som stratigrafisk dækker kalkaflejringer fra det øverste Maastrichtien og det nederste Danien; disse geologiske enheder udgør kulbrintereservoiret i Tyrastrukturen. Mens TWB-8 skærer gennem Tyra gasreservoiret (heie Danien og de øverste Maastrichtien aflejringer), er der kun i de alleröverste Danienafle'-ringer pa E-lx konstateret kulbrinter (olie).

EFP-86 projektet sammenligner både de geofysiske (logging) og de geokemiske (kemiske analyser) data.

De geofysiske data fra boring TWB-8 indikerer lavere porøsitet og permeabilitet i den midterste del af Danien (DGU reservoirenheder LDP og UDT), d.v.s. reduceret reservoirkvalitet. En lignende reduktion af begge petrofysiske parametre er ogsa konstateret i den marginale boring E-lx, omend permeabilitetsværdier her er generelt lavere.

Fordelingen af hovedelementet Ca med dybden i borekerneprøver fra begge boringer viser som forventet lavere indhold i de sektioner, som også har lavere porøsitet.

Kalk med reduceret porøsitet er for begge boringers vedkommende karakteriseret ved høje Si indhold (op til 20% Si); en række sporelementer følger Si, d.v.s. viser også forhøjede værdier. Silicium diagenese i form af silificering af kalkskaller, men også i form af flintdannelse fører generelt til en forringelse af porevolumenet.

Ved at benytte middelværdier for Si and porøsitet i de enkelte reservoirenheder er det muligt at beregne en linear afhængighed for begge parametre. Dermed er det muligt indenfor Tyrastrukturen også at estimere porøsiteten udfra Si indholdet i kalken. Selvom der er en lignende trend for Si og kalkpermeabilitet (aftagende permeabilitet ved stigende Si), er det statistisk ikke muligt at angive en linear afhængighed.

Elementer der følger Si fordelingen med dybden inkluderer Al, Fe and sporelementet Sc. Dermed indikeres, at Si diagenesen også involverer/har involveret lermineraler (smektit); disse elementer kan derfor også benyttes ved reservoirkvalitets estimeringer i Nordsøkalk.

Andre sporstoffer i Tyrakalken er indikative for tilstedeværelse af hydrokarboner: gaszonen er indikeret via lave inhold af elementerne Na og Cl. De er samtidig et udtryk for vandmætningen i formationen.

Sjældne jordartselementer forekommer i meget lave koncentrationer og de viser den fordeling, der er kendetegnende for oxiske aflejringsmiljøer på havbunden, nemlig en udpræget negativ Ce anomali, d.v.s. meget lavere Ce indhold end normale mergelforekomster. Variationer af Ce anomalien med dybden afspejler muligvis aflejringsbetingelserne i Kridt/Tertiærtiden.

Det sporstof, der udviser den mest iøjnefaldende fordeling med dybden i de to boringer er mangan. Indholdet af Mn i kalken korrelerer ikke med nogen af de andre grundstoffer og heller ikke med de petrofysiske parametre; Mn i kalk falder stærkt med dybden, omend der forekommer sektioner (aflejringsperioder) med uændret indhold, samt enkelte zoner med signifikant stigning i Mn indholdet. Den karakteristiske fordelingsform med dybden i kalken er også blevet konstateret i talrige boringer fra det Danske Subbassin. Via Mn indholdet er det derfor relativt let at afgøre, om en kalkprøve stammer fra Kridt (Mn 500 ppm), og inddeling kan endvidere også foretages i reservoirenheder med hver sit karakteristiske Mn indhold. Fordelingen er også karakteristisk for hele det Danske Subbassin. På nuværende tidspunkt er det ikke muligt at give en fyldestgørende forklaring på den med dybden stigende Mn fordeling.

Fordi det både er hovedelementer og sporstoffer, der peger på forskelle i kalk, skønnes det, at multielement geokemiske kort (i 3-D) vil kunne påvise regionale trends med hensyn til reservoirkvalitet. Det er ikke muligt at fremstille disse kort udfra kun to boringer i strukturen.

Projektet er udført under Energiministeriets energiforskningsprogram, EFP-86 (EM-Journal nr. 1313/86-5).

Table of contents

1. Introduction

Oil and gas are natural energy resources connected with the geological environment, confined almost exclusively to sedimentary sequences. The hydrocarbon accumulations obey the same rules of deposition (emplacement of the mineral phase into a geological body) and, e.g., geological alterations as for instance hard mineral deposits. Most of the methods used for identifying hydrocarbon deposits are therefore also related to those applied in normal terrestrial mineral exploration programmes.

Oil and gas frequently accumulating in deep-seated sedimentary sequences are often controlled by tectonic features. The rocks acting as hydrocarbon reservoirs are mainly sandstones and carbonate rocks with appropriate porosity. In the literature, there are relatively few discussions on the inorganic chemistry of carbonate reservoir rocks which influences porosity figures to a considerable extent. Relatively little knowledge also exists on inorganic chemical processes that connect directly with the migration and emplacement of the hydrocarbons in general. This is partly due to the complex processes occurring in sediments both during and after their burial and when reacting with a hydrocarbon phase.

Fig. 1. Tyra gas field top chalk structure map showing gas-oil contact (broken lines) and positions of wells TWB-8 and E-1x (Depth lines in feet).

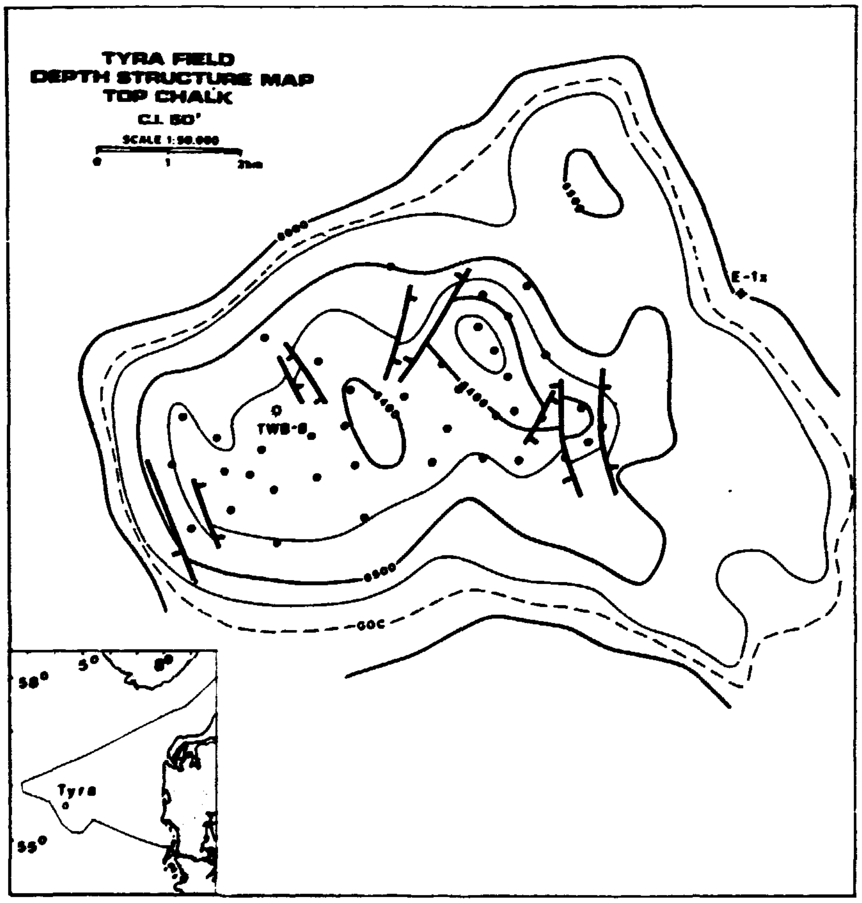

Just as formation temperatures are important for generating oil and gas from suitable source rocks, there is evidence that both petrophysical (e.g., porosity, permeability) and petrochemical properties (chemical composition, diagenetic features) play a comparable role for the reservoir rocks. Such parameters must then be regarded as important for the quality of hydrocarbon reservoirs, and they are therefore important figures for any exploitation step that is taken.

There are close relationships and interactions between the chemical deposit, i.e. oil and gas, and the surrounding sedimentary sequences during and after emplacement stages. When discussing the geochemistry of the hydrocarbon accumulations, geochemical studies have therefore to include both organic and inorganic components, i.e. hydrocarbon accumulations cannot be discussed on organic geochemical principles alone.

1.1 Basic Knowledge on Carbonate Rock Geochemistry

Major hydrocarbon occurrences in the North Sea Central Graben area are contained in carbonate rocks (chalk). Geochemical discussions on these rocks may be based on previously accumulated knowledge, e.g., *Chilingar* et al., 1967; *Reeder*, 1979; *Bathurst*, 1980; *Leeder*, 1982; *Harris* et al., 1985. A general reference list concerning the present investigation is given at the end of this report. This list also contains a number of publications relevant for the present investigation, which however were not referred to in detail.

According to *Chilingar* et al. (1967), carbonate rocks which make up about 15% of the continental crust are polygenetic, i.e. they are composed of both chemical, biochemical, and clastic components. They usually occur in the form of rhythmically repeated sequences reflecting, e.g., climatic or tectonic events during geological times. After deposition, diagenetic changes occur which alter the porosity and permeability of the deposits; they involve organic activitity, chemical processes and the imprint of physical processes.

Because of the generally existing difficulties in defining a proper carbonate rock porosity, *Harbaugh* (1967) differentiates between primary and secondary porosity. Primary porosity is defined as that which arises during depositional stages and which is later reduced by compaction and cementation. Secondary porosity is developed during burial.

Leeder (1982) gives a clear chemical description of the carbonate cycle which because of its fundamental importance is repeated here briefly:

Primary inorganic carbonate precipitation takes place through reactions

$$\begin{array}{c} H_2O + CO_2 \\ \downarrow \\ CaCO_3 + H_2CO_3 \leftrightarrow Ca^{2+} + 2HCO_3^- \end{array}$$

This means that precipitation of $CaCO_3$ is favoured by the reactions that decrease the amount of CO_2 or lower the partial pressure pCO_2 of the solution. This case occurs either when temperatures are increased or if organic photosynthesis takes place.

The normal buffering components of seawater are HCO_3^- and H_2CO_3. In the case of increase of acidity of seawater, the following reactions are possible:

$$H^+ + CO_3^{2-} \leftrightarrow HCO_3^- + H^+ \rightarrow H_2CO_3$$

and

$$CaCO_3 + H^+ \leftrightarrow Ca^{2+} + HCO_3^-$$

In the case where alkalinity increases, the following reactions are encountered:

$$HCO_3^- + OH^- \leftrightarrow CO_3^{2-} + H_2O$$

and

$$Ca^{2+} + HCO_3^- + OH^- \leftrightarrow CaCO_3 + H_2O$$

These reaction chains explain the excellent buffering system existing for seawater.

In general, Mg^{2+} ions present in seawater will supress and often inhibit the growth of the main carbonate mineral calcite.

Leeder (1982) also considers three major diagenetic stages:

- early meteoric diagenesis,
- early marine diagenesis, and
- subsurface diagenesis by formation waters.

The principal reaction zones are shown schematically in Fig. 2.

Early meteoric diagenesis comprises the vadose and phreatic environments and is closely connected with the percolation of meteoric water. During phreatic meteoric diagenesis, the Sr^{2+} amount may be significantly reduced. The low-Sr content in the transition zone Upper Maastrichtian/Danian in the Tyra drill cores could be an expression of such processes, i.e. indicate a period of regression with subsequent fresh water influx.

Fig. 2. Principal reaction zones in the diagenesis of sedimentary deposits (modified after Leeder, 1982).

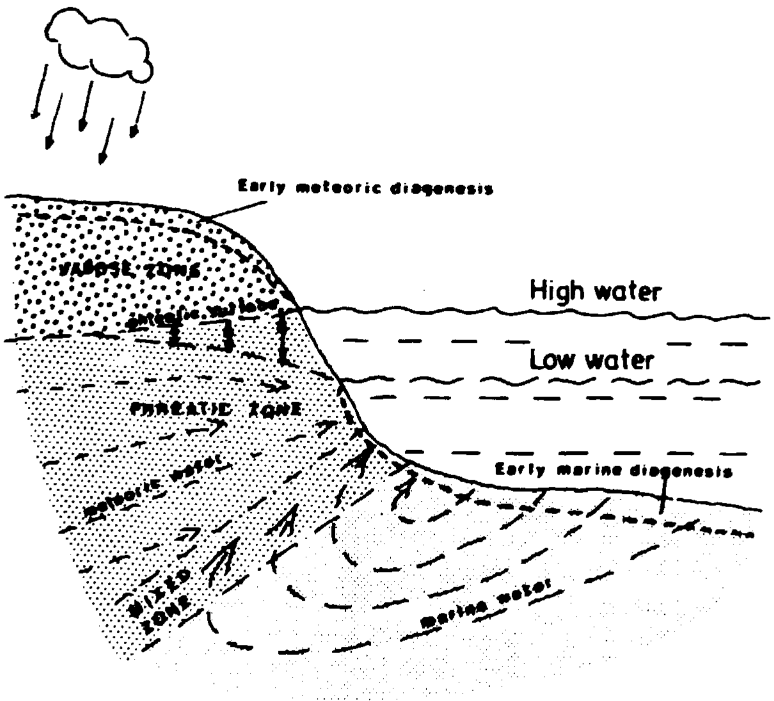

Early marine diagenesis produces beach rocks, fenestrae (birdseye limestone), hardgrounds and geopetal cavity fills. Of interest as regards North Sea chalks is the development of hardgrounds which are frequently observed in connection with the Cretaceous/Tertiary transition. Synsedimentary hardgrounds usually indicate extensive non-deposition, and they reflect the presence of interparticle cement.

Subsurface diagenetical changes caused mainly by circulating formation waters are still not fully understood. Formation waters observed in deeply buried carbonate rocks are usually in equilibrium at the prevailing pressures and temperatures.

These waters, along their circulation paths, may alter aragonite that has been left below the meteoric realm into calcite, and they may change high- into low-Mg calcite. Contrary to early marine diagenesis, ferroan ions are available during subsurface diagenesis and therefore ferroan calcite replacements may develop.

After early diagenesis stages, about 20% porosity is left in the carbonate sediments. Most ancient limestones have a porosity of less than 5% and therefore, large-scale $CaCO_3$ cementation must have occurred during burial stages for these rocks. The frequent occurrence of ancient limestone with preserved high porosity ($A > 20\%$) is probably the result of rigidity enhancement of the rock fabric by calcite precipitation at grain contacts.

Pressure solution is thought to be the dilute source for diagenesis in the deep realm. It has been observed (e.g. *Leeder*, 1982) that much of the late cement consists of ferroan calcite. Fe^{3+} is obtained by the reduction and dissolution of adsorbed ions on clay mineral platelets. Because of the platelet-like form of clay minerals, circulation of pressurized solutions is enhanced yielding large-scale migration of Ca^{2+}, Fe^{2+}, Mg^{2+}, and CO_3^{2-}. Additional Fe^{2+} is supplied by the conversion of smectite to illite. It is also known that such generated ferroan calcite cements may be further changed into ferroan dolomite or ankerite at depths exceeding 2.5 km.

1.2 North Sea Chalk

In general terms, chalk is an organic limestone where $CaCO_3$ containing skeletons are the dominant fraction of the sediment. A practical term for the chalk of the North Sea would be micrite which points to the composition of the matrix as micro-crystalline calcite with grain sizes of less than 0.01 mm.

The dictionary of the American Geological Institute (DIC, 1962) defines chalk as: »A very soft, white to light gray, unindurated limestone composed of tests of floating microorganisms and some bottom-dwelling forms (ammonoids and pelecypods) in a matrix of finely crystalline calcite; some chalk may be almost devoid of organic remains.« The definition given by *Whitten and Brooks* (1976) is more strict and confines chalk to the Upper Cretaceous limestone deposits of Western Europe.

According to *Frykman* (1983), petrographically the chalk material from North Sea drill cores contains a very high percentage of coccolith material, generally above 60% with a very widely varying allochem component. These coccolithic tests were deposited in relatively shallow waters, perhaps a few hundred meters deep, at rates exceeding 10 cm/ka.

The non-carbonate fraction is generally 5% by weight and consists mainly of clay and silica. Silica is present in the form of flint layers and chert nodules. These stem from dissolved silica which in general is highly mobile during early diagenesis. Chertification takes place predominantly in the mixed zone, i.e. in the zone between phreatic and marine realms. Nodular cherts are generated mainly in shallow-water carbonate facies. They often have a meteoric component.

Marly layers in the chalk are generally regarded as expressing carbonate production variability, but may also be caused by variable terrigeneous deposition. Also discussed are carbonate dissolution variations by *Frykman* (1983).

Coccolithic tests consist of low-Mg calcites. They are often coated by organic or other materials which are believed to be the reason for their relatively low degree of diagenetic alteration.

During deposition, chalk has a very high primary porosity, often exceeding 70%; during burial this porosity is quickly reduced. Often no cementation is observed in chalks, although they have been buried at depths greater than 2 km. For instance, Danian chalk from the Tyra well TWB-8 has porosities in excess of 30%. The most probable reason for this is the presence of pore solutions rich in Mg^{2+} at burial stages preventing or delaying $CaCO_3$ cementation.

As regards the chalk as a hydrocarbon reservoir, *Hardman* (1982) pointed out that chalk reservoir quality is defined by the size characteristica (range and distribution) of pore throats. These parameters,however, may be changed during burial involving both chemical and physical changes in the reservoir rocks.

1.3. Framework of the Present Investigation

Investigations with general validity for carbonate rocks are known (e.g. *Chilingar*, 1956; *Holland* et al., 1962; *Hirst* 1962; *Tourtelot*, 1964; *Berner*, 1964; *Weber*, 1964; *Wangersky and Joensuu*, 1972; *Jørgensen*, 1975, 1986a, 1986b). Meanwhile, there has been an ongoing discussion on the geochemistry of source and reservoir rocks in general when interpreting geophysical logging data (e.g. *Nyberg* et al., 1978; *Scott and Smith*, 1973; *Suau and Spurlin*, 1982). These discussions have terminated in the development of a new geochemical well logging device, the GLT Geochemical Logging tool of Schlumberger which uses an array of traditional sondes and a ^{252}Cf based equipment for neutron activation analysis (*Chapman* et al., 1987; *Herron*, 1986; 1987). Elements determined by the logging tool include Si, Fe, Ca, Ti, Gd and Al. In general, such a new logging system reflects the need to characterize the logged sequences by their mineralogical and chemical components so that geophysical log interpretation errors can be minimized.

Contemperaneously to the development of the new geochemical log, inorganic geochemical studies were carried out on the Danish reservoir rocks (*Jørgensen*, 1975; 1981; *Kunzendorf*, 1986) leading to a sequence characterization by the contents of minor and trace elements.

The present investigation concerns Danian and Maastrichtian chalk from the Central Graben area of the North Sea. Following earlier investigations on small chalk samples with a modified instrumental neutron activation procedure (*Kunzendorf* et al., 1986a; 1986b), a project was initiated in 1986 combining the application of the new analytical techniques with existing knowledge on two wells from the North Sea Tyra gas field. Boreholes available for detailed investigations within the 3-year EFP-86 project included TWB-8 and E-1x.

The present project aims at a concomittant interpretation of geophysical log data and geochemical data, applied to detail the understanding of the variation in reservoir quality. Investigations based on two wells alone is the absolute minimum. In order to obtain a fair judgement of reservoir quality variations, the wells were chosen from different topographic locations within the structure. The well TWB-8 intersects the central part of the Tyra structure (Fig. 3), while E-1x is located on its eastern margin.

Investigations include the analysis of some two hundred samples from cores in Lower Danian and Upper Maastrichtian strata in the wells. The applied analytical methods were instrumental neutron activation and X-ray fluorescence. By inclusion of wireline logging data from the wells, a geochemical model explaining some of the variations in reservoir quality is proposed.

The work presented here closely relates to a comparable project carried out in 1987 by the University of Copenhagen, named »Bassinanalyse, geokemi og kemostratigrafi i de danske skrivekridt bassiner«. It is intended that both projects will be able to illuminate the significance of inorganic components in the Danish reservoir rocks and also establish a »chemostratigraphic« scheme. The university project will further correlate this scheme with nannofacies studies.

2. Geological Setting

2.1 Regional Overview

The gas-producing Tyra Field is situated in the Danish Central Graben (Fig. 1) where it occupies an area of about 20 km^2 (top chalk at 6500 feet). A SE-NW cross section of the structure at about 61.75° N and about 60.7° E is shown in Fig. 3 which also outlines the position of the two wells TWB-8 and

Fig. 3. Tyra gas field cross section showing top Danian and Maastrichtian structures and position of TWB-8 and E-1x. Figure made available by Marsk Oil and Gas A/S.

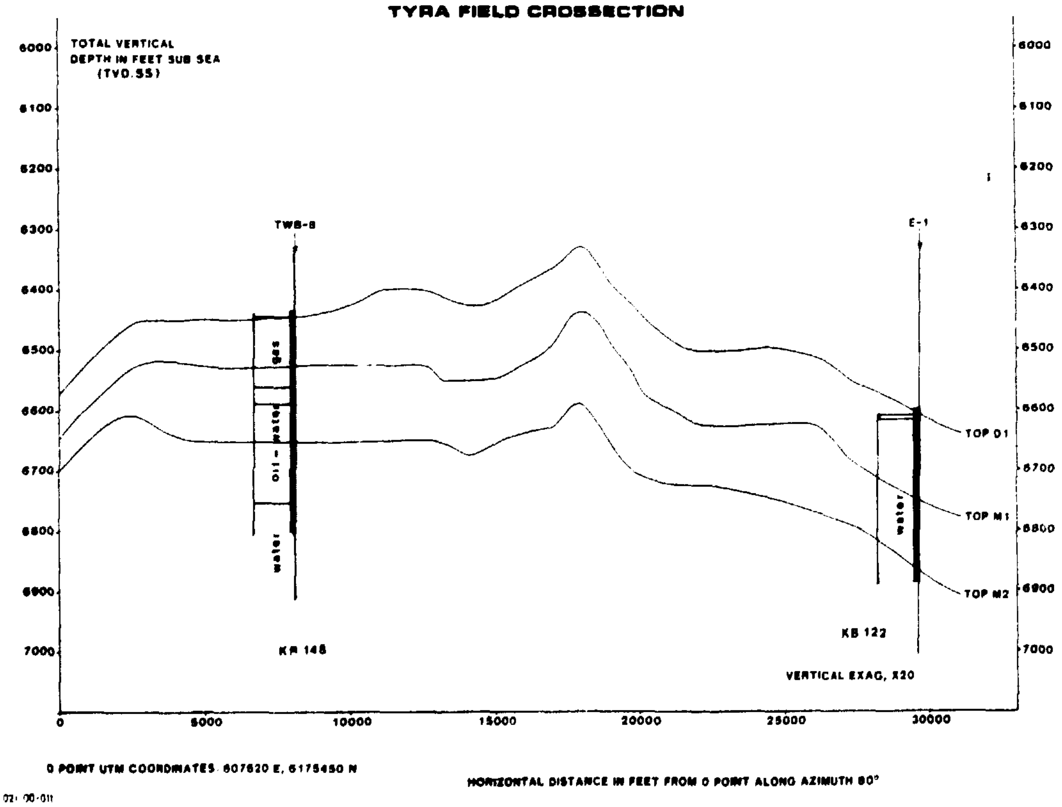

E-lx from which drill core material was investigated. TWB-8 is positioned on a subtopographical high, where both oil and gas are present; E-lx is located on the easternmost margin of the structure where only a very thin oil zone was observed in the uppermost Danian section.

2.2 Tyra Gas Field Chalk Characteristics

A number of stratigraphic and reservoir quality data from the Tyra gas field are available from Marsk Oil & Gas A/S and The Geological Survey of Denmark (DGU). Although there is some debate on the stratigraphic unit nomenclature, the hydrocarbon-bearing chalk sections of the Tyra field may be divided into at least 7 stratigraphic units (Table 1).

For use in the present investigation, a general description of chalk in the Tyra structure was supplied by Marsk Oil & Gas A/S.

Table 1. Proposed stratigraphic units for the Tyra field. Throughout this report DGU reservoir units were used.

Age	Formation	DGU chalk unit	Reservoir unit (DGU)	DUC unit
Danian	Ekkofisk	6	UDP1	D1
			UDP2	
			LDP	D2.1
			UDT	D2.2
			LDT1	D2.3
			LDT2	D2.4
Maastrich-tian	Thor	5+	1M	M1.1
			2M	
			3M	M1.2
			4M	M2
			5M	

This description is given briefly below in an abbreviated form.

The lowermost Maastrichtian reservoir unit, 3M, which also shows the most well-developed reservoir facies, is a soft-to-moderately hard, beige chalk. Macroscopically, the rock appears as a banded and laminated unit. Not many burrows are found and oil staining is observed along some fractures. In general, the chalk shows few indications of diagenetic alteration. Reservoir quality is excellent with porosities above 40% and permeabilities at 9 mD on average. A characteristic feature of this chalk section is that it is often intersected by cm-size floatstones representing perhaps an early diagenetic imprint.

Units 2M and 1M consist of soft to moderately hard, light-yellowish grey chalk with no visible cement. The chalk is characterized by sections with many stylolites. Burrows occur rarely, and few pyrite grains are observed. Ha'rline fractures are numerous. These vary in thicknes on a regional scale in that they are thickest towards the northeast of the Tyra field. Reservoir properties are in general somewhat decreased compared to unit 3M. This decrease is visualized through lower permeabilities (5 to 10 mD) at comparable porosities (30 to 42%).

The top of unit 1M is a strongly cemented hardground.

The lowermost Danian chalk section, LDT2, usually cannot be found in the central parts of the Tyra structure but where deposited, it is a strongly cemented, beige-to dark grey chalk, characterized by horsetail lamination. Burrows and patterned-chalk structures are very abundant. Pyrite nodules (cm scale) and bands of chert nodules also occur. The rock is rich in clay, and, taking into account that many well-preserved trace fossils occur, it was probably deposited during periodes characterized by low rates of sedimentation. Many other features point to strong diagenetic alterations, and the reservoir parameters are generally poor with porosities declining to about 32% and with markedly lowered permeability values.

Further above, section LDT1 is moderately hard, partly banded and mottled, and the chalk is white to greyish-beige. The rock appears cemented and shows a number of secondary structures like stylolites, mm-size pyrite nodule clusters, horsetail-structure lamination and patterned-chalk structures. These features are often concentrically arranged and suggest that they have been exposed to strong diagentic overprinting. Most pronounced for the section as regards chemical changes is the abundance of pyrite. The unit has reduced reservoir quality figures, although porosities generally lie between 36 and 40%, but permeabilities are relatively low, ranging between only 0.9 and 3.5 mD. It should be mentioned that reservoir properties are poorest in subsections with pronounced occurrences of patterned-chalk structures.

Unit UDT is a moderately hard, beige chalk which often has a dense horsetail lamination. Layers of foraminiferal mudstone with relatively high content of pyrite (size 1 um to 1 mm) occur. Microscopically, cement has been observed, and therefore reservoir quality parameters are reduced (porosities rarely are above 30% and permeabilities well below 1 mD). A whitish-beige chalk layer may be interbedded locally in Unit UDT. This layer has better reservoir quality parameters than unit UDT in general, and this is explained by the lower degree of cementation of this subsection.

The overlying unit LDP is a moderately hard, greyish beige, mottled chalk. A relatively dark patterned-chalk structure is present with some dark spots of pyrite. The rock in general has a high content of foraminifera and pyrite-containing patches. Unit UDT has porosities between 38 and 41%, and permeabilities ranging from 2.9 to 3.6 mD.

The uppermost Danian chalk section, units UDP2 and UDP1, are comprised of a moderately hard beige chalk with networks of hairline fractures. The rock contains recrystallized shell fragments and very small chert grains. Reservoir properties are generally better than those of unit LDP (porosities between 43 and 45%, permeabilities between 3.2 and 3.8 mD).

3. Sampling and Analytical Techniques

3.1 Sampling

Chalk samples were collected from selected intervals of the drill core material stored at Marsk Oil and Gas A/S (TWB-8) and The Geological Survey of Denmark (E-lx). Usually, pieces weighing up to 30 g were taken. After removing the remaining drilling mud, the samples were crushed and finely ground in an agate mortar.

For a number of the TWB-8 samples, a somewhat different sample preparation procedure involving hydrocarbon extraction was employed. However, as there were no significant differences between bulk and hydrocarbon-extracted chalk samples it was soon decided to analyze the bulk rock samples alone. Two further reason for doing this was the difficulty of controlling the extraction processes, and that they always include a possibility of dissolution and/or contamination.

For the analysis, 400-mg sample material was used for both short-lived isotope and normal instrumental neutron activation. Conventional X-ray fluorescence requires at leat a few grams of sample material.

3.2 Analytical Procedures

The present project also aimed at the refinement and use of a rapid instrumental neutron activation (INAA) technique based on the gamma-ray intensities of short-lived radioisotopes. However, because only some ten elements can be determined with this method, other analytical techniques were also applied to increase the geochemical data base. These include normal instrumental neutron activation analysis determining some 20 elements and conventional X-ray fluorescence analysis.

Short-lived instrumental neutron activation analysis has been carried out at the delayed-neutron counting facility (uranium analysis) connected with the research reactor DR3 (*Kunzendorf* et al., 1985). In this mode of operation, samples are usually irradiated for 10 s and analyzed for, e.g., Mg, Al, Ca, Ti, and V using counting intervals of 2 and 5 min after termination of appropriate cooling periods. The automatic instrumentation at the irradiation facility allows optimal manipulation of irradiation, cooling and sampling in the minutes range.

Normal INAA analysis was usually carried out on 400-mg samples. After irradiation for 4 hours in the irradiation position 7V2 of the Risø research reactor DR3 (Risø Isotope Laboratory) the samples were cooled for 7 days. Gamma-ray spectrometry was performed with the Mineral Analysis group's Ge(li) detector coupled to a multichannel analyzer (Canberra Series 80). Gamma-ray spectra of the samples were recorded after 1 week (0.5 h counting), 10 days (1 h counting), and 3 weeks (13 h counting) cooling time.

An evaluation of the gamma-ray spectra was carried out by a method based on that reported by *Girardi* et al. (1965) and moderated for use at Risø National Laboratory. While irradiation and gamma-ray spectra recording was conducted at our own laboratory, the final data evaluation was carried out through computer services by the Danish company Tracechem, Copenhagen. Analytical data were generally available within one month, but taking into account the relatively large number of elements analyzed, INAA analysis is a relatively time-consuming operation in the present project.

A number of the chalk samples were also analyzed by conventional X-ray fluorescence analysis (at the Institute of Petrology, University of Copenhagen) to determine standard major, minor, and trace elements in the chalk samples. Silicon values especially were gathered through this method. Furthermore, relatively low uranium values were determined by the delayed-neutron counting facility of the Mineral Analysis Group.

4. Results

Work with the project included both analytical work and interpretation of the geochemical data and of geophysical logging data. The logs were delivered by The Geological Survey of Denmark in the form of magnetic tapes.

To interpret the logging data, computer software was developed for the Risø Burroughs B7800 (later A6) computer enabling the direct plotting of the geophysical logging data by using the Risø RIGGS plotting software. Similar software was used later for plotting the geochemical logs.

4.1 Drill Core TWB-8

4.1.1 Logging Data from TWB-8

Existing wireline logging data for well TWB-8 include data from electrical, acoustic, and radioactive logging devices. A general description of the well-logging devices and their application is given by, e.g., *Helander* (1983). A problem in well-logging data interpretation is the large number of abbreviations and computer codes which also have been altered considerably during past decades. Selected abbreviations of relevance for the present study are given in Appendix VIII. Logging data in digitized form used in the study are tabulated in Appendices VI and VII.

Table 2 Average petrophysical and reservoir data for TWB-8.

Unit	Depth (feet)	Unit thickness (feet)	Porosity (%)	Water saturation (%)	Permeability (mD)
UDP1	6587	17	46	16	4.5
UDP2	6604	10	46	18	4.9
LDP	6614	17	40	34	2.2
UDT	6631	20	31	59	0.6
LDT1	6651	19	38	44	2.1
LDT2	6670	10	37	41	1.9
1M	6680	12	38	28	3.5
2M	6692	34	45	24	9.2
3M	6726	41	40	50	5.1
4M	6767	41	40	72	8.3
5M	6808	61	38	92	5.9

For TWB-8, the gas-oil-contact (GOC) was set by The Geological Survey of Denmark at 6712 feet (Table 2) with a gas zone of 125 feet, 50% water saturation (S_w) was at 6726 feet leading to a GOC- 50% S_w zone of 14 feet, and the oil-water contact (OWC) was determined to lie at 6772 feet with a transition zone (50% S_w-OWC) of 46 feet.

All the avaialable log data for the well TWB-8 were plotted as evaluation plots (Figures 4 to 6). A short general evaluation of these data is given in the following sections.

Fig. 4. Compensated neutron/litho-density log for TWB-8. Log curves include natural radioactivity (GR) and logs belonging to the CNL and FDC-LDT tools.

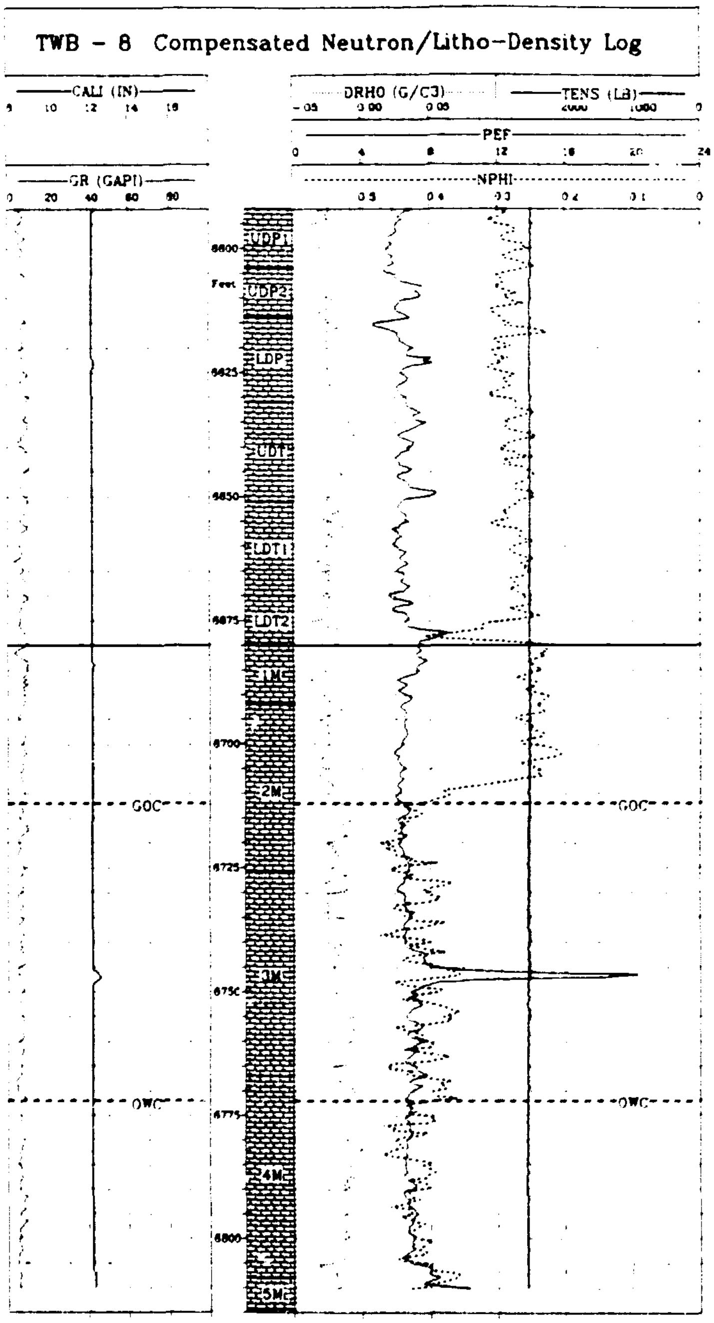

4.1.1.1 Radioactive Logs - CNL and FDC-LDT

Radioactivity logs include natural radioactivity (GR), the Compensated Neutron Log (CNL) including Far Detector (FCNL) and Near Detector (NCNL) count rates and their ratios (NRAT), the Formation Density Compensated Log (FDC) and the Litho Density Tool (LDT) including the logging curves LU1, LU2, LU, LL, LS, LURH, LSRH, SS1, SS2, S1RH, and LITH (see Appendix VIII).

The neutron ratio NRAT (NCNL divided by FCNL) being inversely proportional to NPHI, the neutron porosity, divides the TWB-8 well into 2 main units (Fig. 4):

- the section between 6590-67'0' with neutron ratio of about 3.1 leading to relatively constant NPHI values of about 0.25 to 0.3.
- the section between 6710-6850' with a neutron ratio of about 4, corresponding to NPHI values of about 0.4-0.45.

The NPHI plot with depth clearly defines the thickness of the gas reservoir.

The relatively large number of available single log curves existing for the FDC-LDT evaluation log all show the same tendency, expressed here by the LITH log (Fig. 5):

1) In the UDP1, UDP2 and LDP sections decreasing cps values are observed, dropping from 180 at the top of unit UDP1 to about 100 cps at the transition to unit UDT.
2) For unit UDT, a rather constant value of about 75 cps is found; units LDT1 and LDT2 again show higher but constant values (120 cps).

Fig. 5. Evaluation logs for TWB-8 including Lithology Window Count Rate (LITH), Bulk Density (RHOB) and the Borehole-Compensated Sonic Logs (BHC).

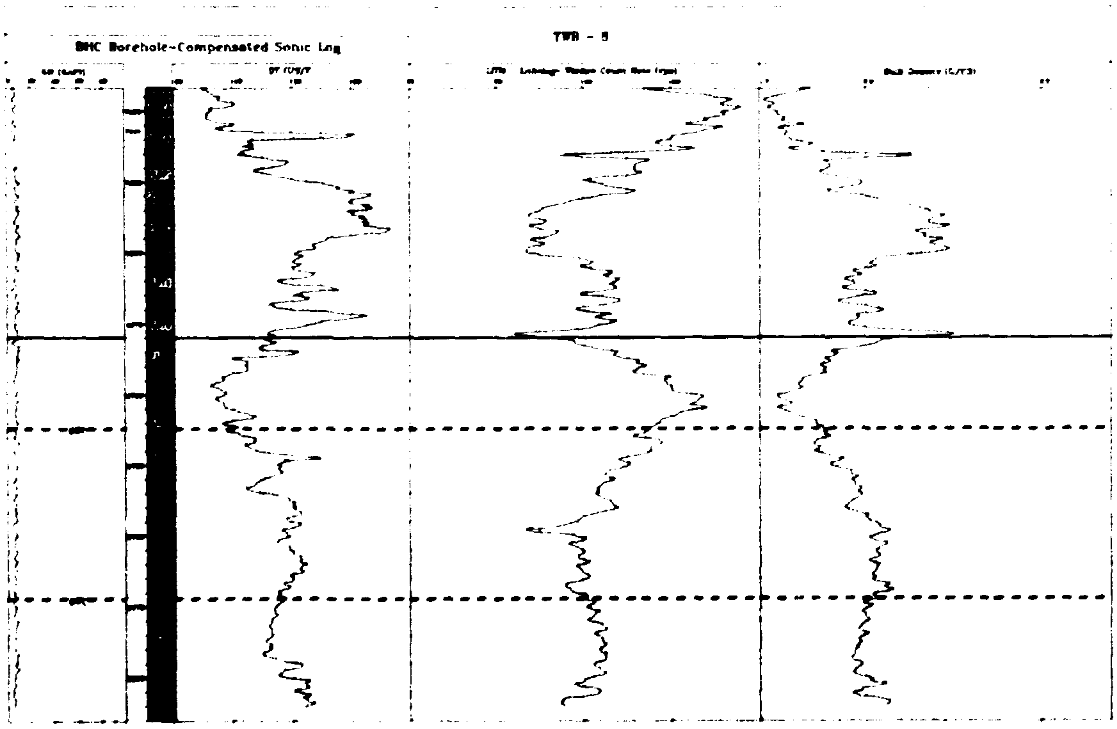

3) From about 6680' to about 6700' depth, LITH values increase linearly to a value of about 170 cps towards the gas-oil contact and they decline then again to a value of about 100 cps at a depth of 6750' within unit 3M
4) LITH values are constant, at about 100 cps, below depths of 6750'.

The LITH log curve is the mirror image of the bulk density curve of TWB-8 (Fig. 5). Density values obtained from cross plots, RHGX (not plotted in the figures) show nearly the same distribution with depth, although some smoother curves appear. In general, density values are higher than the cross plot density values and also, RHGX varies less, holding to about 2.7 g cm^{-3} below depths of 6710'.

4.1.1.2 Sonic Logs

The series of sonic logs available for TWB-8 includes AMPL, CBL, DT, SRAT, and IT. Most interesting in this respect is the DT log curve (Fig. 5) which leads to similar divisions into subsections.

4.1.1.3 Electrical Logs

The electrical logs (Fig. 6) include the Spherically-Focused Logs (SFL), the Self-Potential Log (SP) and the Induction Logs. Available were SFLU, SFLA, ILD, ILM and CILD.

Log plots of resistivity and conductivity are similar. The distributions with depth may be divided mainly into 2 subsections displaying clearly the gas zone:

1) Down to a depth of 6720' constant values of ILM (10 to 20 ohmm), ILD (10 to 20 ohmm) and CILD (about 125 mmho) are observed
2) Values decrease with depth in the rest of the section and stay constant below depths of 6775'.

4.1.2 Geochemical Profiles along Drill Core TWB-8

4.1.2.1 Previous Results

Elemental distributions with depth in drill core TWB-8 based on short-lived instrumental neutron activation analysis were reported previously (*Kunzendorf* et al., 1985; 1986). For detailed discussions of these data the reader is referred to these publications. All the previous analytical data are also tabulated in Appendix III.

Briefly, Ca and Al contents of the carbonate rock samples (Danian and Maastrichtian strata) match the trends observed for the core porosity (see Fig. 7). For the Danian section of the drill core, core porosity figures are significantly decreased at higher Al contents. A pronounced feature is the increasing (from bottom to top) Mn content in the carbonate reservoir rocks, reaching over 1000 ppm Mn in the LDP, UDP2, and UDP1 sections.

The differences in chalk geochemistry for the different reservoir units are displayed in the best way by means of Fig. 8 which shows a clear grouping of the data.

As regards the trace elements, there are fewer clear trends, although V seems to follow the Mn distribution more closely than other elements; rare earth elements Eu and Dy correlate with Al. A distinct feature is the relatively low U content in each of the Danian samples, but the lowermost Danian and the uppermost Maastrichtian sections show higher U.

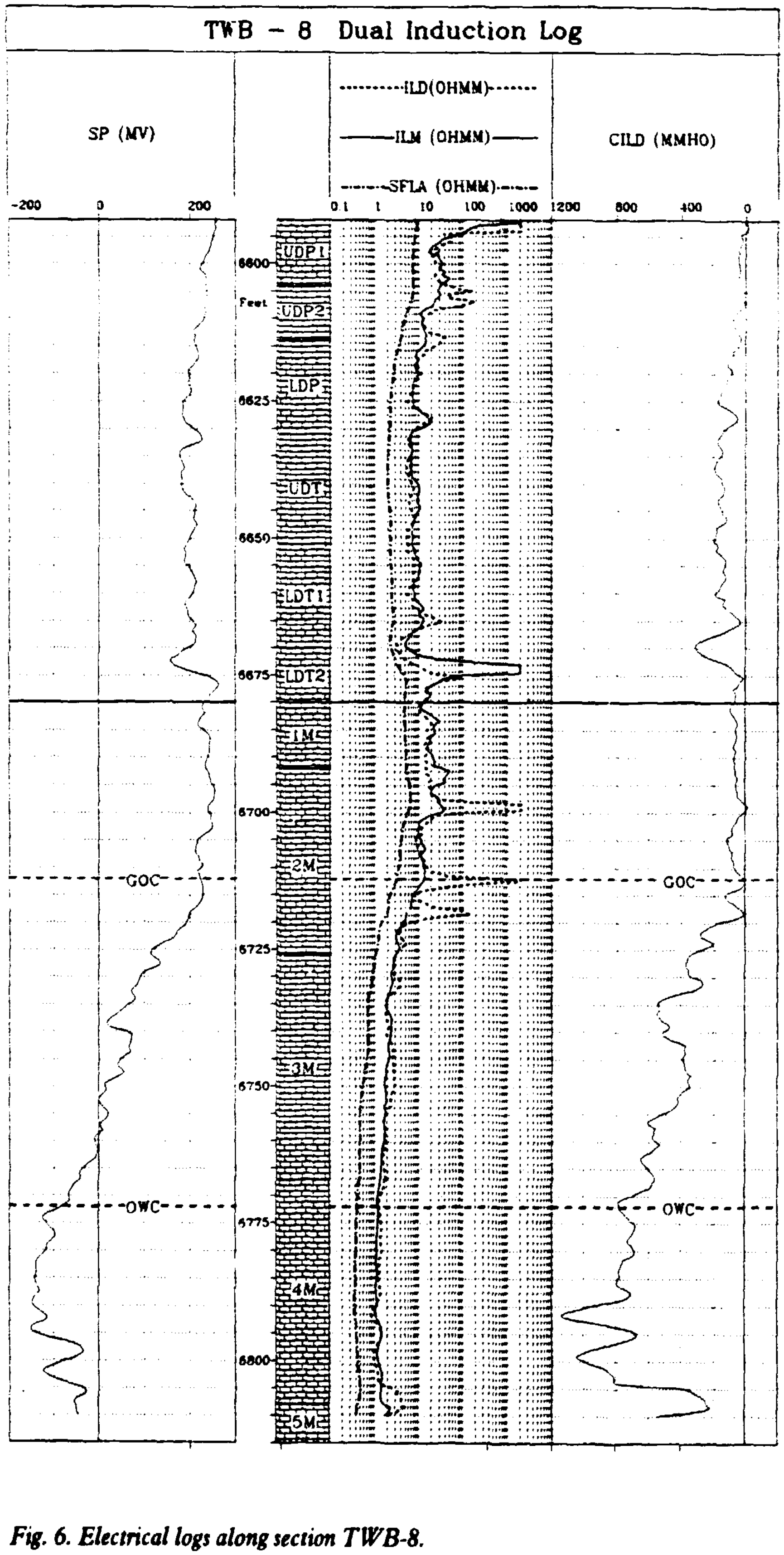

Fig. 6. Electrical logs along section TWB-8.

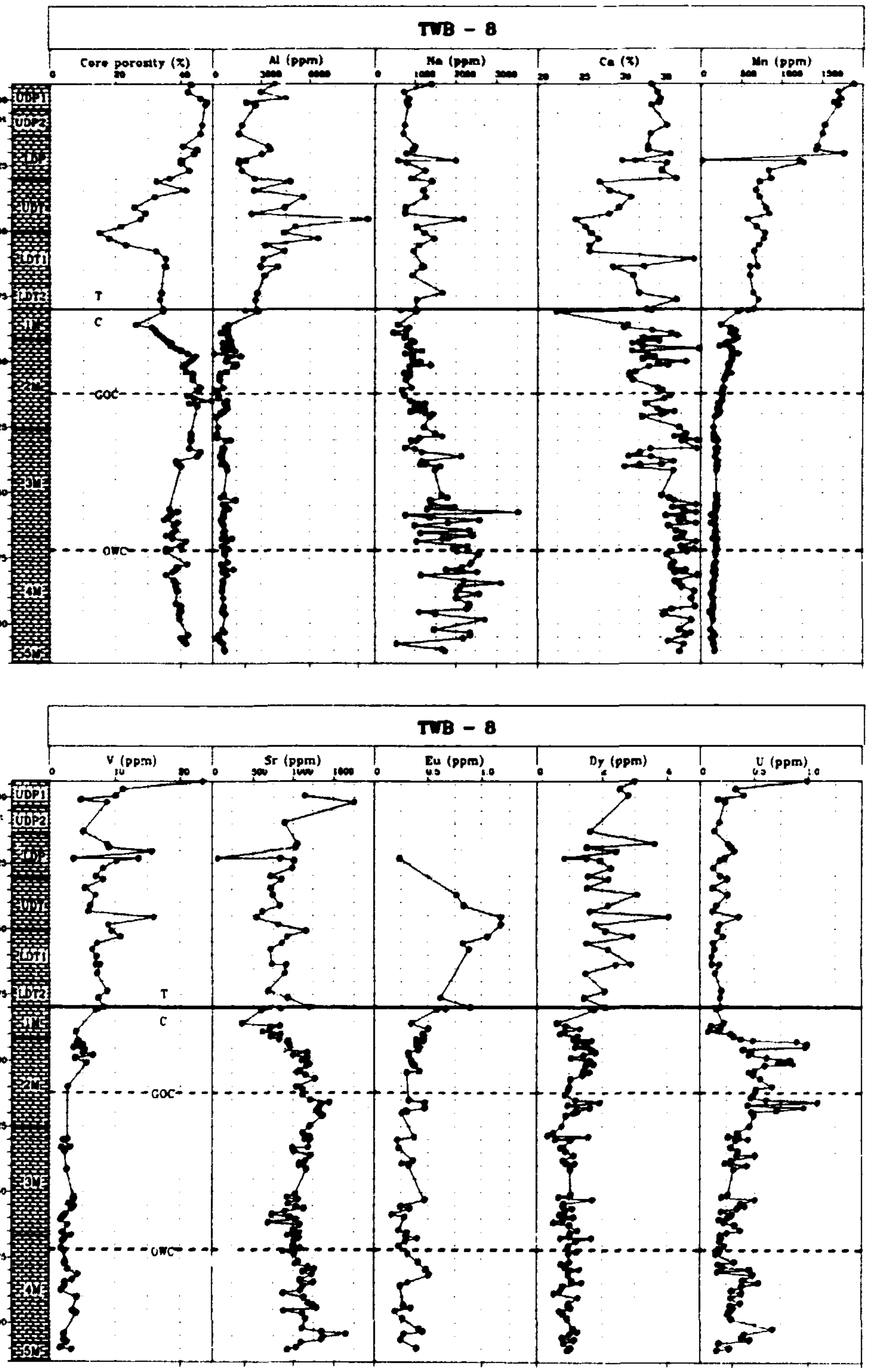

Fig. 7. Geochemical data and core porosity plotted along the TWB-8 section.

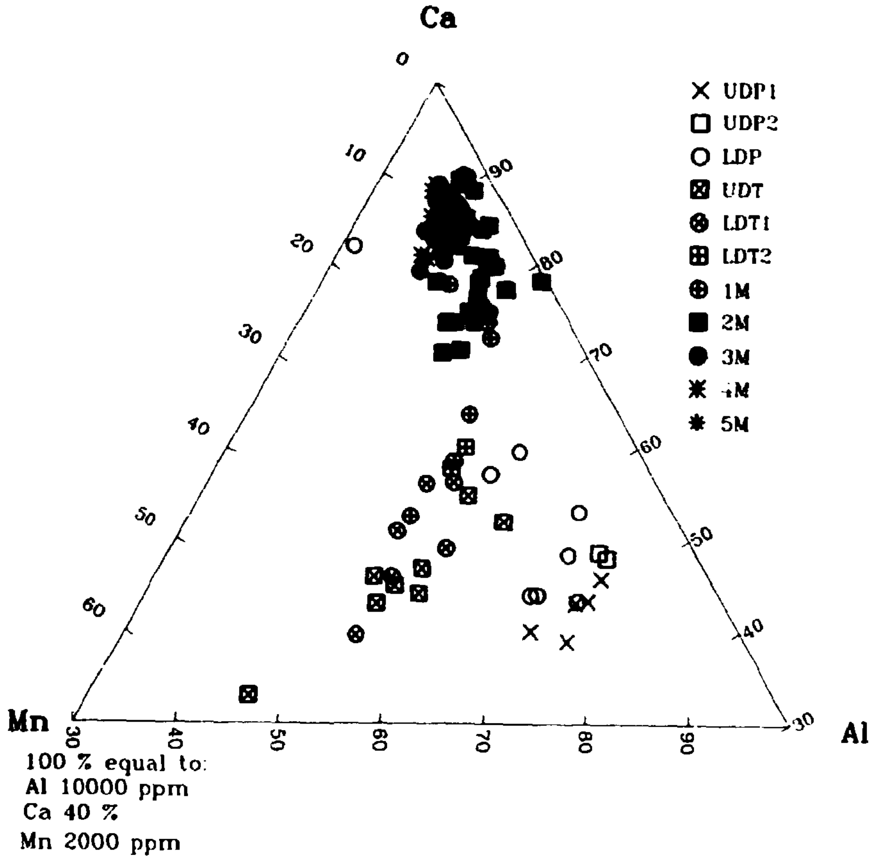

Fig. 8. Triangular plot of Ca, Mn, and Al data showing grouping according to reservoir units, i.e. geology.

Multivariate statistical evaluation of these data is shown in Figs. 9 and 10. The plots are based on the data given in the Appendix III.

Seven factors are necessary to account for 90% of the variability of the analytical data while 5 account for about 70% variability (Table 3). They indicate that there is a modest integration of the data by multivariate statistics.

The plot of factor 1 versus 2 for all analytical data (Figs. 9 and 10) shows a significant grouping in that all Danian samples plot into the right part of the figure while Maastrichtian samples occupy the left part. Also, on dividing further into subgroups, a clear separation of data according to reservoir unit is observed (right part of the figures).

Table 3. R-mode factor analysis of all analytical data from TWB-8.

Factor	Eigenvalue	Percent of trace	Cumulative
1	3.600	30.00	30.00
2	1.753	14.61	44.61
3	1.381	11.51	56.12
4	1.114	9.28	65.40
5	0.970	8.08	73.48
6	0.956	7.97	81.45
7	0.829	6.91	88.36

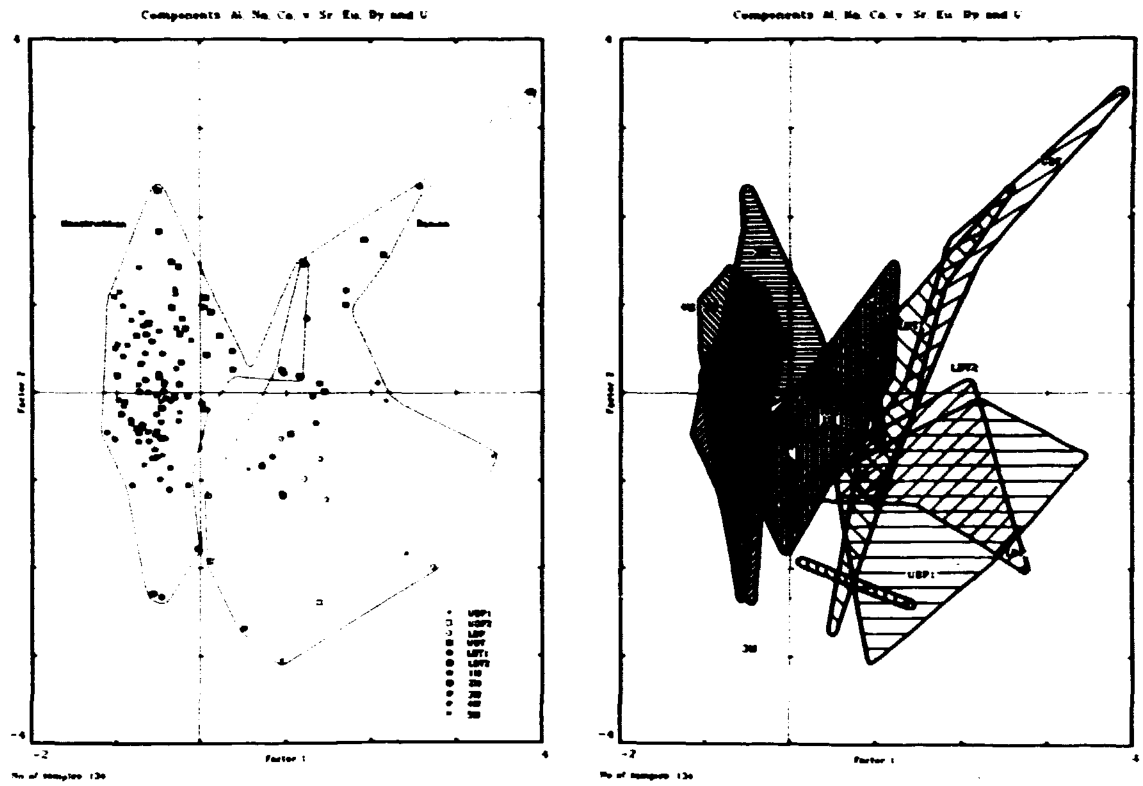

Fig. 9. R-mode factor analysis of geochemical data of TWB-8. Factors 1 and 2 are plotted.

Fig. 10. R-mode factor analysis plot of geochemical data for TWB-8. Factors 1 and 3 are plotted.

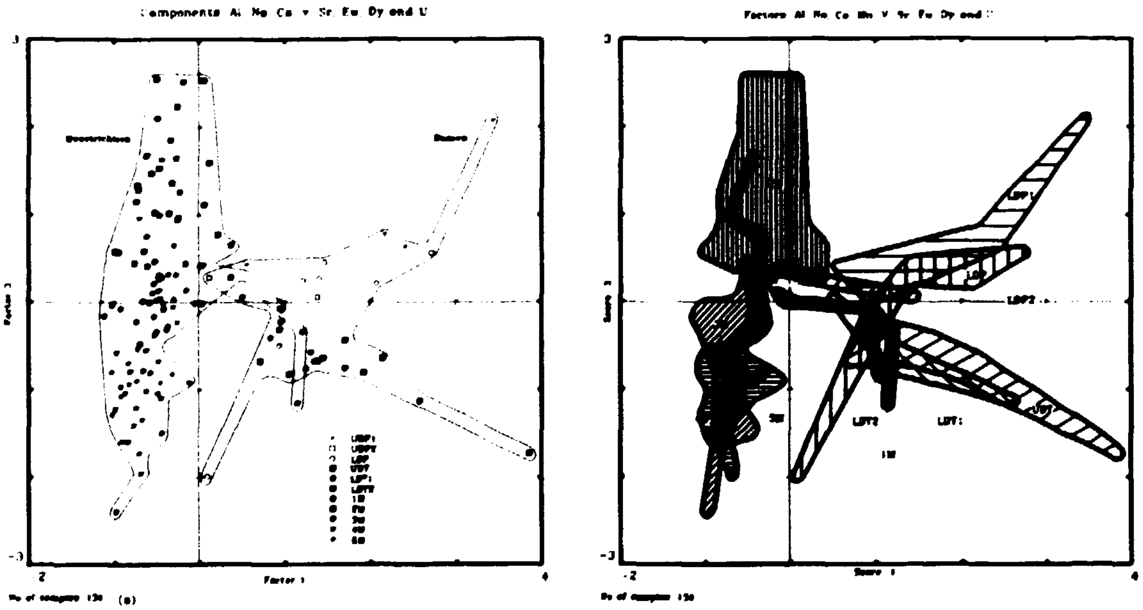

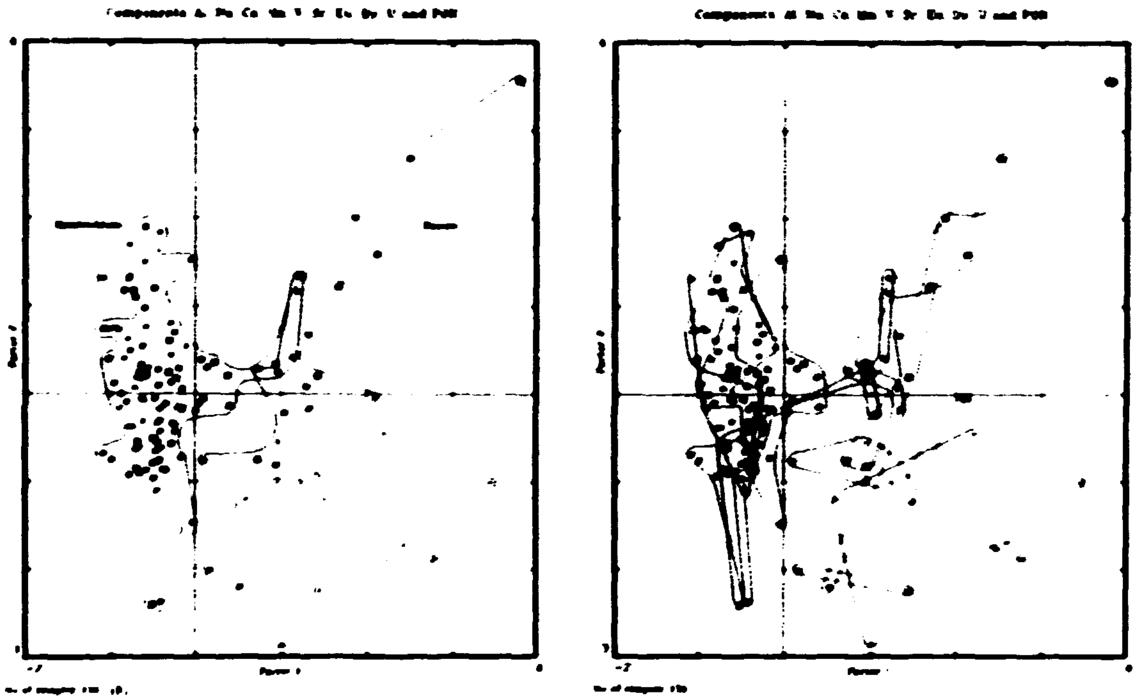

Fig. 11. R-mode factor analysis of geochemical data including core porosity from TWB-8. Factor 1 is plotted against 2.

The same grouping is observed when core porosity is added to the data sets (Fig. 11).

Using the data sets to run cluster analysis, 3 elemental groups may be selected:

1. Na-Cl-Sr-U
2. K-Ca-porosity
3. Mg-Al-V-Dy-Mn-Eu

Basically, this means that U is connected with formation waters, porosity is an expression of Ca contents, and V, Mn, and rare earth elements can be ascribed to an Al-rich phase (probably clay) in the samples.

4.1.2.2 Supplementary Data

Sixteen additional samples were analyzed by normal INAA. The results of these measurements are given in Appendix IV. A plot of the data is shown in Figs. 12 and 13.

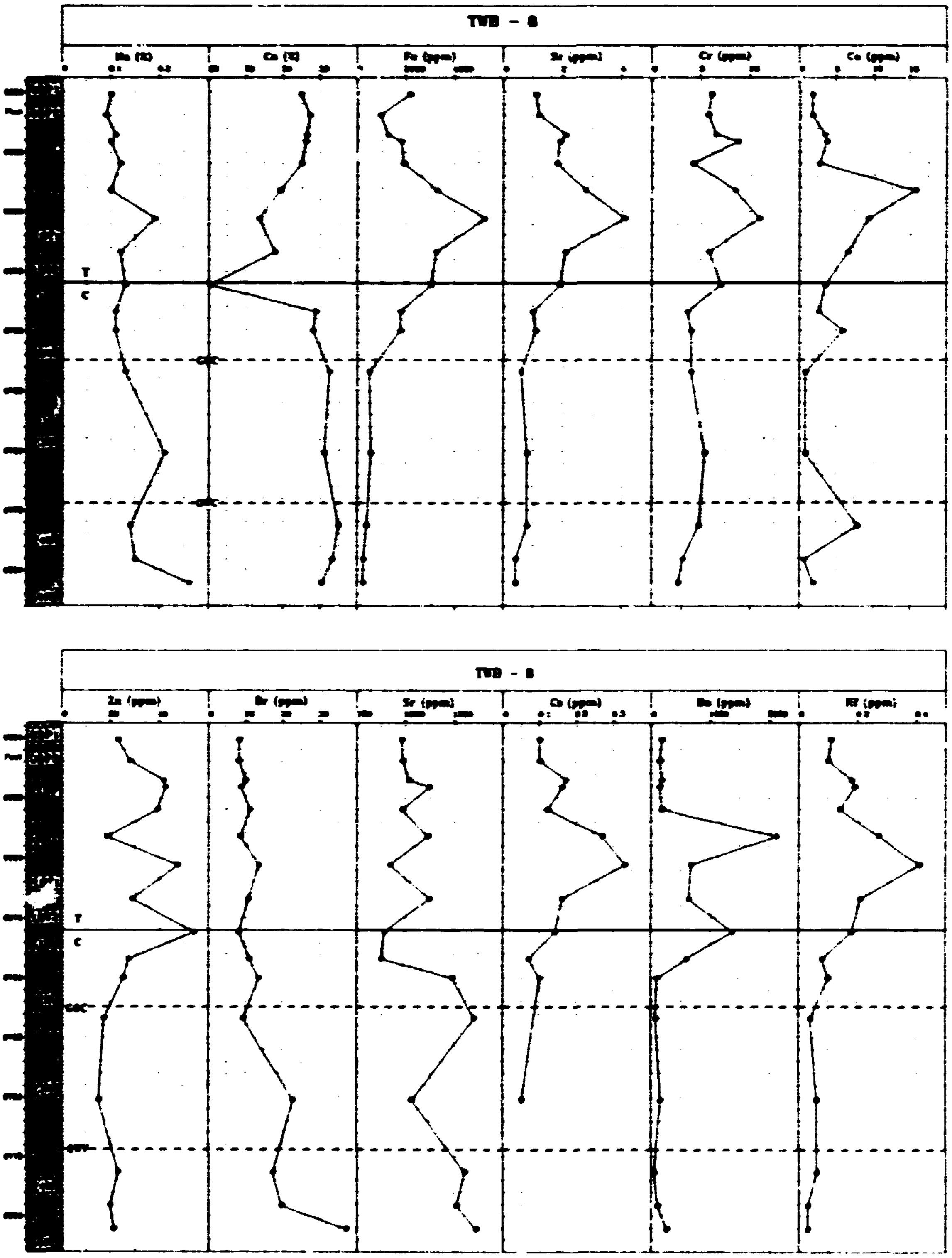

Fig. 12. Elemental contents in additional drill core samples along TWB-8.

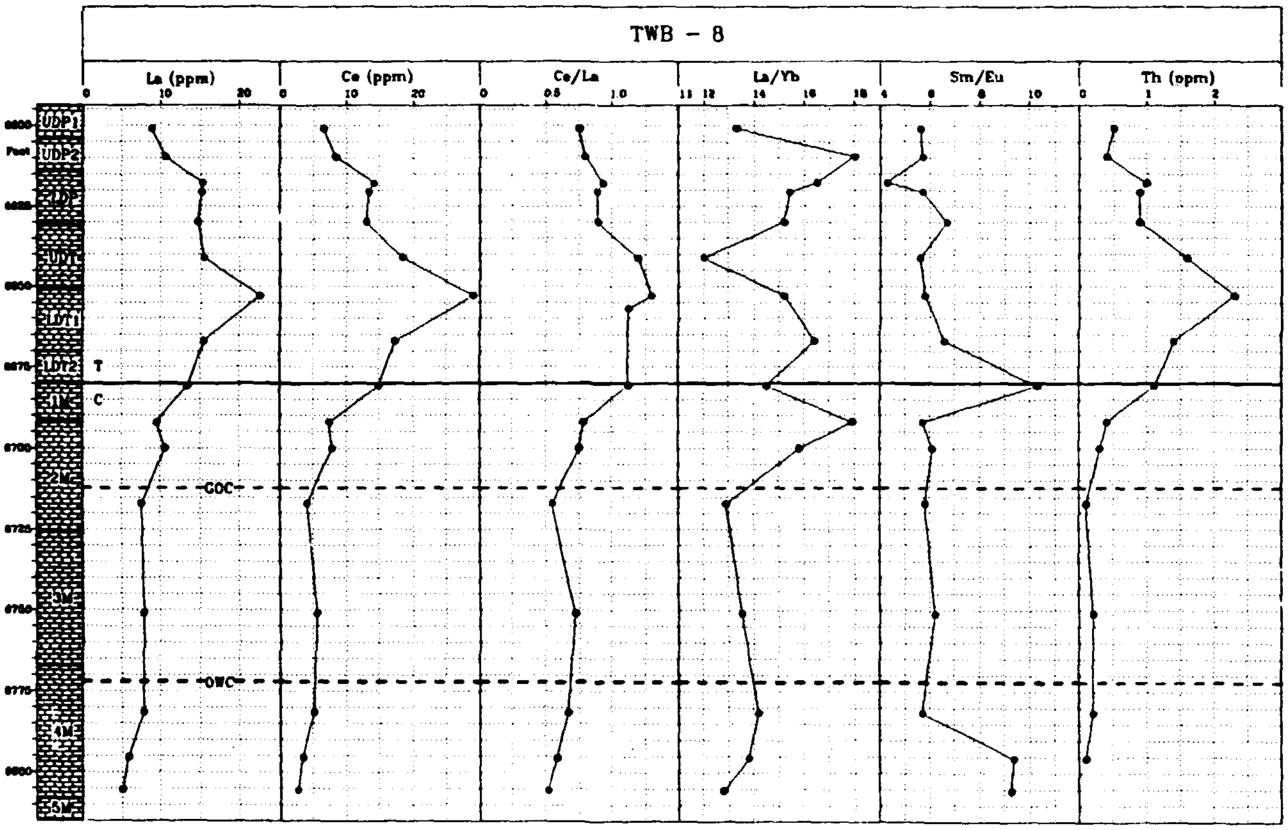

Fig. 13. Elemental contents in additional drill core samples of TWB-8.

The general observation of the distributions with depth is that a number of elements greatly correlate with Fe and also that the low-porosity section in the Danian part has the highest Fe. Some evidence therefore points to the lowered-porosity section of the Danian TWB-8 section being partly due to the occurrence of clay minerals (high Al, see above) which also have elevated Fe contents (up to 0.4%).

As regards the trace elements, Sc follows Fe closely but also displays the high Al values found in the Danian section. This means that, in principle, Sc could be used as an indicator trace element for clay contents in the chalks. The Br distribution with depth strongly resembles that found for Na and Cl, and because the lowest values of both Cl and Br are found in the hydrocarbon-bearing drill core sections, they express the low formation water content in the pore spaces.

Of special importance for investigations of drill cores is the Ba content, baryte being a major component in drilling fluids used for drilling operations. Where the drilling fluids to invade and penetrate the drill core they would seriously influence the analytical data (contamination). High Ba (above 1000 ppm) is observed in only two samples, so actually no Ba contamination need be taken into consideration.

Selected triangular plots are given in Fig. 14.

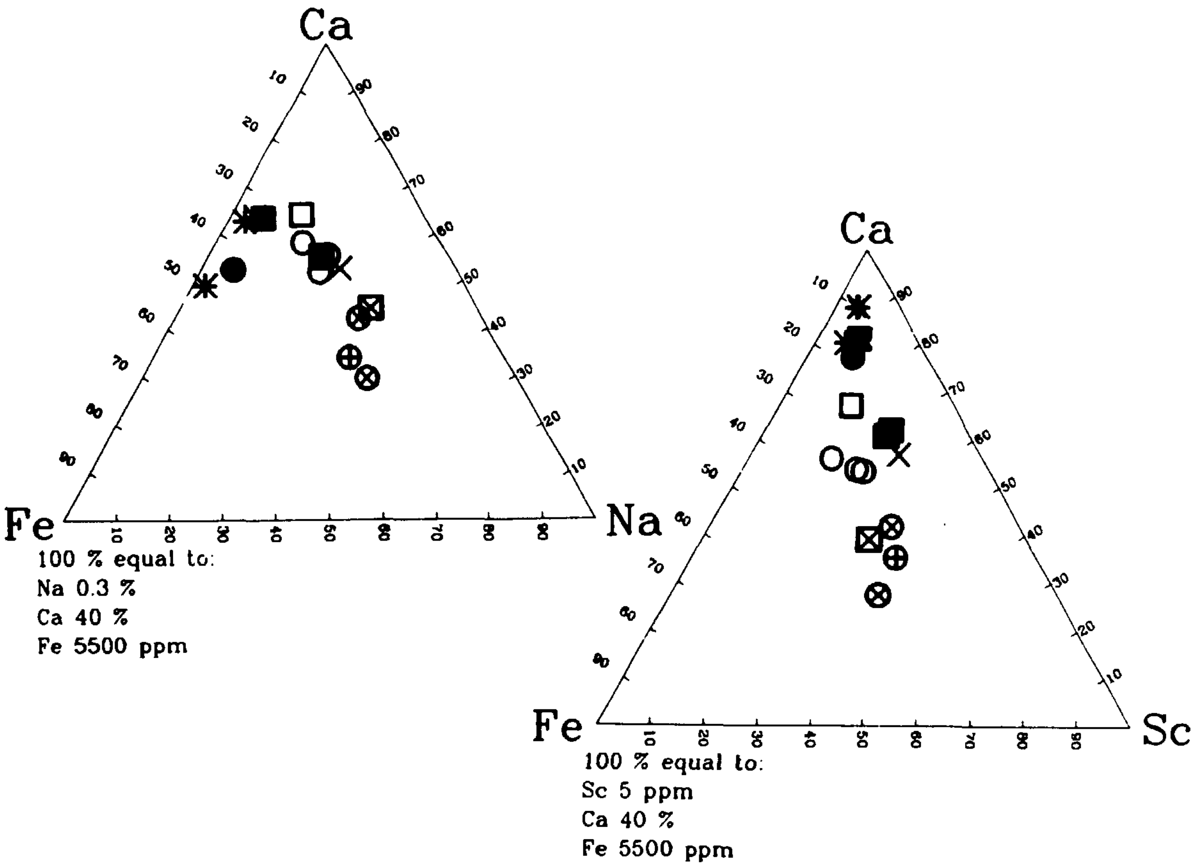

Fig. 14. Triangular plots for average Ca, Fe, Na and Sc showing pronounced grouping according to geology. Symbols as in Fig. 8.

Rare earth elements (REE) also correlate with elements Fe, Al and Sc, and they are therefore best ascribed to the clay fraction in the carbonate sediments. As shown in Fig. 13, there is a significant change in the Ce/La ratio, from about 0.6 to about 1.2, at the Maastrichtian-Danian border suggesting that Danian deposition of carbonate sediments probably occurred in more oxidized waters. There is also some fractionation trend with higher La/Yb ratios in the Danian strata, while the ratio Sm/Eu (not plotted) largely remains constant throughout the investigated sections. The latter ratio usually expresses terrestrial input (feldspars) into the sedimentary environment by elevated Eu values.

REE patterns of all samples normalized to North American shale (Fig. 15) show a similar tendency: a more-or-less shale-like pattern (except for Ce) suggesting that REE occurs mainly in the clay fraction of the chalk. The negative Ce anomaly, expressed as very low (< 1) Ce/La ratios are typical for oxic depositional environments. Ce is one of the two REEs that may exist in the tetravalent state in which it is readily precipitated and separated from the other, mainly trivalent, REEs.

A characterization plot based on these rare earth element ratios is shown in Fig. 16; it clearly groups the Danian and Maastrichtian strata.

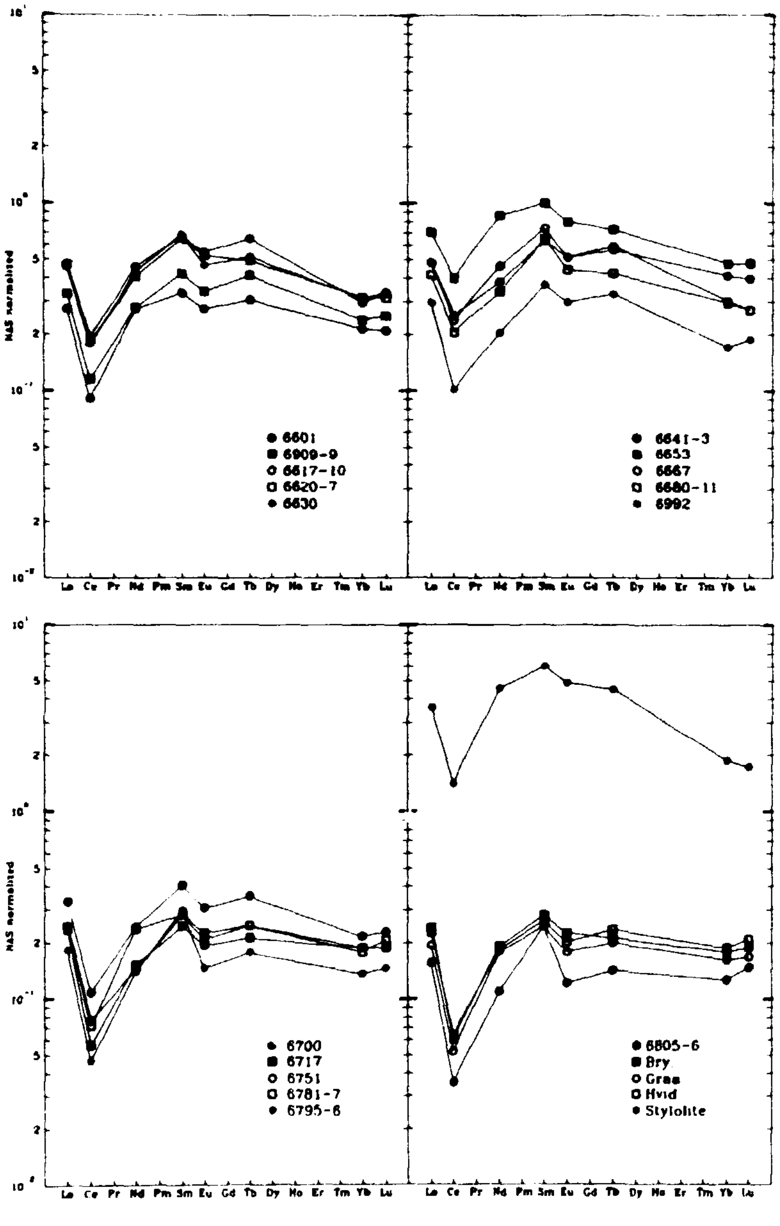

Fig. 15. North-American shale normalized rare earth element patterns of selected drill core samples along TWB-8.

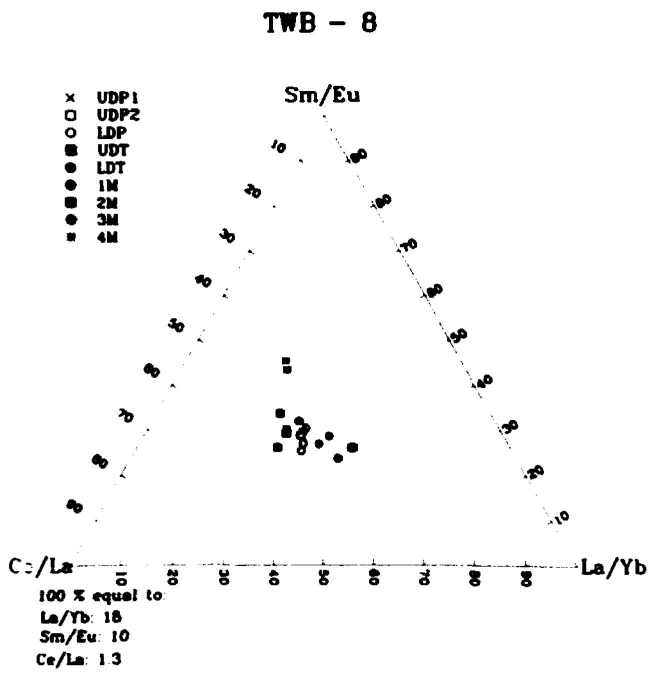

Fig. 16. REE characterization plot.

4.1.2.3 Average analytical data for TWB-8.

As already mentioned, most of the data from drill core samples TWB-8 were generated during an earlier project (see. *Kunzendorf* et al., 1985; 1986). Converting the previous data into values for the reservoir units used by The Geological Survey of Denmark (DGU), i.e. calculating average chemical data for the units, some interesting features can be evaluated (Table 4 and Fig. 17).

Table 4 Average analytical data of the Danian section for drill core TWB-8 using short-lived isotpes. All data in %, except V, Mn, Sr and Eu which are given in ppm.

Element	UDP1	UDP2	LDP	UDT	LDT1	LDT2	1M	2M	3M	4M	5M
Na	0.25±0.42	0.07±0.03	0.10±0.04	0.12±0.05	0.11±0.[illegible]	.13±0.04	749±192	978±217	1527±618	2018±568	1680±57
	n=6	2	8	8	6	2	9	29	29	30	2
Mg	1.17±0.97	-	-	-	-	-	3320	2685±573	2443±629	2652±1175	3325±375
	4						1	2	10	13	2
Al	1.70±3.39	0.17±0.01	0.24±0.08	0.48±0.22	0.39±0.13	0.27±0.01	1379±850	758±408	676±237	703±220	725±65
	6	2	8	8	7	2	9	30	30	28	2
Cl	0.12±0.05	0.20±0.00	0.20±0.08	0.18±0.08	0.18±0.09	0.19±0.01	1399±557	2592±823	2332±1213	3385±1955	2915±148
	6	2	7	8	5	2	9	29	29	31	2
Ca	34.44±0.51	34.80±1.00	34.16±2.28	27.90±2.24	30.40±4.59	34.60±3.25	32.33±4.36	34.21±2.24	36.38±2.47	37.50±1.30	37.30
	5	2	8	8	7	2	9	27	29	27	1
V	46.6±86.1	5.0	9.5±3.7	8.3±3.4	7.6±1.5	8.0±1.0	6.6±1.9	4.5±1.1	2.7±0.7	2.6±0.8	2.4±1.1
	6	1	8	8	7	2	4	10	17	19	2
Mn	1466±632	1515±15	1100±534	725±88	670±71	666±48	431±117	299±73	184±20	161±26	147±1
	6	2	8	8	6	2	9	29	29	31	2
Sr	1084±696	892	815±351	787±184	849±91	807±172	749±230	1138±157	1042±128	1137±159	978±74
	3	1	7	8	6	2	9	29	29	31	2
Eu	2.1	-	0.2	1.0±0.2	0.9±0.1	0.6	0.6±0.2	0.4±0.1	0.3±0.1	0.3±0.1	0.4
	1		1	4	3	1	8	19	14	17	1
Dy	3.6±1.7	1.6	2.0±0.8	2.3±0.9	2.2±0.6	1.8±0.5	1.2±0.5	1.3±0.3	0.9±0.3	1.0±0.3	1.0±0.1
	4	1	8	8	6	2	9	29	29	31	2

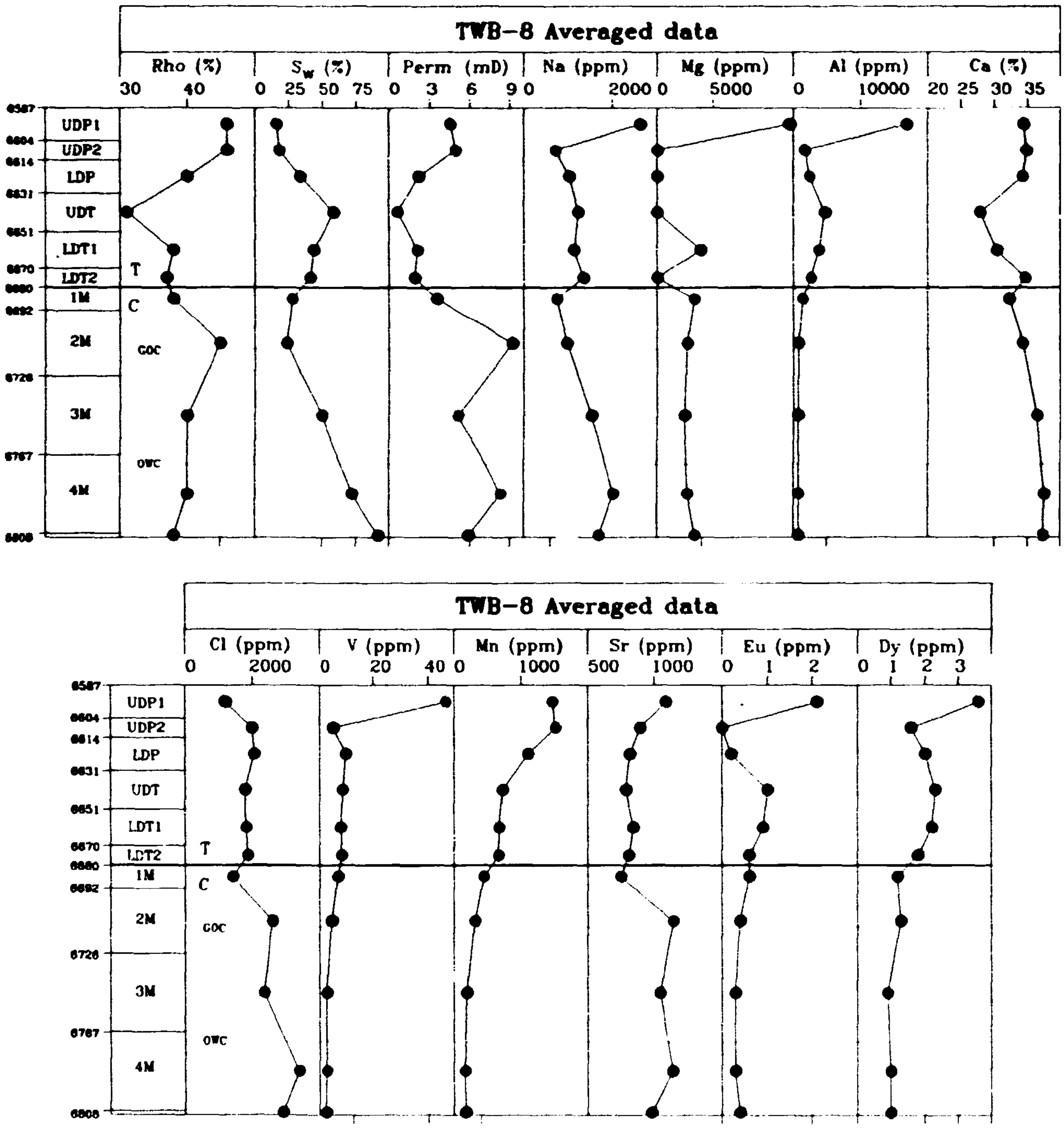

Fig. 17. Average analytical data distribution along drill core TWB-8.

As already mentioned, Ca is significantly reduced in sections LDP and UDT also, reflecting reduced porosity values at increased Al contents. Water saturation peaks as well in the area of high Al contents. In the gas zone, between 6614' and 6690', therefore, the reservoir quality is significantly reduced.

On comparing average petrophysical data (rho, S_w, permeability) with average elemental data, some significant grouping of Maastrichtian and Danian strata may be obtained (Fig. 1°\

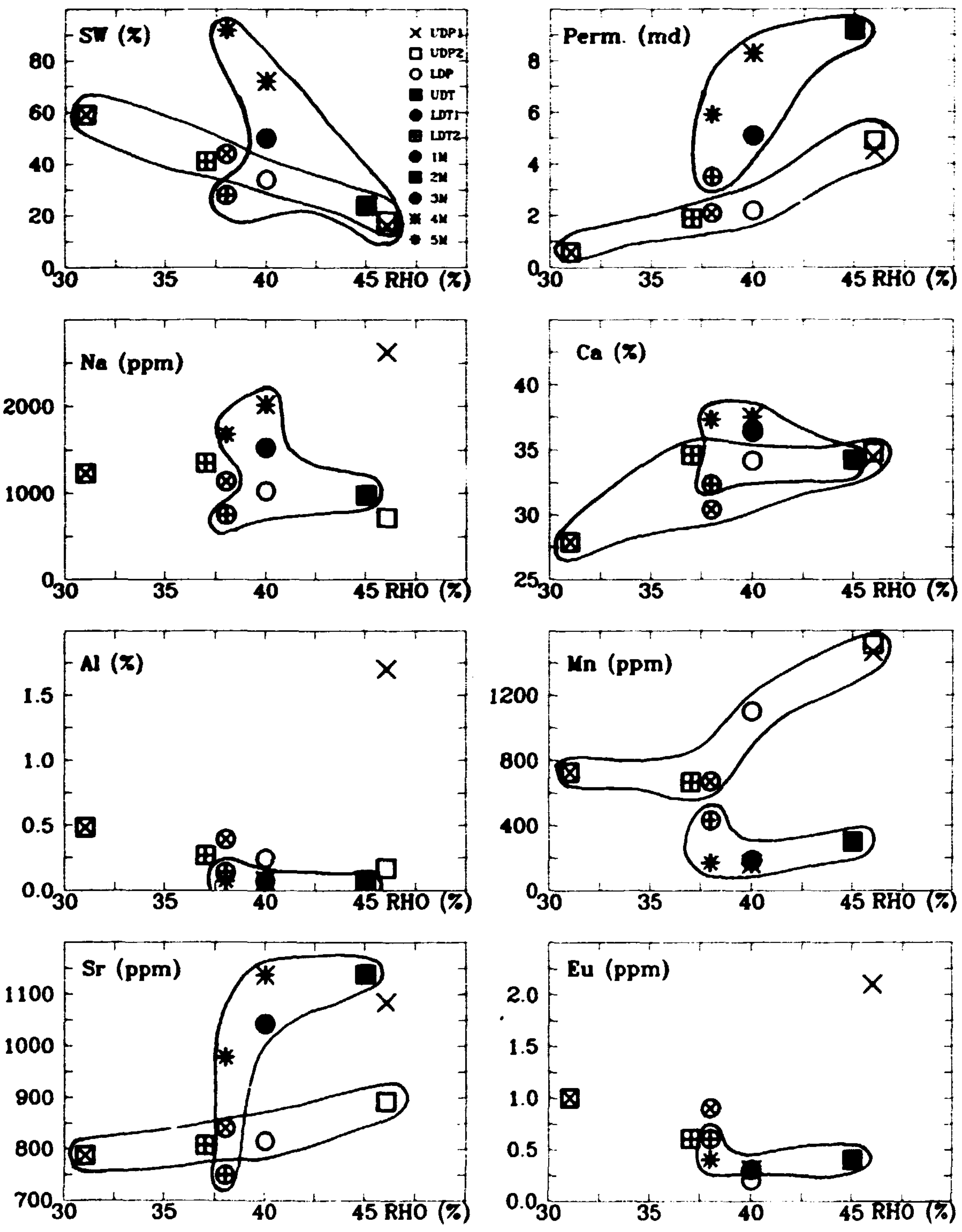

Fig. 18. Selected X-Y plots for average analytical data of TWB-8.

There is no clear correlation of elemental data with rho, although grouping into Danian and Maastrichtian groups is observed for, e.g., Sr, where Maastrichtian samples generally have higher Sr at comparable rho.

For water saturation, S_w (not plotted), there are some positive correlations with the average analytical data. As expected, there is a significant correlation between S_w and Na involving all chalk units. Also, water saturation divides Maastrichtian and Danian carbonate sediments into groups when plotted against Mn, Sr and Dy. Most interesting is perhaps the plot S_w vs. Ca where Maastrichtian samples show an increasing tendency while those of the Danian show decreasing S_w with decreasing Ca.

On comparing the permeability values, there seems to be significant correlation between permeability and average Na, Cl, Ca, and Sr. Permeability vs. average Mn also divides Danian strata (increasing tendency) and Maastrichtian strata (constant average Mn at increasing permeability).

4.1.3 Comparison of Log Data with Element Contents

Logging data are physical measurements of petrophysical properties in sedimentary formations. These properties in turn are closely related to the chemical composition of the rocks. It is therefore worthwhile to compare the chemical core data directly with the log values to establish relationships between chemistry and e.g. rock porosity or permeability. These comparisons should then lead to a better definition of petrophysical parameters via core data.

From the continuous log data we used the log value corresponding to the depth of the core sample taken for chemical analysis. In the correlation analysis, we follow the conventions suggested by Marsk Oil and Gas A/S, i.e. division into Danian units D1 and D2, and into Maastrichtian units M1 and M2, sometimes choosing further subdivisions according to the Mn distribution with depth. In the X-Y plot examples, however, the division of data is made according to reservoir units.

4.1.3.1 Comparison of Log Data with Ca Core Data from TWB-8

Correlation analysis results using log data and analytical results for Ca are given in Table 5.

Table 5. Correlation matrix for well-logging and Ca data.

Tool	DANIAN	D1	D2	MAAST	M1	M2	All data
GR	-0.15	0.63	0.20	-0.28	0.06	-0.05	-0.23
SP	0.36	0.35	0.17	-0.48	-0.03	-0.09	-0.44
NPHI	0.11	-0.71	0.00	0.45	-0.01	-0.10	0.45
ILM	0.37	0.66	0.15	-0.41	-0.06	-0.24	-0.25
ILD	0.46	0.59	-0.24	-0.39	0.22	0.13	-0.06
CILD	-0.52	-0.26	-0.40	0.43	-0.23	-0.03	0.39
SFLA	0.42	0.56	0.25	-0.46	0.32	0.57	-0.28
RHOB	-0.57	-0.75	-0.45	0.50	0.07	0.24	-0.01
PET	-0.05	-0.83	0.42	0.27			0.20
DT	0.33	0.61	-0.02	-0.34	0.09	0.21	0.06
LITH	0.51	0.83	0.36	-0.47	-0.07	-0.30	-0.03
AMPL	0.00	0.25	-0.44	0.49			0.48
RHGX	-0.58	-0.86	-0.51	0.51	-0.10	0.34	0.31

It is usually not sufficient to discuss correlation coefficients without actually plotting the data. The reason for this is that in many cases analytical data (even very large numbers of data) tend to show high correlation in case the range of the data is limited. This means that, although regression analysis gives a high correlation coefficient, there might be no linear dependence at all. X-Y plots in general have the advantage that they flag grouping of data, in the present case with depth in the core.

As seen from the data in Table 5, significant correlations exist for:

- GR and Ca in D1 (r = 0.63),
- NPHI and Ca in MAAST. (0.45),
- ILM and Ca in D1 (0.66),
- ILD and Ca in DANIAN (0.46) and D1 (0.59),
- CILD and Ca in MAAST. (0.43),
- SFLA and Ca in DANIAN (0.42), in D1 (0.56) and M2 (0.57),
- RHOB and Ca in MAAST. (0.50),
- PEP and Ca in D2 (0.42),
- DT and Ca in D1 (0.61),
- LITH and Ca in DANIAN (0.51) and in D1 (0.83),
- AMPL and Ca in MAAST. (0.49), and
- RHOGX and Ca in MAAST. (0.51).

Here, as mentioned above, DANIAN, D1, and D2 correspond to data from the whole Danian, units D1 and D2, respectively, while MAAST., M1 and M2 correspond to data from the whole Maastrichtian, units M1 and M2, respectively.

On inspecting these correlations in further detail it becomes clear that the correlation GR vs. Ca in D1 is not significant because only a few analytical results are available. The good correlation expressed by a relatively high correlation coefficient therefore is quite misleading.

An interesting grouping is obtained when plotting SP data vs. Ca (Fig. 19). While for Danian samples (UDP1 to LDT2) SP values are relatively constant

Fig. 19. Selected well-log data plotted vs. Ca content in drill core samples.

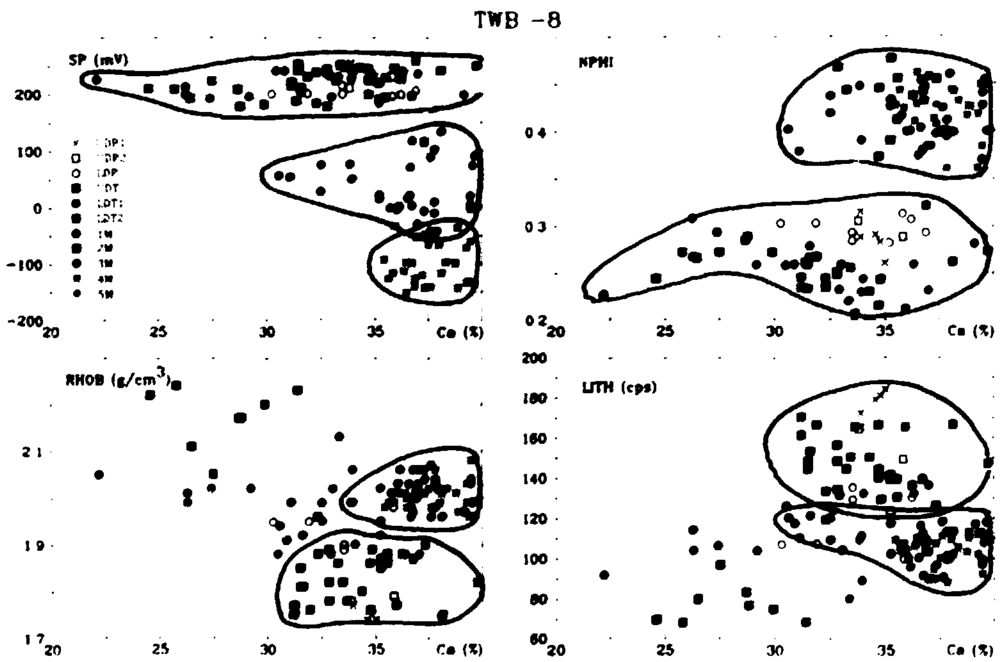

at largely varying Ca, most of the Maastrichtian SP data of the lowermost units (3M to 5M) are significantly lower, and by this a clear grouping of data is obtained. Characteristically, the group with Danian data includes also the uppermost Maastrichtian units (1M and 2M).

Plotting NPHI data against Ca, a clear grouping for the Maastrichtian samples is again observed. A distinct feature is that data from unit 2M fit equally into the two groups. As can be seen from the figure, the good correlation coefficient (r = 0.45) we find is an artifact produced by two distinct data groups; and therefore is without meaning.

The induction log data plotted against Ca (not shown in Fig. 19) also suggests grouping of data and in reality no positive correlation, although correlation analysis predicts rather high correlation coefficients. A similar pattern is derived for the SFLA data.

The plots RHOB vs. Ca and LITH vs. Ca (Fig. 19) also show some grouping rather than significant positive correlation, although the groups do overlap.

4.1.3.2 Comparison of Log Data with Al Core Data from TWB-8

Data from the following logs of TWB-8 were compared with Al core data: GR, SP, NPHI, ILM, ILD, CILD, SFLA, RHOB, PEF, DT, LS, LITH, AMPL, and RHGX. Correlation data are given in Table 6.

There are only a few significant element-log correlations (correlation coefficients greater than 0.4). The gamma-ray count rate (in API units) of section D1 correlates well with Al (r = 0.65), while there is no correlation between GR and Al for the whole Danian-Maastrichtian section.

Other significant correlations (correlation coefficient r in parenthesis) between logs and Al are: SP-Al for M1 (0.50), CILD-Al for D2 (0.50), RHOB-Al for DAN (0.43), for D2 (0.56) and for M2 (0.40), and RHOGX-Al for D2 (0.52).

Table 6. Correlation coefficients of log-data vs Al contents for TWB-8.

Tool	DANIAN	D1	D2	MAAST.	M1	M2	All data
GR	0.15	0.65	-0.07	0.20	–	–	0.09
SP	-0.08	0.32	-0.07	0.12	0.50	-0.36	0.24
NPHI	-0.27	-0.33	-0.22	-0.41	-0.53	-0.06	-0.37
ILM	-0.02	0.10	-0.22	0.27	0.26	-0.35	0.20
ILD	-0.34	-0.54	-0.46	0.10	–	–	0.10
CILD	0.38	0.04	0.50	-0.13	-0.35	0.35	-0.23
SFLA	-0.20	0.24	-0.30	0.33	0.41	0.93	0.21
RHOB	0.43	0.10	0.56	-0.18	-0.25	0.40	0.29
PET	-0.22	-0.03	-0.57	-0.11	–		-0.23
DT	-0.21	0.06	-0.14	0.28	0.32	0.08	-0.26
LITH	-0.32	-0.08	-0.45	0.17	0.23	-0.31	-0.18
AMPL	0.07	-0.20	0.33	-0.22	–	–	-0.35
RHGX	0.37	-0.04	0.52	-0.32	-0.46	0.23	-0.11

On inspecting the relevant data in detail by X-Y plots, it is evident that the correlation GR-Al in the DI section (not plotted) is an artifact and generated by too few scattered data. Contrary to this, a significant correlation seems to exist for SP-Al in the MI section alone, but inspecting the data in detail (Fig.20), the characteristical feature is the way the data is grouped.

Fig. 20. Selected well-logging data plotted against Al content in drill core samples.

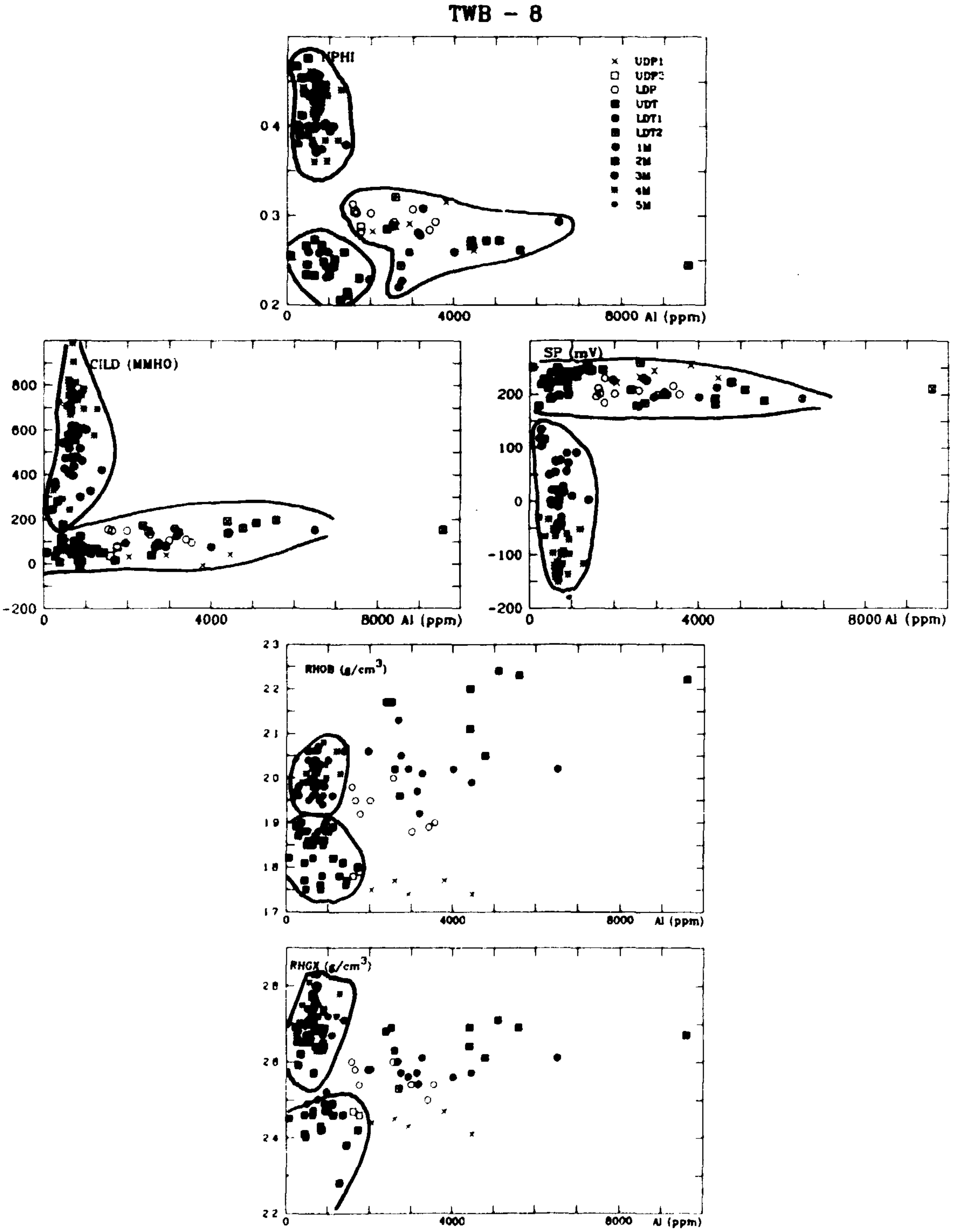

When plotting neutron porosity values (NPHI) against Al, a clear pattern is shown (Fig. 20). Danian and Maastrichtian samples make up three significant groups, but there is no positive correlation, rather a negative one, as should be expected. Al usually connected with the clay mineral fraction should express lower porosity values at higher Al content. It can be seen from the figure that some of 2M (and 1M) samples show high NPHI values, while others (gas-bearing) clearly group within the Danian samples.

Most of the induction logs plotted versus Al show an erratic picture with little or absent grouping of data. Only the plot of CILD-Al data shows 2 main groups, whereas the calculated positive correlation for the D2 section in doubtful.

While correlation analysis predicts a significant positive correlation between RHOB-Al in the Danian section, the grouped data in the plot (Fig. 20) do not confirm this. Also, calculated positive correlations between RHOB and Al for D2 and M2 are rather doubtful. It appears that there is perhaps some further grouping in the Maastrichtian strata. There are too few data for D2 to be sure that the observed positive correlation between RHGX and Al is real, but a grouping of data is observed here as well.

Table 7. Correlation coefficients of log-data vs. Na core data for TWB-8.

Tool	DANIAN	D1	D2	MAAST.	M1	M2	All data
GR	0.35	-0.17	0.22	-0.42	–	–	-0.29
SP	-0.25	-0.45	-0.23	-0.47	–	–	-0.67
NPHI	-0.13	0.49	-0.12	0.47	-0.32	-0.10	0.44
ILM	-0.38	-0.10	-0.15	-0.49	-0.28	-0.47	-0.48
ILD	-0.27	-0.26	-0.27	-0.28	-0.01	-0.36	-0.28
CILD	0.38	-0.44	0.32	0.69	0.34	0.40	0.67
SFLA	-0.33	0.32	-0.41	-0.61	0.13	-0.76	-0.56
RHOB	0.53	0.18	0.50	0.58	-0.10	0.27	0.48
PEF	0.01	0.40	-0.53	0.46	-0.13	0.10	0.36
DT	-0.40	0.13	-0.30	-0.57	–	–	-0.41
LITH	-0.46	-0.27	-0.37	-0.57	0.18	-0.33	-0.47
RHGX	0.53	0.30	0.49	0.58	-0.41	0.41	0.58

4.1.3.3 Comparison of log data with Na core data from TWB-8

Data from the following logs were compared with sodium core data: GR, SP, NPHI, ILM, ILD, CILD, SFLA, RHOB, PEF, DT, LS, LITH, AMPL, and RHGX. Correlation data for this comparison are given in Table 7.

There is no significant correlation of Na with GR data in the whole investigated section. If we introduce a threshold value for significant positive correlation at > 0.4, only RHOB ($r = 0.48$) and RHGX (0.58) correlate significantly with Na in the drill core section as a whole. A higher correlation (0.69) is obtained for CILD and Na. Good correlation between Na and LITH and AMPL is found for the lower parts of the Maastrichtian section.

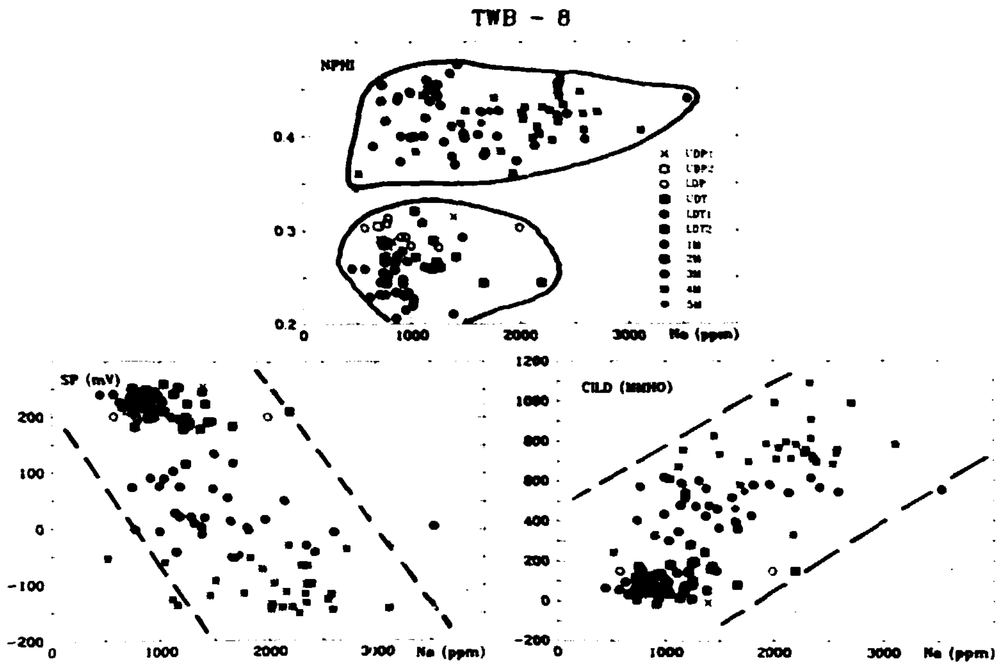

Fig. 21. Selected well-logging data plotted vs. Na content in drill core samples.

By plotting the SP and Na data (Fig. 21), two main groups are obtained within which the general trend shows decreasing SP values with depth at increasing Na. In the figure, 1M and 2M data plot within the Danian group. A similar group separation with depth may also be deduced by plotting NPHI vs. Na.

Although the correlation coefficient for the data set CILD-Na is rather high (0.69) by inspecting the data (Fig. 21), it is clear that the apparent correlation may also be interpretated as the presence of two groupings of data.

4.1.3.4 Comparison of log data with Mn core data from TWB-8

Characteristic for the comparison of logging data with drill core Mn analyses is the presence of a number of significant and high positive correlations. An overview of the correlations is presented in Fig. 22.

Highest positive correlations (> 0.8) are observed between log data and Mn for

DI section:	SP (0.96), ILM (0.85), SFLA (0.96) and DT (0.97)
DANIAN section:	ILD (0.82), LS (0.90), and LITH (0.90)
MAAST. section:	SFLA (0.94), DT (0.97), LS (0.85) and LITH (0.85)

These high correlations call for a more detailed investigation.

When all the available Mn data vs. the respective SP data (Fig. 23) are plotted, it becomes evident that one should be sceptical about the high correlation in the DI section because only few data are available. There is a significant grouping, suggesting at least 4 groups: group 1 includes the data for reservoir units UDP1, UDP2, and LDP; group 2 contains mostly data from UDT, LDT1, LDT2 and partly 1M; group 3 is composed of mainly data from 2M; and group 4 incorporates all data from 2M to 5M.

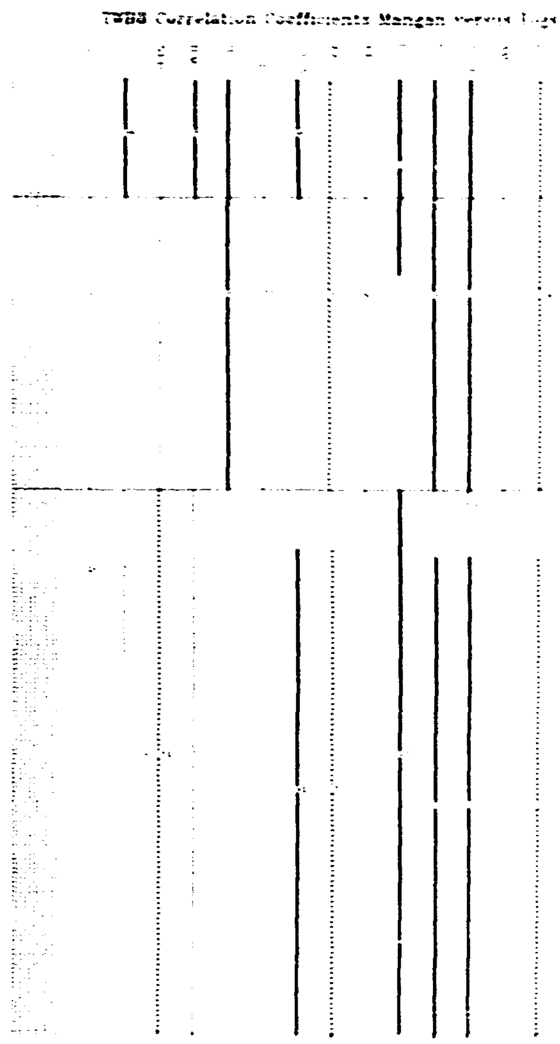

Fig. 22. Correlation coefficient plot of Mn vs. log data.

SFLA data plotted against Mn (Fig. 23) suggest a positive and significant correlation for all the Maastrichtian samples (samples from reservoir unit IM are slightly removed). The Danian samples make up four clear'y separated groups.

On inspecting the curve ILM vs. Mn (Fig. 23), a significant grouping is again seen, the data being split up into 3 main groups. There is a significant positive correlation within the group containing the Maastrichtian data (r = 0.73).

The curve for DT vs. Mn (Fig. 23), although giving very high positive correlation coefficients for some subsections, is most significant for the Maastrichtian data. Three major groups are suggested by the plot: two groups with positive correlation of data and one with negative correlation. The latter group contains both Danian (UDT, LDT1) and Maastrichtian (IM) data.

LITH and RHGX vs. Mn show the same grouping of data, i.e. three distinct data groups (Fig. 23).

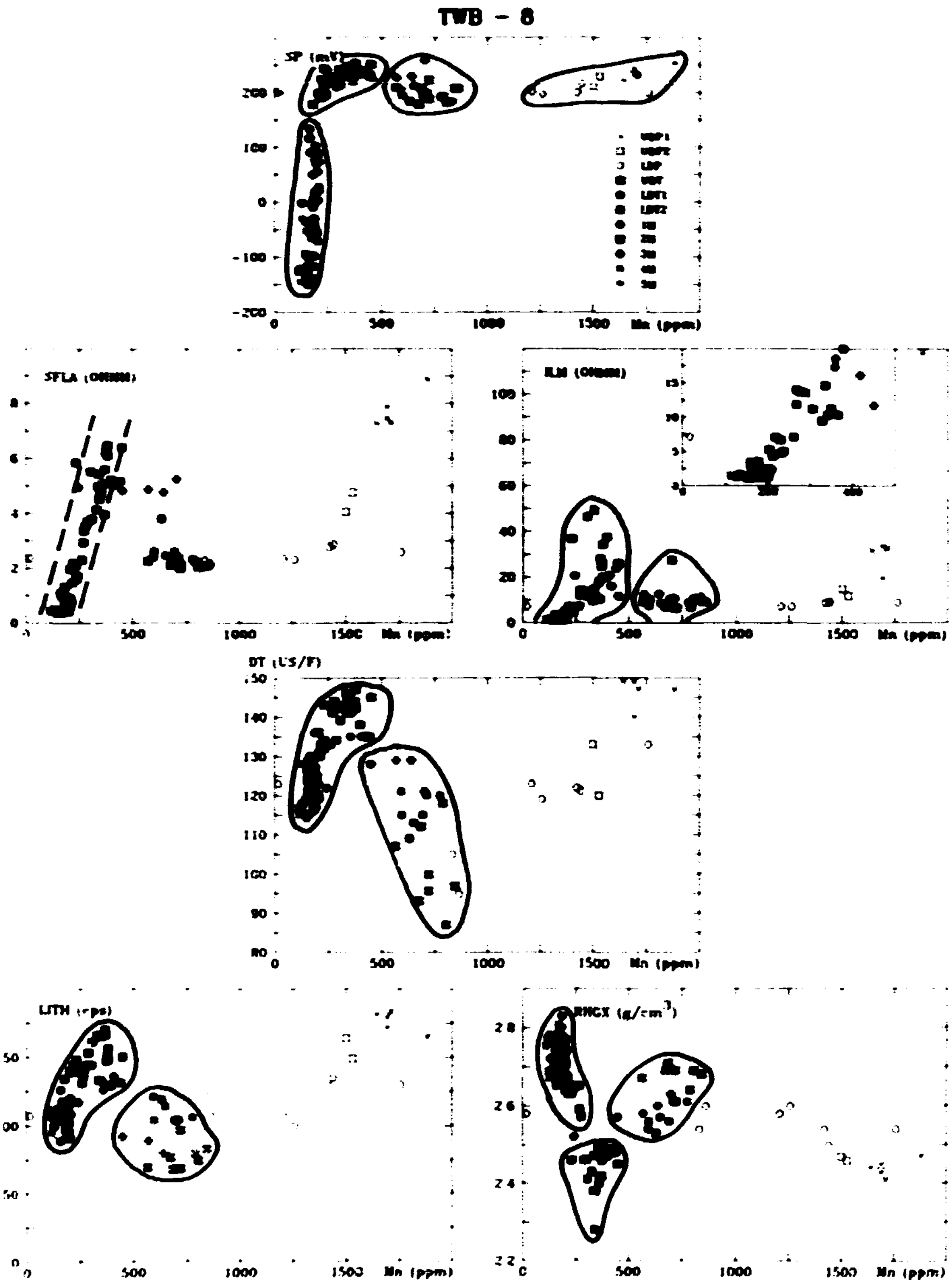

Fig. 23. Selected well-logging data plotted against Mn contents in drill core samples.

4.1.3.5 Comparison of Log Data with U Core Data from TWB-8

Data for the following logs were compared with U core data: GR, SP, NPHI, ILM, ILD, CILD, SFLA, RHOB, PEF, DT, LS, LITH, AMPL, and RHGX. Correlation data are given in Table 8.

Table 8. Correlation coefficients of log-data vers. U core data for TWB-8.

Tool	DANIAN	D1	D2	MAAST.	M1	M2	All data
GR	-0.27	-	0.02	0.18	-	-	0.08
SP	0.43	0.40	0.20	0.48	-0.05	0.25	0.31
NPHI	-0.26	-0.69	-0.37	-0.19	-0.12	0.19	- 0.01
ILM	0.32	0.11	-0.18	0.37	0.05	0.57	0.38
ILD	0.36	-	-0.37	0.35	0.17	0.48	0.33
CILD	-0.45	-	0.45	-0.51	-0.14	-0.35	-0.33
SFLA	0.57	-	-0.13	0.38	-0.11	0.60	0.28
RHOB	-	-	0.62	-0.58	-0.36	-0.29	-0.48
PEF	-	-	0.26	-0.34	-0.37	-0.34	-0.22
DT	-	-	-0.14	0.53	-	-	0.50
LITH	-	-	-0.58	0.62	0.44	0.27	0.49
RHGX	-	-	0.51	-0.41	-0.52	-0.54	-0.30

When comparing the data in the table, it may be concluded that D1 shows a significant correlation between SP and U, whereas SP, CILD, RHOB and PEF correlate with U in the section D2. For the Maastrichtian, U correlates positively in the M1 section with LITH only, whereas in the section M2 U correlates with EP, ILM, ILD, SFLA, and LITH.

On comparing the log and geochemical data in the form of X-Y plots (not shown), the general tendency of grouping rather than positive correlation is confirmed.

4.2 Drill Core E-1x

4.2.1 Log Interpretation Data for E-1x

Average petrophysical and reservoir data for the well E-1x are given in Table 9.

GOC and 50% Sw are not present in E-1x, and the OWC is calculated at 6742'. A zone of > 7 feet comprises the 50% S_w-OWC, i.e. a very thin oil zone exists in the uppermost Danian.

All available logging data for E-1x were considered. These data were recorded in 1982. The logging equipment differed from that applied when logging TWB-8 (at later times). This means that a number of logging tools were different and generally not as advanced when logging well E-1x. Logs are included for E-1x: SP, IL, GR, DT, CAL1, RHOB, SNP, MLL, MINV, and MNOR.

A number of interpretational plots for E-1x are given in Fig. 24, while porosity and s_w with depth are plotted in Fig. 25.

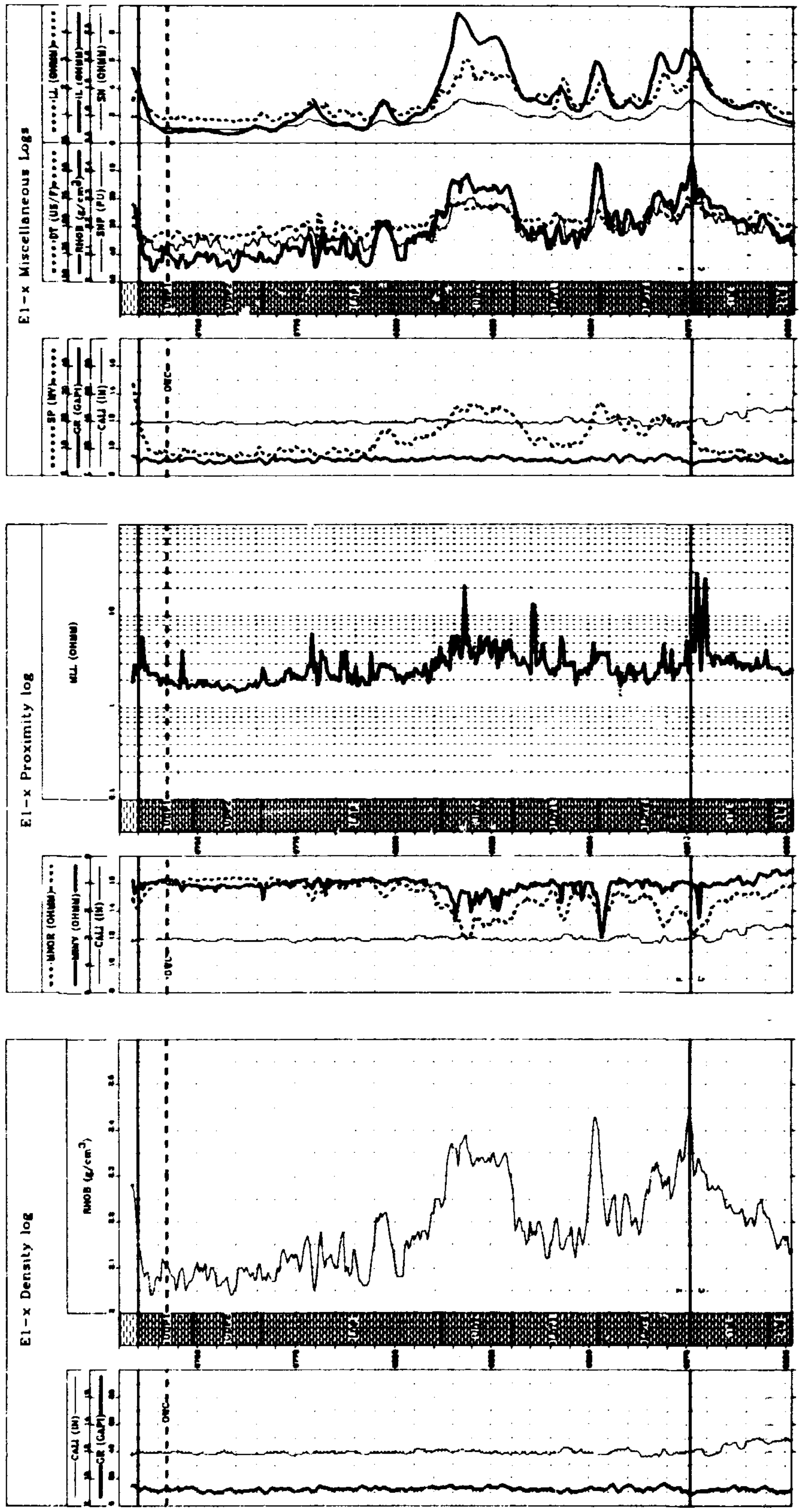

Fig. 24. Log evaluation plots for well E-Ix.

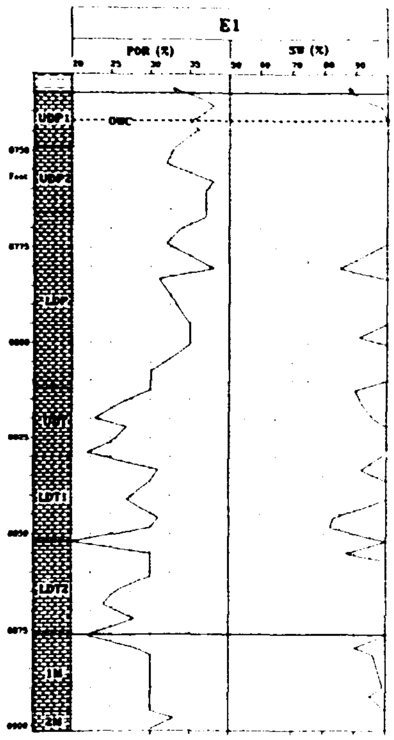

Fig. 25. Interpretational porosity and s_w with depth in hole E-1x.

4.2.1.1 Logs Involving Radioactivity Measurements

Natural radioactivity is very low (about 12 GAPI) throughout the well and there is only very little graduation in the GR data (Fig. 24).

The SNP tool giving data in porosity units (PU) points to a porosity degradation in unit UDT (Fig. 24) which shows a constant value of about 20 PU. While SNP values in Danian units UDP1, UDP2, and LDP generally lie at about 35 PU, and they gradually decrease towards the Creataceous-Tertiary boundary; only about 18 PU are observed at the boundary. An increase with depth is then found in units 1M and 2M.

Table 9. Average petrophysical and reservoir data for E-1x.

Unit	Depth (feet)	Thickness (feet)	Porosity (%)	Sw (%)	Permeabil. (mD)
UDP1	6735	14	35	-	0.9
UDP2	6749	17	35	-	0.9
LDP	6766	46	33	-	0.7
UDT	6812	18	25	-	0.3
LDT1	6830	22	30	-	0.5
LDT2	6852	24	27	-	0.3
1M	6876	20	29	-	0.6
2M	6896	44	32	-	1.2
3M	6940	82	31	-	1.2
4M	7022	51	30	-	1.5
5M	7073	75	29	-	1.3

4.2.1.2 Electrical Logs

Results for the microspherically focused log and the microlaterolog, both measuring resistivity near the borehole are shown in Fig. 24.

MLL values are slightly decreasing in unit UDP1 towards the transition zone to UDP2 and stay constant within this rock unit. MLL values are slightly higher in unit LDP, while they are significantly increased in unit UDT and are somewhat lower again in units LDT1 and LDT2. The transition to the Maastrichtian strata is marked by high MLL values, decreasing rapidly to a constant level comparable to that for UDT.

Log curves with a behaviour very similar to that of MLL are displayed for MINV, MNOR, LL, IL, and SN. They all show a maximum value in unit UDT.

Very similar data are also recorded by the self-potential tool SP.

4.2.1.3 E-1x Density Logs

The plot of RHOB (Fig. 24) shows values of 2.07 g cm^{-3} for Danian units UDP1 and UDP2. Increasing RHOB values are observed for section LDP, increasing to about 2.2 g cm^{-3} at the bottom of the LDP section. Section UDP shows the highest RHOB, about 2.35 g cm^{-3}, whereas in section LDT1 the value for RHOB drops again to about 2.17 g cm^{-3}. Apart from a relatively high-RHOB upper part of section LDT, increasing values are generally observed for this section.

From the C-T boundary onwards, RHOB decreases with depth from a value of about 2.4 g cm^{-3} to about 2.2 g cm^{-3} in the Upper Maastrichtian section.

4.2.2 Geochemical Profiles along E-1x

Major element contents (Na, Ca, Fe, Al, and Mn) determined by both INAA and XRF are given for all samples in Appendix V, and they are plotted with depth in Figs. 26 to 29.

While Na contents are constant (about 0.2%) throughout the drill core section (Fig. 26), there is a slight decrease of Ca (from about 35% to 30%) in sections UDT, LDT1, and LDT2, i.e. towards the Cretaceous-Tertiary boundary. Ca values are high again in the Maastrichtian samples. The tendency for Ca is somewhat mirrored by Al contents being slightly higher in the lowermost Danian samples. Aluminium contents in general are significantly decreased in the Maastrichtian samples.

Iron content in the samples were determined by both INAA and XRF. The depth profiles for both measurements are compared in Fig. 29. Although there is some difference for both Fe measurements the general tendency is clearly displayed: reduced Fe values are found in the Maastrichtian strata, while in the Danian Fe is relatively constant at about 0.2%. Compared with TWB-8 there is no Fe enrichment observed within the Danian samples.

For manganese the distribution with depth strongly resembles that observed in TWB-8 (Fig. 26). Content continuously decreases from about 4000 ppm (unit UDP1) to the top LDP unit (about 1500 ppm) and then reaches a nearly constant value at about 1000 ppm down to the Cretaceous-Tertiary boundary. Maastrichtian samples then have much lower Mn (less than 500 ppm).

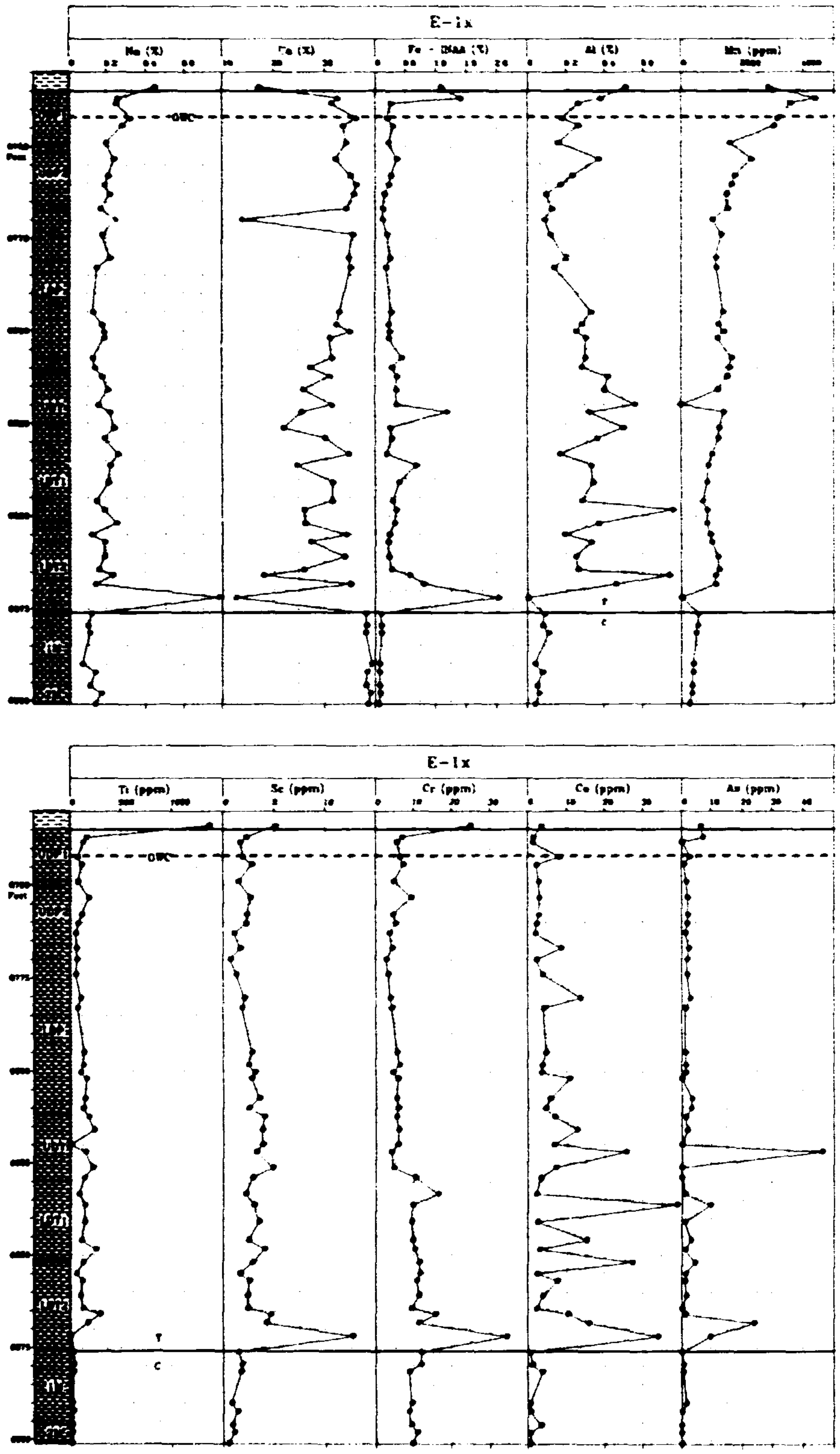

Fig. 26. Na, Ca, Fe, Al, Mn, Ti, Sc, Cr, Co, and As distributions with depth in drill core E-1x.

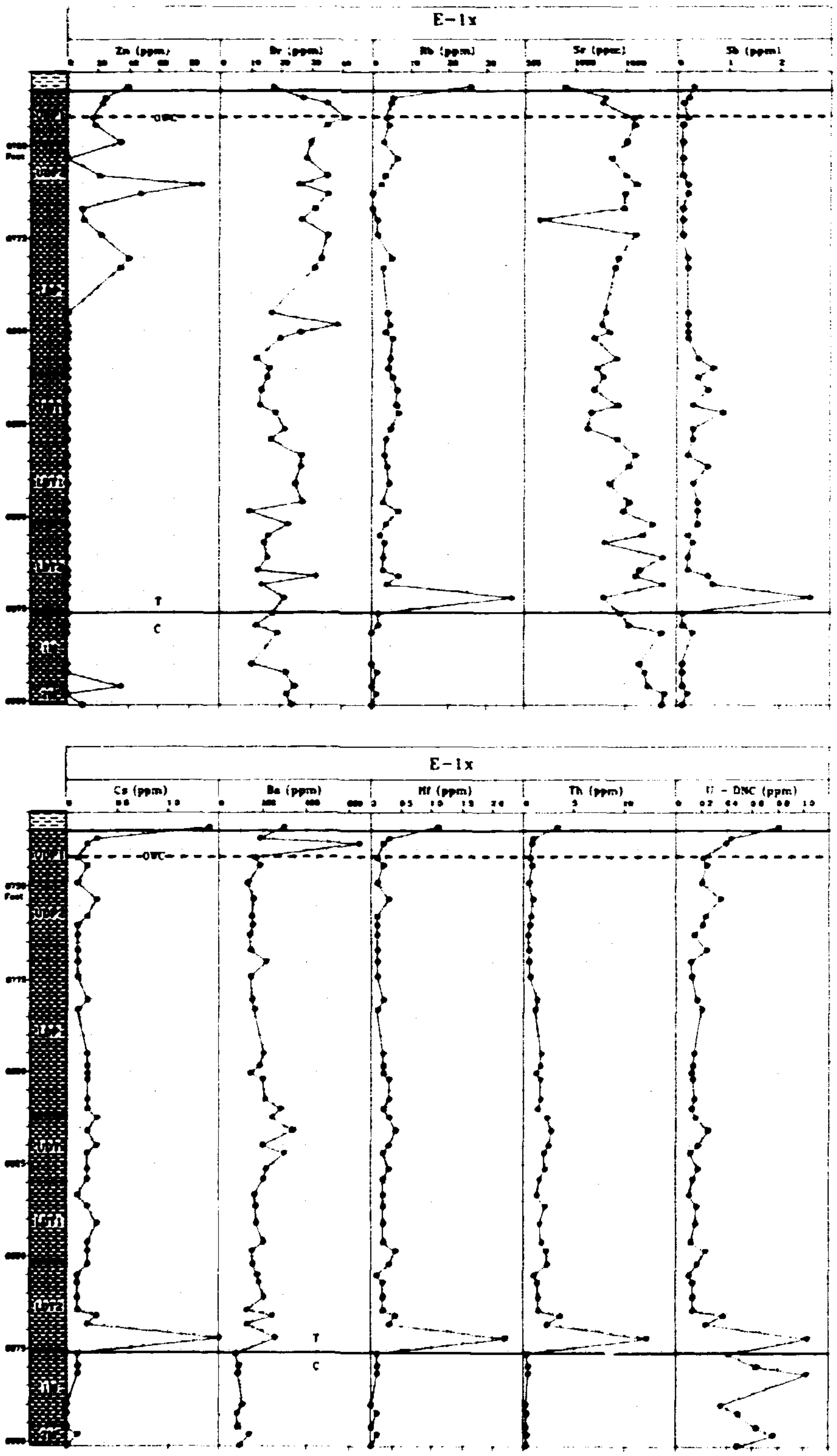

Fig. 27. Zn, Br, Rb, Sr, Sb, Cs, Ba, Hf, Th and U distribution with depth in drill core E-1x.

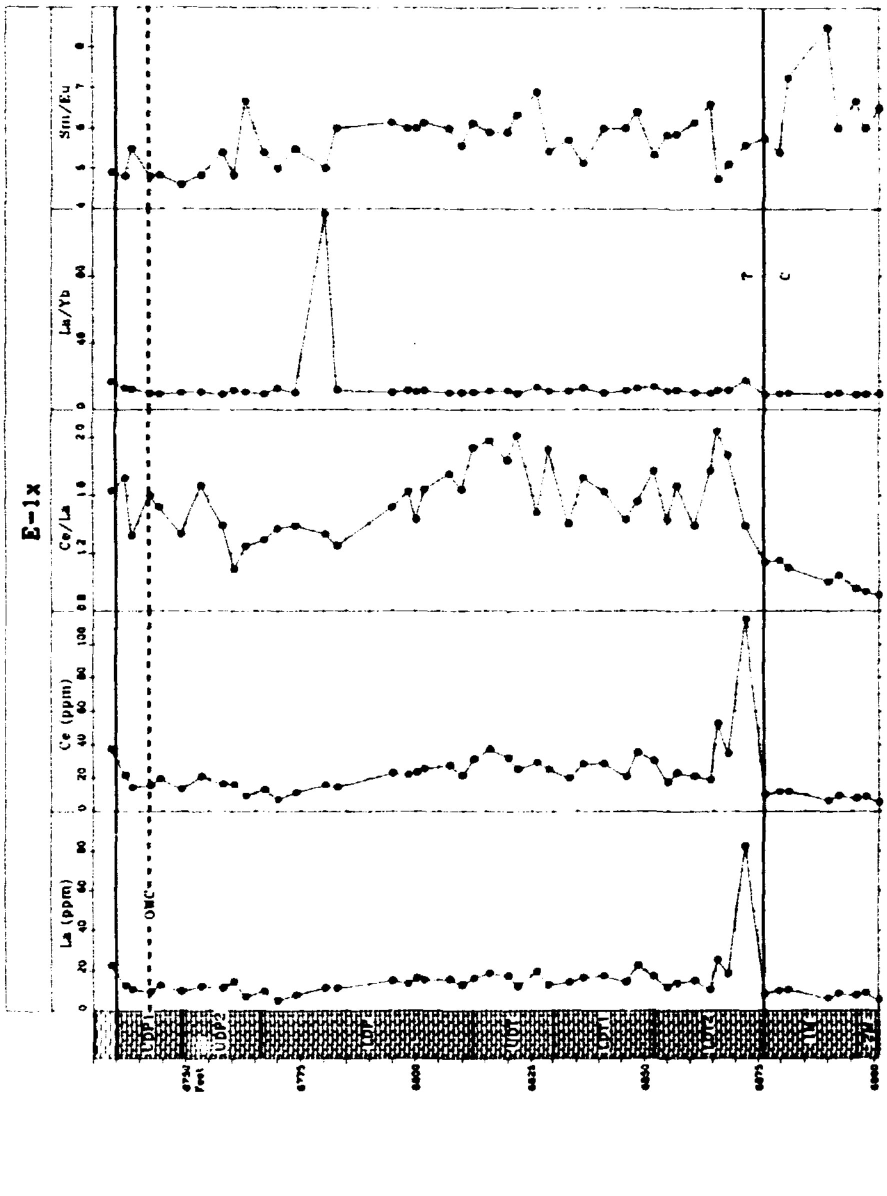

Fig. 28. Selected rare earth element contents and ratios plotted vs. depth in drill core E-1x.

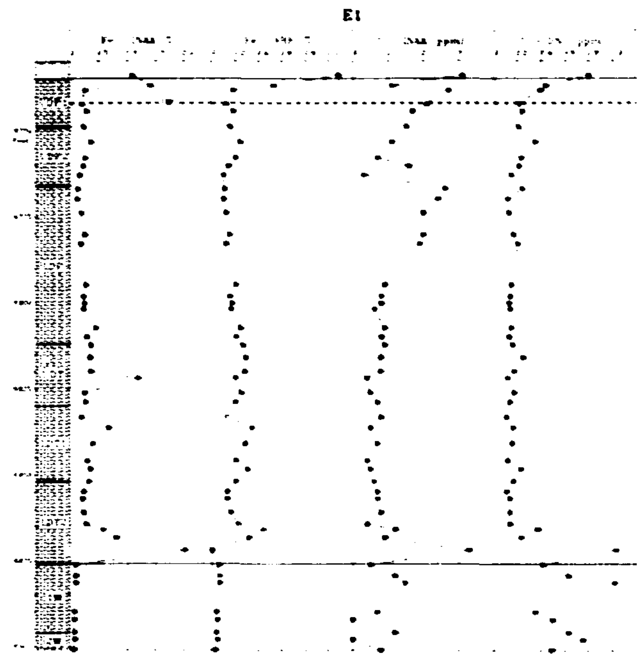

Fig. 29. Fe and U determined by two independent analytical methods plotted vs. depth in drill core E-lx.

As regards Ti, Sc, Cr, Co, and As, the content of each in the chalk samples is very low (Fig. 26); for Ti, Sc and As, there is practically no trend with depth, although Sc values are somewhat higher in the Danian rocks compared with their Maastrichtian counterparts. A clear trend with depth is seen for Cr in that contents in the lowermost chalk units LDT1 and LDT2, but also in 1M and 2M are significantly higher, at generally 10 ppm. Frequently observed fluctuations in the contents of these elements may be explained by the small sample amount analyzed suggesting problems of inhomogeneity.

While Rb contents are very low showing no clear trend with depth (Fig. 27), values for Br, Sr and Sb differ somewhat from each other. There is a slight increase in Sr contents in units LDT1 and LDT2, and for Sb values are slightly higher in the lowermost Danian samples.

Most of the Danian samples show rather constant contents of Cs, Ba, Hf, Th, and U along the drill core (Fig. 27). However, clearly lower values for Cs, Ba, Hf, and Th are observed in the Maastrichtian samples, while U in these samples is significantly higher. Uranium analyses by DNC differ somewhat from those obtained by INAA (Fig. 29), but the distribution with depth is quite similar.

As regards the rare earth elements of which 2 of the 7 analyzed elements are plotted in Fig. 28, they are expectedly low throughout the E-lx drill core section. However, some clear trends are observed. Viewing only La and Ce, these elements are relatively low and constant in Danian sections UDP1 and UDP2 with very low contents at the top of unit LDP. They then increase again towards unit UDT and stay constant throughout the Danian. Maastrichtian strata have generally lower REE content.

Selected rare earth element ratios (Fig. 28) show that Ce/La is different in sections UDT, LDT1, and LDT2 (higher) but was significantly reduced in the Maastrichtian strata. This again (see sect. 4.1) would suggest a significant change in redox conditions at the end of the Maastrichtian. Depositional redox conditions in the carbonates may be viewed through the behaviour of Ce. As they are preferentially removed under oxic depositional conditions, it is concluded that available oxygen was increased in the Danian. There is no clear trend for the other two selected rare earth element ratios (La/Yb, and on Sm/Eu), although the higher Sm/Eu ratios in the Maastrichtian samples could be interpreted to stem from increased terrestrial input.

4.2.3 Average Analytical Data for E-lx

Average analytical data for the E-lx drill core section are given in Table 10. Not all of these data were obtained by INAA, i.e. the table also contains XRF data.

The average data are also plotted in Fig. 30 vs. depth. It is clear that there is a significant grouping in element distributions with depth, i.e. for a number of elements similar distributions with depth are observed.

Fig. 30. Average analytical data plotted vs. depth in drill core E-lx. The data are grouped according to depth distributions that are similar to each other.

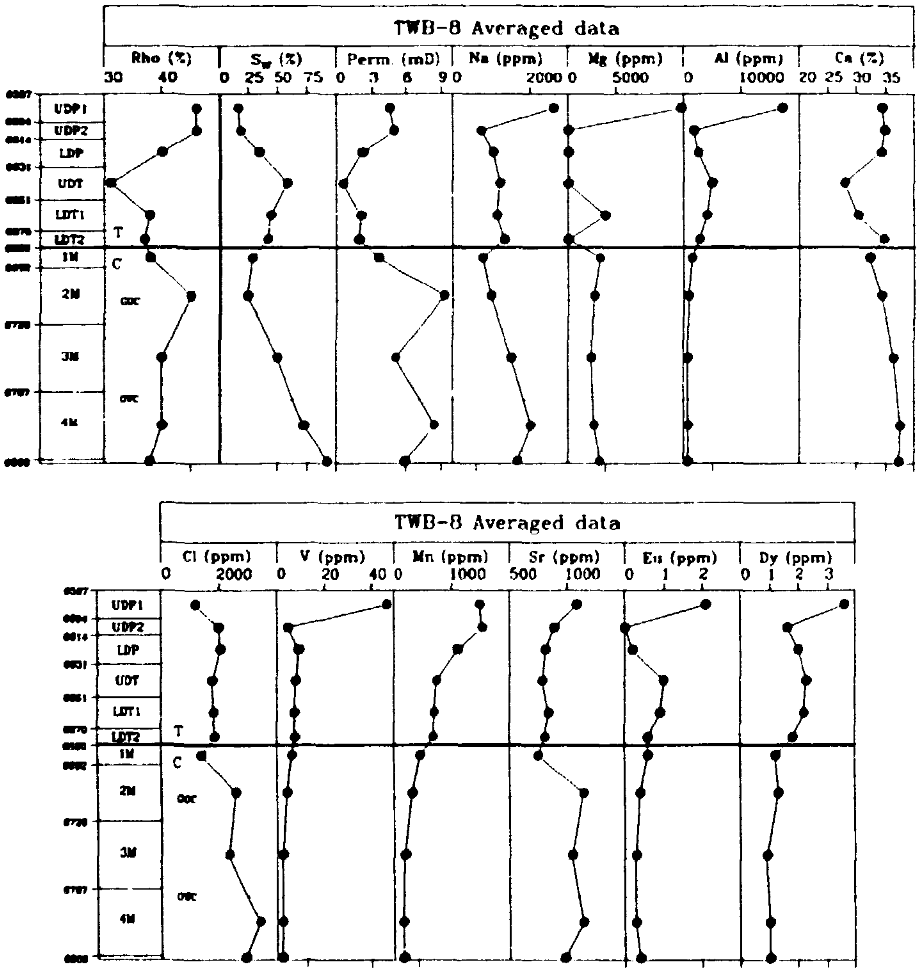

Table 10. Average analytical data for drill core E-1x.

Element	UDP1	UDP2	LDP	UDT	LDT1	LDT2	1M	2M
Na	0.31±0.08 N=5	0.21±0.02 5	0.18±0.04 11	0.20±0.03 6	0.21±0.04 5	0.26±0.22 8	0.11±0.03 5	0.14±0.03 3
K	0.36±0.30 2	-	-	-	-	-	-	-
Ca	33.10±7.40 5	34.70±1.60 5	31.20±6.20 11	27.60±3.80 6	29.70±4.20 5	26.60±8.20 8	38.40±0.57 5	38.60±0.50 3
Fe	0.65±0.56 5	0.24±0.07 5	0.23±0.09 11	0.46±0.36 6	0.38±0.18 5	0.58±0.62 8	0.09±0.02 5	0.07±0.01 3
Determined by XRF:								
Al	0.32±0.13 5	0.21±0.10 6	0.22±0.09 11	0.43±0.09 6	0.38±0.23 5	0.37±0.19 7	0.08±0.03 5	0.05±0.01 3
Ti	374±558 5	105±54 6	110±39 11	197±45 6	156±67 5	153±76 7	31±9 5	18±4 3
Mn	3410±611 5	1772±304 6	1352±204 11	1352±137 6	884±121 5	1104±148 7	478±81 5	313±55 3
Fe	0.42±0.40 5	0.17±0.05 6	0.16±0.04 11	0.25±0.04 6	0.25±0.08 5	0.23±0.11 7	0.06±0.01 5	0.04±0 3
Sc	2.8±1.4 5	2.0±0.7 11	2.3±0.8 6	3.8±0.7 5	3.0±0.7 8	4.2±3.6 5	1.5±0.4 5	0.8±0.3 3
Cr	10.3±8.2 5	5.5±2.2 5	4.7±1.2 11	6.1±2.3 6	11.1±3.0 5	14.5±8.2 8	10.2±1.6 5	9.9±0.9 3
Co	3.4±2.9 5	2.7±0.4 5	6.0±3.5 11	10.4±8.0 6	12.3±15.7 5	12.9±11.9 8	1.3±1.4 5	1.6±1.7 3
Zn	24.1±8.8 5	47.7±28.5 4	23.3±13.9 5	-	-	-	-	23±18 2
As	4.4±3.1 4	1.7±0.4 5	2.0±0.8 10	16.4±25.6 3	3.2±3.8 5	6.2±8.4 7	0.9±0.6 3	-
Br	31.0±9.3 5	30.9±4.3 5	26.0±8.9 11	16.3±3.3 6	22.8±7.6 5	18.2±6.5 8	16.0±5.0 5	23.5±1.3 3
Rb	8.7±9.4 5	3.8±1.9 4	3.7±1.5 10	9.5±4.9 6	4.3±1.6 5	7.8±11.8 8	1.6±0.1 3	1.2 1
Sr	1319±280 5	1492±86 5	1295±247 11	1265±135 6	1496±96 5	1616±227 8	1628±153 5	1813±91 3
Sb	0.1±0.1 5	0.1±0.1 5	0.2±0.2 11	0.5±0.2 6	0.4±0.2 5	0.7±0.8 8	0.1±0.1 3	0.1±0.1 3
Cs	0.4±0.5 5	0.2±0.1 5	0.2±0.1 11	0.2±0.1 6	0.2±0.1 5	0.3±0.5 8	0.1±0.0 3	0.1 1
Ba	295±203 5	143±11 5	182±45 11	249±57 6	167±20 5	183±51 8	87±11 5	104±27 3
Hf	0.4±0.4 5	0.1±0.1 5	0.2±0.1 11	0.3±0.1 6	0.2±0.1 5	0.5±0.7 8	0.1±0.0 3	0.1 1
Th	1.3±1.2 5	0.6±0.2 5	1.2±0.5 11	2.3±0.4 6	1.8±0.4 5	3.3±3.7 8	0.3±0.1 5	0.2±0.1 3
U	0.41±0.24 5	0.23±0.08 5	0.15±0.04 11	0.16±0.05 6	0.15±0.05 5	0.29±0.31 8	0.58±0.27 5	0.62±0.14 3
La	13.8±5.3 5	11.2±2.8 5	12.4±3.6 11	16.3±3.0 6	17.1±3.4 5	24.4±23.9 8	8.9±1.8 5	7.5±1.6 3
Ce	21.7±9.3 5	15.1±4.4 5	18.6±6.7 11	30.1±4.5 6	26.6±6.4 5	39.1±32.7 8	9.7±2.3 5	7.0±1.6 3
Nd	12.6±4.7 5	12.1±2.7 5	13.5±5.1 11	18.3±1.9 6	17.7±3.4 5	29.5±28.2 8	8.2±1.5 5	8.9±2.0 3
Sm	2.9±0.9 5	2.6±0.4 5	3.6±1.2 11	5.0±1.0 6	4.9±1.0 5	7.2±7.3 8	2.4±0.5 5	1.9±0.6 3
Eu	0.6±0.2 5	0.5±0.1 5	0.6±0.2 11	0.8±0.2 6	0.8±0.3 5	1.3±1.3 8	0.4±0.1 5	0.3±0.1 3
Tb	0.4±0.1 5	0.4±0.1 5	0.5±0.1 11	0.6±0.1 6	0.7±0.1 5	1.0±1.0 8	0.3±0.1 5	0.2±0.1 3
Yb	1.1±0.2 5	1.1±0.3 5	1.1±0.5 11	1.5±0.2 6	1.5±0.3 5	1.9±1.3 8	1.0±0.2 5	0.8±0.2 3
Lu	0.1±0.1 5	0.1±0.0 5	0.2±0.1 11	0.2±0.0 6	0.2±0.0 5	0.2±0.2 8	0.1±0.0 5	0.1±0.0 3

Group 1 which also contains petrophysical parameters porosity (RHO) and estimated permeability (mD) includes elements Ca and Br; it shows a general decrease of data down to unit UDT. Higher values are found in unit LDT1, decreasing again in LDT2. Maastrichtian units 1M and 2M have generally increased values. The plots also suggest that for E-1x there is a positive correlation between the Ca content in drill core samples and the porosity of the formation.

Group 2 includes elements Fe, Sc, Rb, Sb, rare earth elements, Hf, and Th. The distribution with depth for these elements is approximately the mirror-image of group 1 distributions. Because of this, group 2 is thought to contain largely elements of the residual fraction incorporating both clays and other residual minerals. The rare earth North American shale normalized distributions are plotted in Fig. 31 showing the increased negative Ce anomaly for Maastrichtian samples.

Group 3 incorporates elements Na, Cs and Cr showing distribution patterns similar to each other. If there are higher elemental contents for unit UDT, this element group could be included into group 2.

Group 4 is made up of elements showing little similarity in their depth distributions. It includes elements Co, Zn, As, Sr, Ba and U. Apparently these elements are resting in some phases clearly differently with respect to those of the other groups. However, some of these elements could also be added to some of the other groups, e.g., Co to group 3.

Fig. 31. Average North-American shale normalized REE patterns in drill core E-1x.

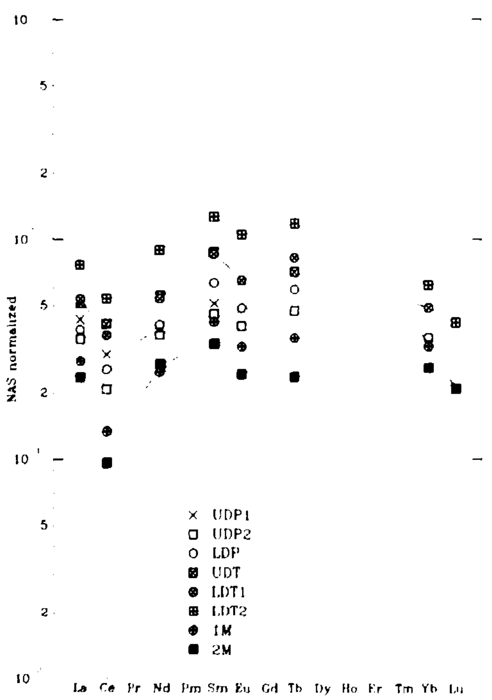

4.2.4 Comparison of Selected Analytical Data with Log Data

Because drill core samples from E-lx were analyzed for a large number of chemical elements (normal INAA), comparisons for all of these elements may be carried out. However, only a few of them are selected.

Some results of correlation studies between log data and selected element contents for drill core samples E-lx are given in Fig. 32.

The only positive correlation between Ca and log data is for DT in the Danian section. Inspecting the data of Ca vs. DT (Fig. 32) however, reveals that there is merely a grouping of data, where Danian and the few Maastrichtian data split into 2 groups. Correlation analysis of log data vs. Al shows correlation coefficients close to 0.5, very rarely exceeding 0.55.

Fig. 32. Selected analytical data plotted vs. selected logging data the well E-lx.

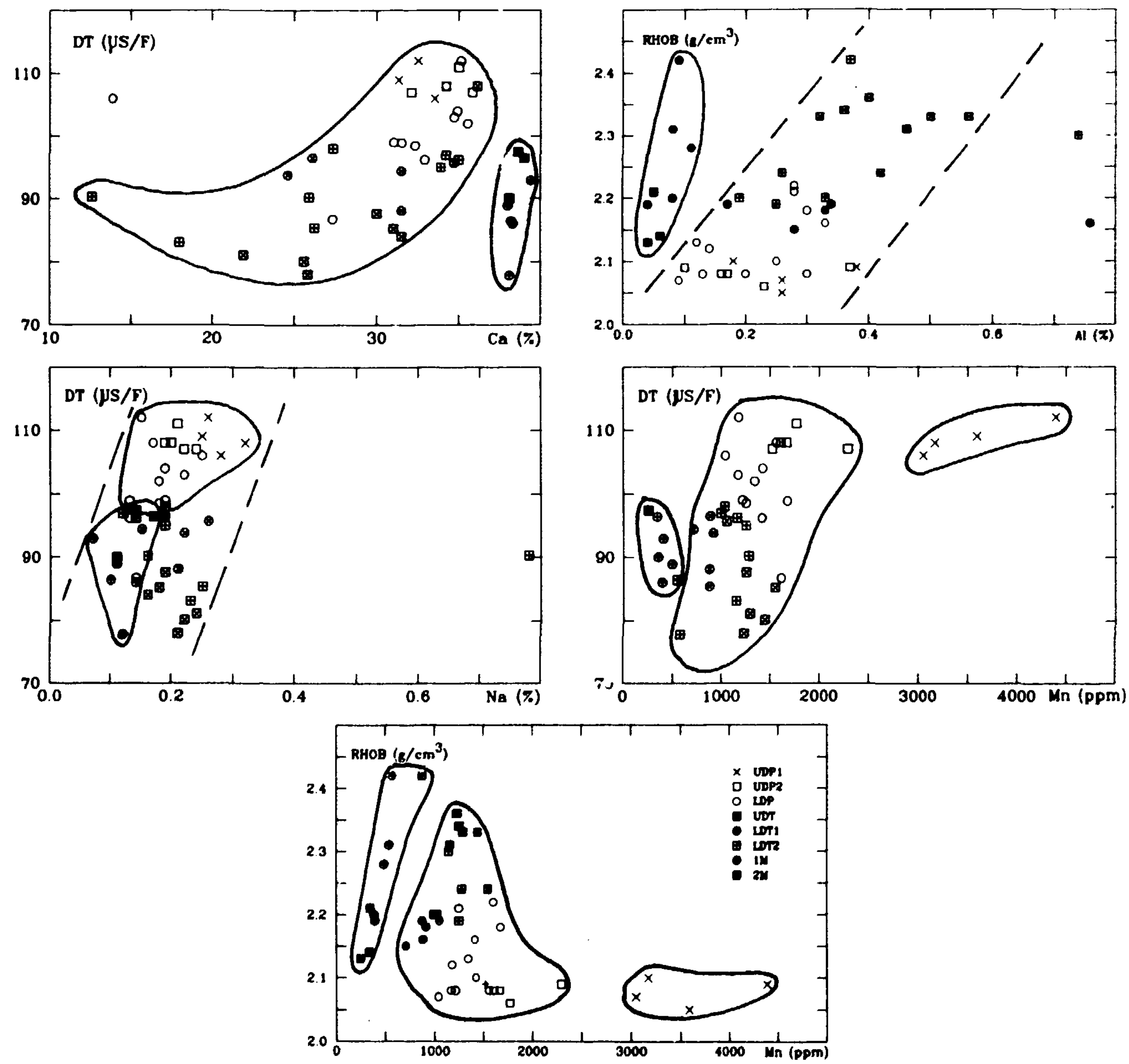

A typical example for Al is given in Fig. 32. As was the case in several other examples, a clear grouping is present, but in reality no linear dependence is shown by the plot. It is interesting that UDT and LDT2 show generally higher RHOB values than the rest of the Danian samples.

Among all the possible correlations, the only positive one (r = 0.45) is between Na and SNP for the Maastrichtian samples.

As an example, grouping of data is observed for Na vs. DT (Fig. 32) where the Danian data are split into 2 groups with perhaps further subdivision into two subgroups, the one with the lowest DT clearly being confined to the oldest Danian. A similar tendency is observed for Na vs. RHOB (not plotted).

Correlation analysis of Fe contents vs. log depth for drill hole E-Ix data shows that only the combinations with the SN and the IL log give positive correlation coefficients above 0.4 for the Danian. When plotting the data (not shown in Fig. 32) for these two combinations, however, it is obvious that the correlation is an artefact because Fe content varies only little.

Correlation data of Mn vs. log parameters suggest that there is no significant correlation for the Danian samples while the few data for RHOB, SP, SN, IL, LL, MINV, and MNOR all give correlation coefficients with Mn that exceed 0.8.

The selected plots of data (e.g. DT vs. Mn and RHOB vs. Mn, Fig. 32) show the normal trend, namely grouping of data.

4.2.5 Multivariate Statistical Analysis

The results of R-mode factor analysis of analytical data for drill core samples from well E-Ix are plotted in Fig. 33.

Although only a limited data set is used, it appears that the geochemical drill core data separate the different reservoir rock units and also that the Maastrichtian strata are clearly separated using geochemical data alone. In addition, the thin oil-bearing zone on top of the Danian (unit UDPI) may also be separated through factor analysis of geochemical data.

Fig. 33. Factor score plot of factors 1 and 2 for R-mode factor analysis of data from E-Ix.

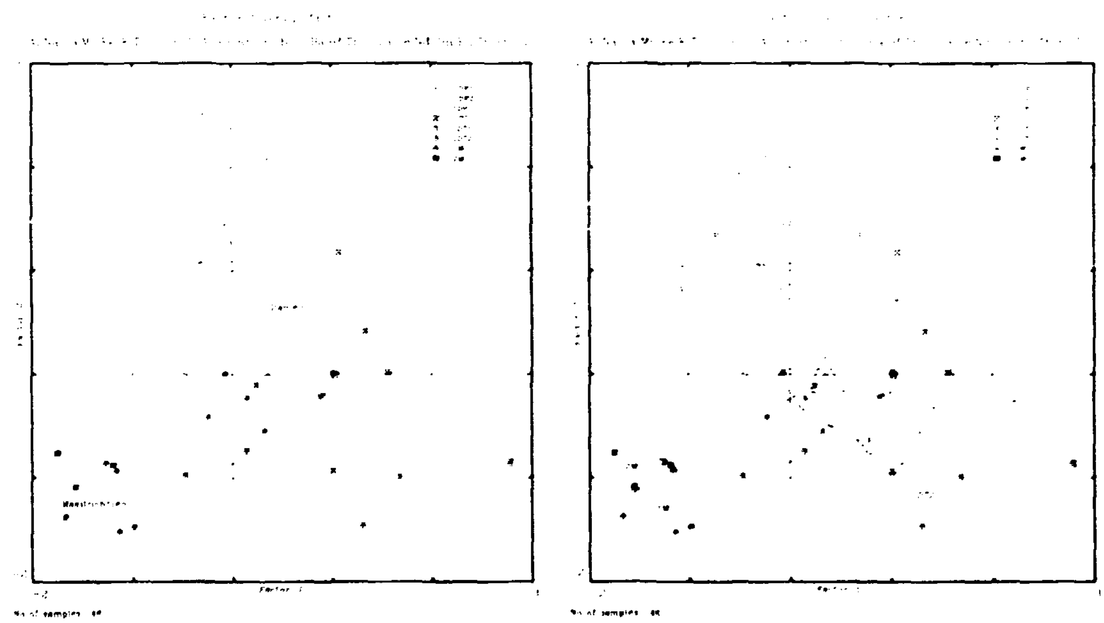

5. Discussions

5.1 General Considerations

General discussions of the data used in the present investigation should comment on their validity and quality before they are used for final interpretational purposes.

The geochemical data were generated from drill cores influenced by chemical and physical processes produced by the drilling operations; these operations were followed by geophysical sensing (well logging) in which measurements are made on rock formations influenced by the drilling.

5.1.1 Well Logging Considerations

In the evaluation of oil and gas reservoirs, a number of well-logging techniques are used which are important to be observed. It is not possible, however, to discuss these techniques in more detail within the framework of the present investigation. Only some pertinent observations are presented in the following.

While porosity usually is determined by the sonic log, the formation density log or the neutron log, for estimates of water saturation and hydrocarbon saturation electrical logs are preferred (resistivity logs).

As mentioned above, in interpretating in well logging it is very important to consider the processes involved in the drilling operations. Drilling is carried out using drilling fluids leading to the establishment of distinct influence zones around the drill hole (Fig. 34). All the logging results have to consider some sort of influence spacing within and around the drill hole, into

1. Mud cake with h_{mc} thickness
2. Flushed zone
3. Transition zone
4. Undisturbed zone.

Fig. 34. Schematic drill hole representation showing three major zones of influence by the drilling operations.

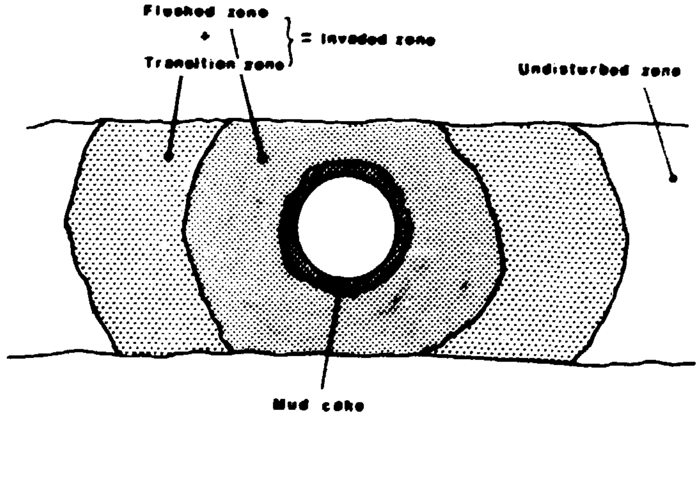

Generally, the mud cake zone with a thickness often varying between . and about 20 mm has a moderate resistivity, while the flushed zone contains both mud and oil or gas (if present). In the transition zone, both mud and formation fluids may be present grading into the undisturbed zone which also has, e.g., the true resistivity. It is often the case that formations with high porosities have the lowest invasion depths; mud filtrate, during its penetration into the formation, in unfavourable cases may seal the formation. General figures for an inversion depth (mud cake thickness + flushed zone thickness + transition zone thickness) are less than 1' in formations with high porosity, while for low-porosity formations these depths may increase to up to 10'.

There are some basic equations connected with the different well logging tools; these are not discussed here, however.

A number of standard log interpretational methods are known leading to the determination of the important parameters porosity (Ø), water saturation (S_w), and permeability (k_a). Interpretational methods including standard and cross plot techniques have been described in some detail by Helander (1983) and need not be repeated here. Of some importance in this respect, however, are so-called »quick-look« methods combining a number of logs to determine the important parameters.

5.1.2 Drill Core Investigations

Other important information about the hydrocarbon reservoir is generally gained by the investigation of drill cores. However, as coring is much more expensive than plain drilling, only a few wells are cored throughout.

There are some problems connected with the collection and evaluation of measurements on drill cores. These have to be considered when discussing analyses of drill cores. Processes that influence the core material are:

1. Ahead-flushing of rocks by drilling fluids,
2. Pressure alterations of the core, and
3. Temperature alterations of the core.

Flushing generally reduces the hydrocarbon content in the core at the same time increasing its water content. Flushing influence is less pronounced, however, in the drill cores because the core usually is removed immediately after it has been cut and protected largely by the coring rods. Pressure and temperature influences may alter values of core porosity, permeability and resistivities in that they often alter the primary structures within the rock by subsequent stress variations in the core. There is little alteration of the geochemistry of the core, but samples for chemical analyses should always be taken within the core and not from its marginal regions because of possible surface contamination by drilling mud.

As regards core analysis, whole-cores, plugs or sidewall cores may be used. Determinations on cores result in data on core porosity, permeability, and residual fluid saturation; these, however, need the removal of residual fluids in the core samples mainly by solvent extraction.

The most important core measurements are those of porosity which include estimates of bulk volume, pore volume, and grain volume. Permeability in terms of vertical and horizontal values may be determined based on the use of liquid or air flows. A number of other measurements are usually carried out on cores.

5.2 The Well-Logging Results

As already mentioned, the petrophysical parameters porosity, water saturation, and permeability of the reservoir are usually estimated from the geophysical measurements, i.e. from well logging.

The logging data from both wells alone could be used to evaluate some parameters closely related to chemical properties of the reservoir rocks. There is some problem in comparing the data because logging of the wells was established with different tools at different times and comparison is therefore difficult. However, if we choose some of the physical tools that are comparable, e.g., all the electrical tools, the radioactivity measurements and the sonic results, comparison by multivariate statistics (R-mode factor analysis) including data on both wells may be carried out. Average data are given in Table 11.

Results of this comparison by using all available data (those ascribed to core-sampling depths) for Danian and Maastrichtian units are plotted in Fig. 35.

It appears from the figure that at least for drill hole TWB-8 (left side of Fig. 35) the data is separated according to geology and also to hydrocarbon occurrences but this separation is not evident at drill hole E-1x. Also, the reduction in reservoir quality as seen in units UDT and upper part of LDP (well TWB-8) is, although separated, not clearly displayed through the figure.

Table 11. Average well-logging data for drill holes TWB-8 and E-1x.

Formation	SFLA/ MNOR	GR	ILD/ IL	DT	RHOB	NPHI/ SNP	SP
UDP1 (TWB-8)	7.8	7.1	26.0*	146	1.75	0.29	236
UDP1 (E-1x)	1.3	12.6	1.1	107	2.13	0.33	11
UDP2 (TWB-8)	4.4	6.9	21.0	127	1.79	0.30	221
UDP2 (E-1x)	0.8	11.7	0.7	108	2.08	0.38	4
LDP (TWB-8)	2.5	7.9	8.0	118	1.93	0.30	200
LDP (E-1x)	1.1	11.5	0.9	103	2.12	0.35	10
UDT (TWB-8)	2.1	9.0	6.0	101	2.17	0.27	199
UDT (E-1x)	2.2	12.8	2.2	83	2.30	0.25	22
LDT1 (TWB-8)	2.5	8.3	9.0	118	1.99	0.28	200
LDT1 (E-1x)	1.7	11.4	1.4	92	2.21	0.31	15
LDT2 (TWB-8)	4.5	8.5	20.0	115	1.99	0.28	222
LDT2 (E-1x)	1.8	12.4	1.5	93	2.25	0.27	20
1M (TWB-8)	5.0	8.4	14.0	132	1.95	0.24	235
1M (E-1x)	2.0	11.1	1.6	87	2.30	0.27	12
2M (TWB-8)	3.9	8.2	27.0*	139	1.83	0.33	223
2M (E-1x)	1.3	10.5	1.0	93	2.17	0.32	7

* one value ILD = 2000 (error ?) excluded in average calculations

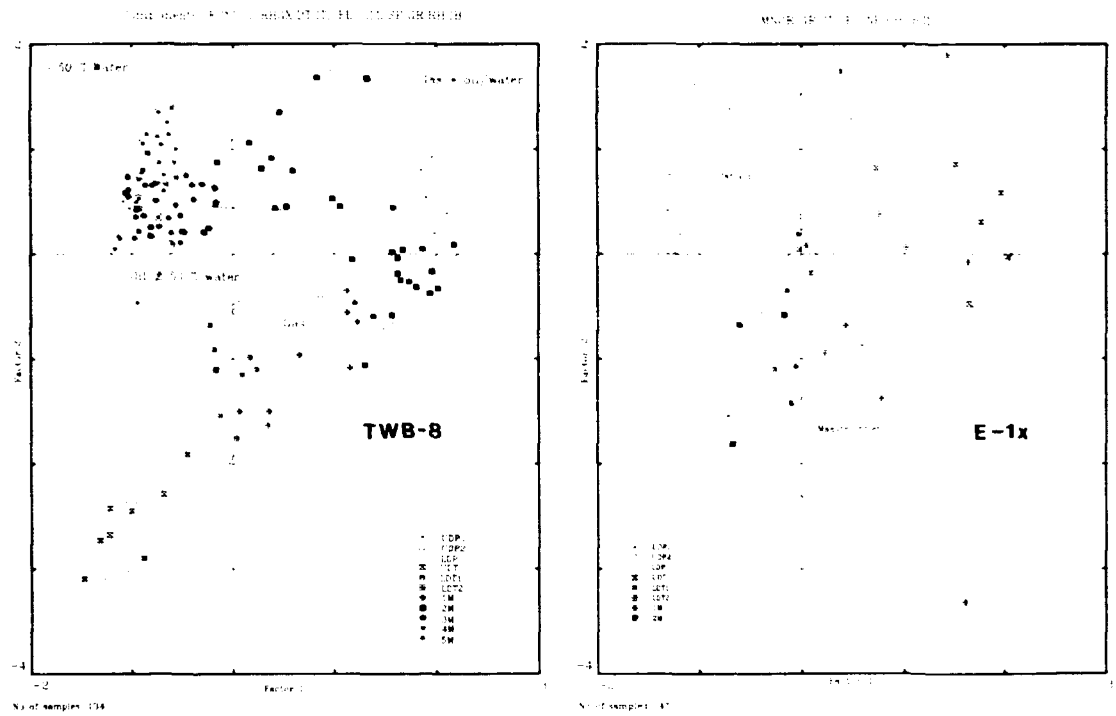

Fig. 35. R-mode factor analysis of logging data from TWB-8 and E-lx.

It appears from the figure that at least for drill hole TWB-8 (left side of Fig. 35) the data is separated according to geology and also to hydrocarbon occurrences but this separation is not evident at drill hole E-lx. Also, the reduction in reservoir quality as seen in units UDT and upper part of LDP (well TWB-8) is, although separated, not clearly displayed through the figure.

5.3 The Geochemistry

The geochemical databases for drill core sections of the two Tyra wells differ because they were constructed from analyses using various analytical strategies. Because a relatively large number of both major and trace elements in the carbonate rocks were determined, these data are sufficient to describe geochemically the different geological units involved.

From the average analytical data of the different rock units for both drill cores, characterization plots can be constructed showing the differing reservoir unit geochemistry (Fig. 36). The average data matrix for TWB-8 (Table 12) was built up from the the additional data (see chapter 4.1.2.3), which unfortunately lacks the analysis for unit LDT2.

Table 12. Average analytical data for drill cores TWB-8 and E-lx.

Formation	Na	Ca	Fe	Sc	Cr	Co	Br	Sr	Cs	Ba	Hf	Th	La	Ce	Sm	Eu	Yb
UDP1 (TWB-8)	0.10	32.4	2170	1.1	6.0	1.7	8.3	983	0.1	171	0.11	0.5	8.8	6.6	1.9	0.34	0.7
UDP1 (E-1x)	0.28	33.4	5375	2.2	6.6	3.3	34.5	1425	0.2	294	0.20	0.8	11.5	17.8	2.5	0.50	1.1
UDP2 (TWB-8)	0.09	33.6	936	1.2	5.7	1.7	8.2	987	0.1	142	0.10	0.4	10.6	8.4	2.4	0.42	0.7
UDP2 (E-1x)	0.21	34.6	2440	2.0	5.5	2.7	30.9	1492	0.2	143	0.14	0.6	11.2	15.1	2.6	0.50	1.1
LPP (TWB-8)	0.11	32.9	1667	1.9	6.5	3.3	9.9	1042	0.2	158	0.17	0.9	15.0	13.5	3.8	0.64	1.0
LDP (E-1x)	0.18	31.2	2309	2.3	4.7	6.0	36.0	1295	0.2	182	0.18	1.2	12.4	18.6	3.6	0.62	1.1
UDT (TWB-8)	0.10	29.6	3260	2.8	8.5	15.7	8.5	1110	0.3	2120	0.27	1.6	15.4	18.4	3.6	0.64	1.2
UDT (E-1x)	0.20	27.6	4633	3.8	6.1	10.4	16.3	1265	0.2	249	0.28	2.3	16.3	30.1	5.0	0.82	1.5
LDT1 (TWB-8)	0.16	27.9	4230	3.1	8.4	8.0	12.1	1021	0.3	654	0.31	1.9	19.0	23.2	5.0	0.82	1.2
LDT1 (E-1x)	0.21	29.7	3800	3.0	11.1	12.3	22.8	1496	0.2	167	0.24	1.8	17.1	26.6	4.9	0.84	1.5
LDT2 (TWB-8)	0.00	0.0	0	0.0	0.0	0.0	0.0	0	0.0	0	0.00	0.0	0.0	0.0	0.0	0.00	0.0
LDT2 (E-1x)	0.18	28.7	3757	3.0	11.7	9.9	17.8	1664	0.2	172	0.24	2.0	16.1	28.3	4.6	0.84	1.4
1M (TWB-8)	0.13	20.2	3000	1.9	7.0	3.5	8.1	891	0.1	1370	0.18	1.1	13.3	14.9	3.7	0.55	0.9
1M (E-1x)	0.11	38.5	850	1.5	9.7	1.5	15.7	1673	0.1	90	0.10	0.3	9.0	9.7	2.4	0.38	1.0
2M (TWB-8)	0.16	35.6	785	0.7	3.9	2.9	18.6	1202	0.1	187	0.06	0.2	7.7	5.2	1.7	0.27	0.5
2M (E-1x)	0.14	38.6	700	0.8	9.9	1.6	23.5	1813	0.1	104	0.10	0.2	7.5	7.0	1.9	0.30	0.8

For the average chemical data, there is a relatively clear grouping in Fig. 36 showing that chemical data of comparable reservoir units from the two wells often plot close to each other. For instance, in the Mn-Al-Ca plot, data from TWB-8 (large symbols) plot close to data from E-lx (small symbols). This indicates that the rocks from both drill cores are similar geochemically and that variation generally occurs between the reservoir units. To illustrate the latter observation, we note that the position of the points UDT is quite different than, e.g., that for 2M.

On the other hand, knowing that there is core porosity reduction in unit UDT in the respective core section of TWB-8 (reduction from 40 to less than 20%) but not as clearly developed in core E-lx, the plots in Fig. 36, therefore, give no strong indication of reservoir quality reduction. As a consequence, the reservoir quality variations must be sought merely in the chemical diagenetic changes usually not expressed through the bulk chemistry.

The average data for the two wells (logging and geochemical results) may be combined into a final multivariate statistical analysis to evaluate possible trends within the Tyra structure. The results of R-mode factor analysis are shown in Fig. 37.

The data in Fig. 37 (right plots) show a separation of drill holes. Perhaps subgrouping is also seen showing decreased reservoir quality (mainly units UDT and LDT1).

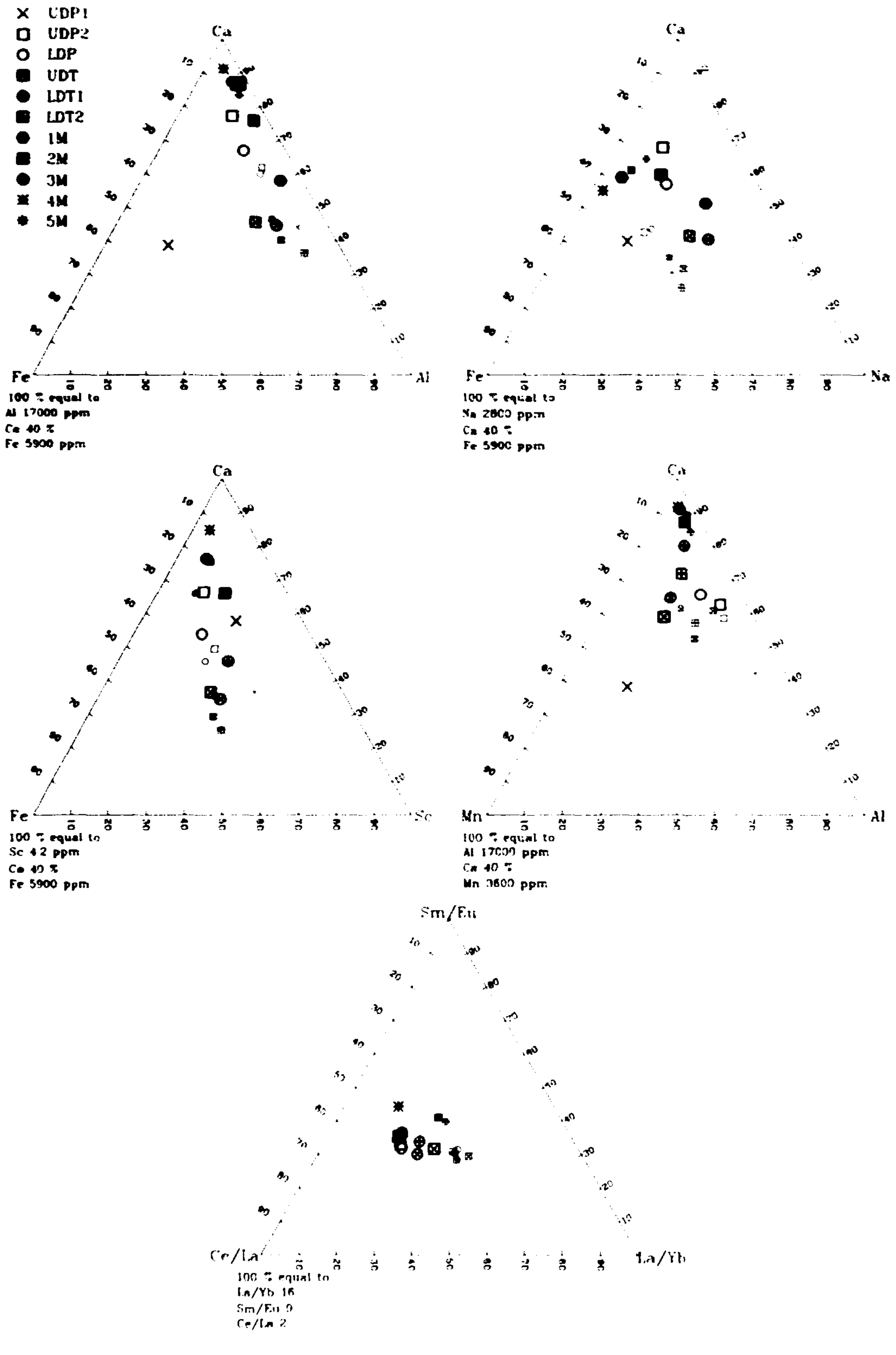

Fig. 36. Selected characterization plots for drill cores TWB-8 and E-1x.

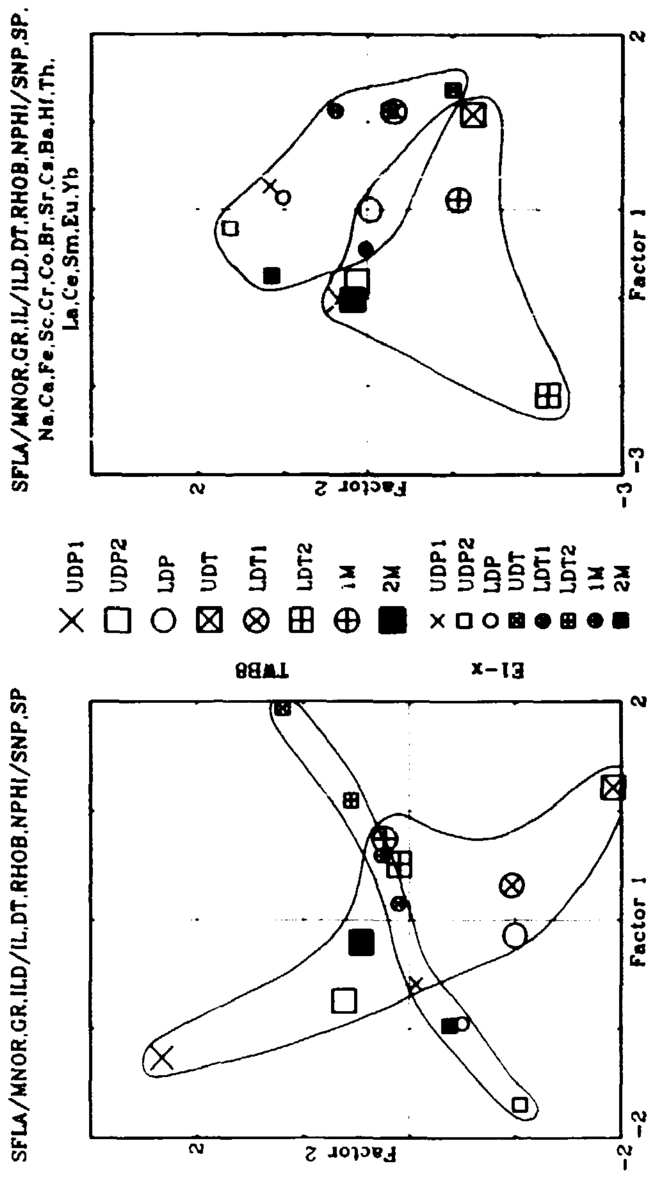

Fig. 37. Average data for chalk units combined in R-mode factor analysis. Left: logging data alone, right: all data.

5.4 Considerations for the Tyra Field Reservoir Quality

5.4.1 General Considerations

Reservoir quality measures are tightly coupled to the processes applied to sedimentary basin evolution. For chalk, diagenetic considerations have been discussed in greater detail by, e.g., *Sippel and Glover*, 1964, *Neugebauer*, 1973; 1974, *Håkansson* et al., 1974, *Mapstone*, 1975, *Scholle*, 1977, and *Hardman*, 1982, and some of the features of chalk diagenesis have been discussed in general terms in chapter 1.

Of these, the comprehended work of *Scholle* (1977) may provide a good background to discuss the chemical data generated during the present investigation. He mentions that chalk diagenesis may be divided into early diagenesis and burial diagenesis.

The early stages of diagenesis consist of relatively simple processes in which dewatering of the calcareous sediment through compactional features is mainly dominant. In reality however, early processes may be much more complex involving chemical graduation of the calcareous shells as well; the most important of these processes is the enforcement of shell structures leading to an improvement in rigidity of the sediment. Common features generated during early diagenesis are carbonate cements and replacement glauconites and phosphates. A distinct product of near-surface cementation are hardgrounds (connected with erosional surfaces) having considerably reduced porosities (O < 20%) and occurring within otherwise porous chalks with porosities exceeding 30%.

A significant feature of chalk is its low initial permeability. This prevents the penetration of meteoric water into chalk. As a result, meteoric water can migrate only along bedding planes or created chalk surfaces such as undulating surfaces. According to *Scholle* (1977), the only way to alter porosity in chalks is by burial. This view, however, is oversimplified and does not explain local porosity variations within chalk reservoirs. As a consequence, *Scholle* (1977) suggests pressure solution processes that progress with depth, the solutions being preferably transferred via thin clay seams. Such processes lead to carbonate cementation, i.e. porosity deterioration. That these processes were active in chalk is confirmed by the occurrence of solution seams visible on a macro scale, predominantly connected with chalk layers showing increased clay content.

Most of the previously reported geochemical work on chalk is based on stable isotopes and includes only a few major and minor elements. Generally the work is based on relatively few chemical analyses despite generally large size of the sedimentary basins on which conclusions were made. A siginificant observation is δO18 values decrease with depth in chalk, i.e. with porosity. For North Sea chalk it is reported that the deepest chalks have the highest Sr and Mg but most chalk samples from the Deep Sea Drilling Project showed a decrease of Sr with depth of burial.

For the hydrocarbon deposits of the North Sea, where the reservoirs are located at depths of 2 to 3 thousand meters, chalk porosities are often above 30%, although burial diagenesis predicts lower values. *Scholle* (1977) reports porosities for oil-producing Danian and Maastrichtian chalks to be on average between 20 and 30%, but locally significantly higher values are observed. Permeability is very rarely higher than 3 mD. These contradictory features (e.g. high porosity at large burial depth) are at present explained by overpressurizing, both in the sealing rocks (Tertiary shales) and in the reservoir chalks themselves. However, there is also some evidence that oil migration into the chalks occurred during relatively early burial stages, thereby preventing porosity deterioration at later burial.

Basin evolution studies were recently also applied to sandstone diagenesis and porosity modifications by *Bjørlykke* et al. (1989). It is worthwhile to review their findings briefly because, in general, they apply also to carbonate rocks.

Referring to earlier geochemical and isotopic investigations on circulating water in the reservoirs, the authors point to the importance of water stratification merely than to upward flow; meteoric water is thought to penetrate the reservoir on a horizontal more than a vertical scale. Flow rates of meteoric water are estimated to be higher than compactional water flow and therefore the reservoir is generally more heavily influenced by meteoric water. Mixing processes (meteoric/seawater) especially lead to enhanced corrosion of carbonate minerals.

- Carbonate cement development in siliclastic sedimentary rocks has been studied by stable isotopes. Accordingly, early carbonate cements in sandstone reservoirs were found to have $\delta^{13}C$ values close to zero but cements that precipitate under the influence of meteoric water (early diagenesis) are characterized by negative $\delta^{13}C$ values.
- Silica cements in these rocks, on the other hand, are generally confined to the deeper burial stages (pressure solutions, stylolitization). Another possibility for silica diagenesis is probably convective pore water flow but few investigations exist on this topic.
- Clay minerals may be converted into other species during burial. The authors suggest that clay diagenesis may continue after hydrocarbon emplacement.

Bjørlykke et al. (1989) also discuss secondary porosity and its change with depth of burial in a sedimentary basin, in general. Porosity alteration is *thought to be obtained by slightly acid pore fluids and such processes are best* described under the heading chemical diagenesis. Important in this respect is the generally valid observation that porosity in siliclastic sedimentary rocks decreases with depth of burial. At the same time, as the temperature increases chemical processes are also enhanced with depth of burial. After burial and during the course of subsiding, sediment porosity is altered by mainly three processes:

- mechanical compaction: fragile mineral grains due to pressure may be re-orientated or destructed leading to reduced porosity;
- chemical compaction: mineral grain dissolution at grain contacts are usually dominant at burial depths exceeding 2 km (pressure solutions);
- cementation: precipitation of authigenic minerals principally related to chemical compaction;

Regarding carbonate cements, oxygen isotope measurements of samples from arkosic sandstones show that the earliest carbonate cement is a dolomite usually forming at temperatures of 30 to 40° C (*Boles and Ramseyer*), while calcite cement formation is observed at 50-60 and also at 70-80° C, the latter is caused mainly by plagioclase replacement. Also, a (Fe + Mn)/Mg ratio of ca. 3 is characteristic for the calcite cements; most importantly, Mn is very high in nonmarine sections with calcites. Porosity enhancement in the reservoir is obtained by the dissolution of plagioclase leading to Al enrichment. In general, these authors point to the importance of cement growth in single reservoirs.

5.4.2 Tyra Field Reservoir Quality and Chemistry

Based on the geophysical and geochemical results of the present study, a number of observations can be deduced. These observations explain in part why there are local reservoir quality variations and also why the reservoir quality in the marginal parts of the structure are generally poorer, although the results from no more than two drill holes are not ideally suited for making general evaluations on the structure.

For comparison, the petrophysical parameters porosity (POR), bulk density (RHOB), permeability (PERM) and neutron porosity (NPHI) are plotted in Fig. 40.

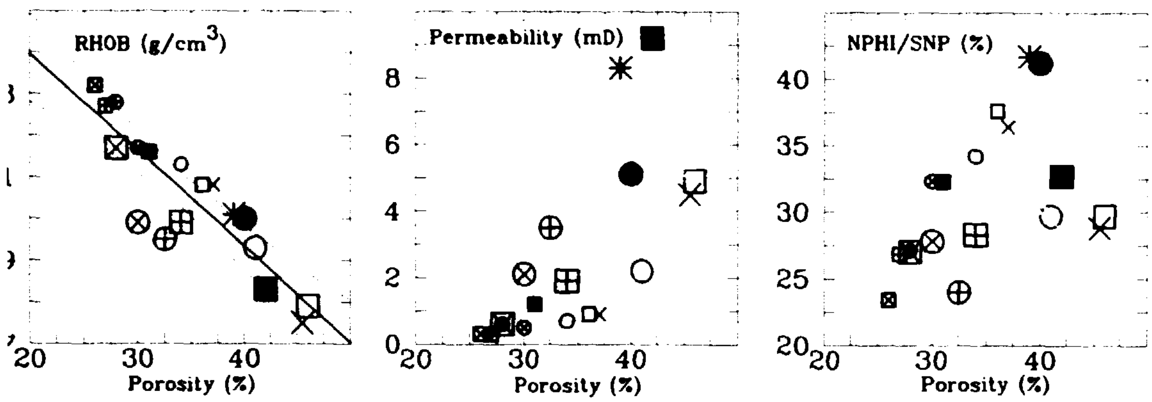

Fig. 38. Average petrophysical parameters plotted against each other. (For symbols see Fig. 37)

5.4.2.1 The Bulk Chemistry

The bulk chemistry of chalk from the central part of the Tyra structure (TWB-8) has already been shown through the multivariate statistical attempts (see Chapter 5.3) to differ only slightly from the easternmost margin (E-lx). There is therefore only a weak indication through the bulk chemical data that chemistry is producing large-scale reservoir quality variations. A systematic chemical analysis of Tyra reservoir chalk samples including such a large number of major, minor, and trace elements is however new and has no counterpart in the recent literature. Therefore, chemical variations with depth and on a regional scale (central to marginal parts of a chalk structure) are at present unique findings.

Fig. 39. Average Ca content plotted vs. porosity.

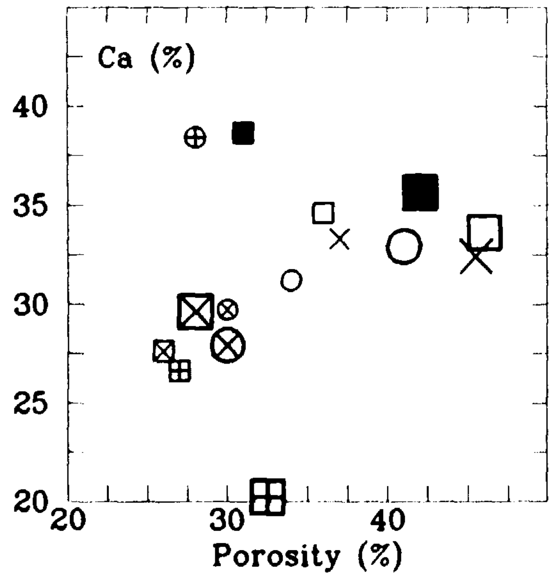

5.4.2.1.1 Major Elements

By systematic evaluation of the chemical data it becomes clear that there are some chemical graduations of the reservoir chalk. For chalk composed of more than 80% of calcitic material only one major element has to be considered, namely Ca. Two observations are apparent through our data. Firstly, there is a significantly lower Ca content in the middle part of the of the central Danian TWB-8 section (reservoir units UDT and LDT1). This is unobserved in E-1x lying in the marginal part. Secondly, Ca contents in general are higher in the Maastrichtian strata. The Ca reduction in the middle part of the Danian TWB-8 section is closely related to Si and this is discussed in the section on Si diagenesis.

Although there are some outliers, it is apparent in the plot of average porosity values against Ca (Fig. 39) that porosity in the Tyra rocks generally increases with increasing Ca content, i.e. all high-porosity reservoir rocks of TWB-8 have high Ca content. In contrast, E-1x reservoir units are characterized by significantly lower Ca.

5.4.2.1.2 Minor Elements

Of the minor elements, Al contents are generally lower in Maastrichtian drill core material from both wells. Such graduations must be ascribed mainly to occurrences of clay minerals, although bulk Al contents still are low, on average below 1000 ppm. As a unique feature of TWB-8, Ca reduction goes along with an increase of Al (and other elements) at the Danian section, leading to an Al content of more than 8000 ppm in the lowest sample of section UDT. Such increases in Al in carbonate rocks are usually interpreted as clay supply during quieter depositional stages.

The plot of average Al vs. prorosity (Fig. 40) shows no clear trend and therefore clay is regarded to be of minor importance in porosity reduction in the Tyra chalks.

Fig. 40. Average Al and Fe contents plotted vs. porosity.

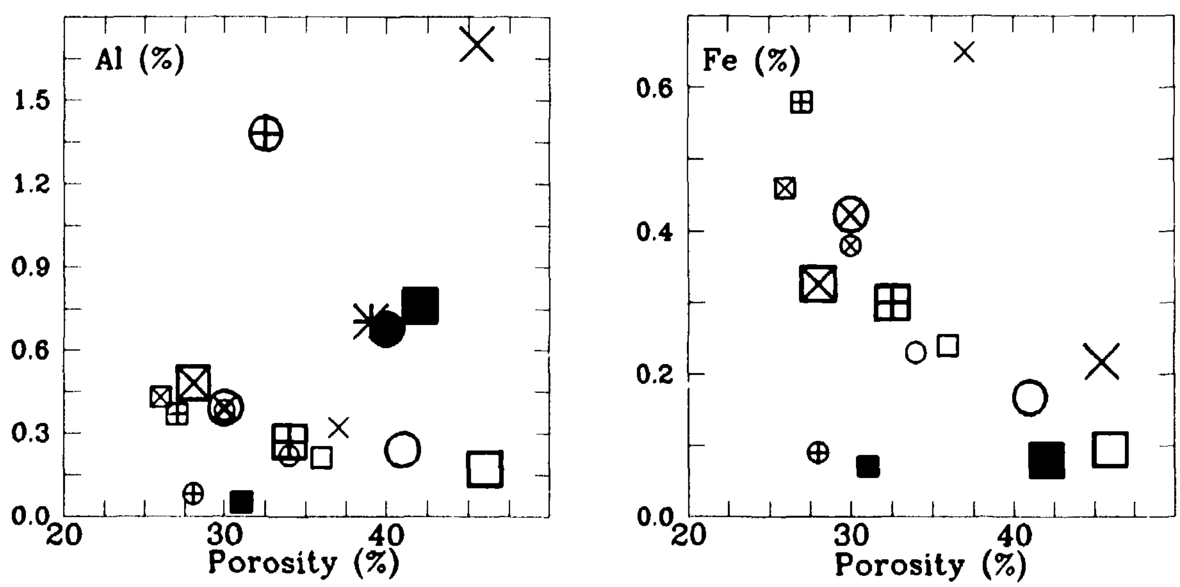

Sodium contents in the chalks can be interpreted as an expression of the presence of marine waters in the pore spaces; they precipitate in the form of NaCl after the samples are dried. Although it is very difficult to interpret Na on a more regional scale, the general observation is that due to the presence of hydrocarbons, sodium content is significantly lower (about 1000 ppm) in the respective TWB-8 section when compared to the hydrocarbon-free E-lx section (about 2000 ppm). Because Na significantly decreases above the OWC for TWB-8, the distribution with depth (see Fig. 7) clearly marks both the oil-water contact (OWC) and the gas-oil contact (GOC) (further reduction in Na to a plateau value).

Strontium is the minor element that has been studied most intensively in carbonate rocks. The reasons for this are primarily its geochemical affinity to Ca and its occurrence, usually at the 1000 ppm level in ancient carbonate rocks, thereby being more readily determined. During dissolution of Ca minerals or Ca mineral phases Sr may be fractionated, generally entering the solute phase and being transported to precipitation centers, even at large distances. The Sr distribution trends with depth for both wells are similar, the highest Sr content being found in the Maastrichtian rocks. There is therefore little evidence of reservoir quality changes by chemical processes involving Sr diagenesis.

Iron is an important minor element in carbonate rocks and found mainly when carbonate dissolution locally leads to pH reduction. In such cases, pyrite precipitation may occur in the course of carbonate diagenesis, as for example when the chalk of the Tyra field becomes evident because of macroscopically visible pyrite grains within otherwise homogeneous chalk occur and the Fe content in chalk samples increase (see Figs. 12 and 26). Comparing average Fe data with porosity values for the two wells (Fig. 40), it becomes obvious that reduced porosity goes along with elevated Fe contents.

Manganese and silicon are discussed separately.

5.4.2.1.3 Trace Elements

Of the trace elements, more than 20 different ones have been determined in the chalk samples. The trace element distributions with depth not only support some observations for major and minor elements, but they also add significantly to the general geochemical information on carbonate reservoir rocks. We have divided them into groups of trace elements with some geochemical similarity and discuss obvious features in their distribution with depth within the different groups.

<u>Sc, Br, Rb, Ba, and Hf.</u>
Scandium is usually confined to the clay fraction, and in this respect it should follow Al closely. When the depth distributions of the element for both drill cores are compared (Figs. 12 and Fig. 26), it becomes clear that the Sc distribution in core TWB-8 does indeed follow that of Al (Fig. 7). For this drill core also, there is an increase in Sc values from section LDT to 1M. It is important to mention that, as was the case for Al, scandium values are generally higher in drill core E-lx; we therefore also point out that there is more clay in the carbonate sections. The comparison of average Sc data with porosity values (Fig. 41) indicate that chalks from the Tyra structure with relatively low porosity all show Sc contents greater than 2 ppm.

Bromine is a standard trace element determined by INAA. It is closely related to chlorine in the carbonates, i.e. to the content of formation waters. It therefore also follows the distribution trend of Na already discussed, showing

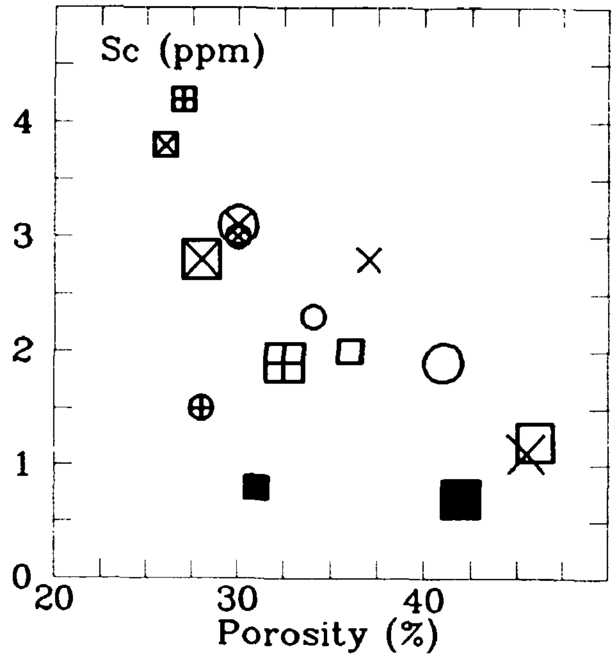

Fig. 41. Average Sc content plotted vs. porosity.

a general increase with depth in drill core TWB-8. While Br values in this core are usually at 10 ppm and exceed 20 ppm only in the Maastrichtian section, in drill core E-1x, Br values throughout are higher than 20 ppm with a slight tendency to decrease with depth. This behaviour is an indication of the absence of hydrocarbon in the marginal well E-1x.

The content of Rb, which often is associated with K thereby expressing the amount of feldspar in the rock samples, is very low, generally at or below 10 ppm. It is therefore not an important trace element in the Tyra carbonate rocks.

Barium content is important when studying drill core sections from the Tyra gas field. Firstly, Ba is often connected with marine phases (baryte, phosphates). Secondly, high Ba contents in core samples from hydrocarbon exploration wells are usually identified with the contamination of core samples by drilling fluids which often contain additives in the form of baryte. After comparing all the available data, we find perhaps a slight Ba contamination in two additional samples from drill core TWB-8 (Fig. 12) but the Ba values are generally low and at an expected level.

Hafnium which geochemically is closely related to Zr can be taken as an expression of the residual (clay) fraction in chalk. The element often follows Sc, and similar trends are therefore also valid for Hf.

<u>Cr, Co, Zn, As, and Sb</u>

Of these five trace metals, Cr is expected to be entirely connected with the residual fraction in the chalks. If there were heavy mineral horizons in the carbonates they would evident, among others, through high Cr contents. However, Cr values in general are very low (< 10 ppm), and even the high-Al section of TWB-8 is found to be only 10 ppm. Comparing the depth distribution of Cr in E-1x, there is a significant increase in Cr in samples below chalk unit UDT (jump from 5 to 10 ppm Cr, Fig. 26).

Cobalt - which in the marine environment may be connected with both a biogenic phase or phases directly precipitated from seawater - is often connected with Fe. Therefore, the depth distribution for Co in both investigated drill cores closely follows that of Fe. The same tendency is seen for zinc, but because of the generally very low Zn content, other analytical tools probably have to be applied to determine it.

Arsenic and antimony are of little importance in carbonate sediments. They are geochemically connected with hydrothermal processes and because of the very low content in the chalk samples such influences are regarded as hypothetical.

Radioactive elements

Of the radioactive elements, uranium is often involved in diagenetic changes in sedimentary rocks, while thorium is generally connected with the residual phases. It is quite clear from Figs. 7, 13 and 27 that the Danian strata of both drill cores have the lowest U content, usually not exceeding 0.2 ppm. Uranium content is higher in the uppermost Maastrichtian chalks; values being generally above 0.5 ppm U are found in samples from both drill cores. In this respect, the U distribution with depth clearly defines the transition of Maastrichtian to Danian strata. In contrast to U, thorium normally connected with the residual phase shows a similar distribution patterns with depth as, e.g., Al.

The plot of average data for the two wells vs. porosity (Fig. 42) shows that at reduced porosity Th values are elevated, while there is no linear dependency between U and porosity.

Fig. 42. Average U and Th contents plotted vs. porosity.

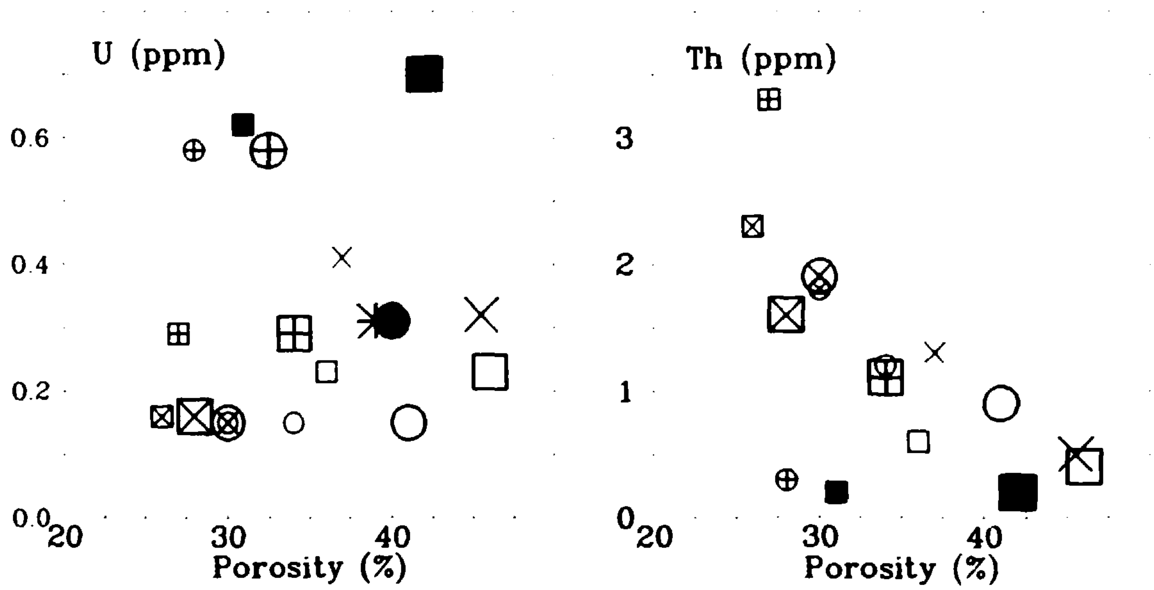

Rare earth elements

On comparing the REE distributions of the two drill cores with depth, no clear change in content of REE with depth seems to be present. When the Ce/La ratios of the chalks of both wells are compared it appears, however, that Danian strata have generally higher ratios. On the other hand, on a regional basis (central to marginal part) there is no graduation between values for TWB-8 and E-1x.

If we take the Ce/La ratio as an expression for the depositional environment (fractionation of Ce in an oxidizing environment), it could be argued that deposition during Danian times took place in a more oxidized milieu (higher Ce/La ratios) compared with the Upper Maastrichtian. The ratio also suggests that the depositional environment at the end of the Cretaceous was altered.

According to *Jarvis* (1984) who investigated Late Cretaceous chalks from northern France, the REE in the chalks are mainly confined to carbonate fluorapatite and sometimes to iron phases. The highest REE contents are generally found in hardgrounds. The process favoured for REE accumulation from seawater is via settling of ferric hydroxide coatings and sinks. This would explain the similar depth distribution trends for Fe and the REE in the Tyra field samples.

5.4.2.2 Si Diagenesis

The sample descriptions for TWB-8 (Appendix I) document the presence of flint layers and hardened chalk horizons in chalk unit LDP grading into obviously silicified chalk (units LDT1 and LDT2) sections. This variation is expressed logically by the petrophysical parameters and by the variation of reservoir quality.

The diagenesis of silica in marine sediments has been described in general terms by *Calvert* (1974). Accordingly, most profiles of dissolved silicon in marine sediments show a concentration gradient towards the sediment-seawater interface suggesting a flux of dissolved silicon into the overlying water column. The reason for this is that biogeneous silica in marine sediments usually is not stable even at low temperatures. One consequence is the formation of chert and porcellanites in marine sediments. Most investigations suggest a relatively slow conversion process of biogeneous debris via some transitional products finally into quartz. Submarine hydrothermal activity may add to the silica supply mechanism on the ocean floor.

Early investigations by *Lovering and Patten* (1962) including simple experiments showed that cold neutral solutions supersaturated with silica were able to move over long distances in carbonate rocks. At contact with them they generate CO_2 or Na; silica would precipitate in turn.

It is also known that dissolved silica in surface sediments reacts with poorly crystalline Fe-Mn oxyhydroxides generating both the mineral todorokite and Fe-rich smectite. Such a process could also be invoked to explain the Si-enrichment which, in the Tyra reservoir rocks, often is coupled to Al and Fe.

After analysing selected samples from TWB-8 for Si, we founds especially high Si values in chalk sections UDT and LDT1 (Fig. 43). These Si values are 3 to 4 times higher than in the other hydrocarbon-bearing chalk units. They correlate closely with Al (Fig. 8) and Fe (Fig. 12) suggesting that dissolved silica was precipitated from silica-bearing solutions at clay horizons, thereby further reducing core porosity.

A similar pattern for Si is also observed in drill core E-1x (not plotted).

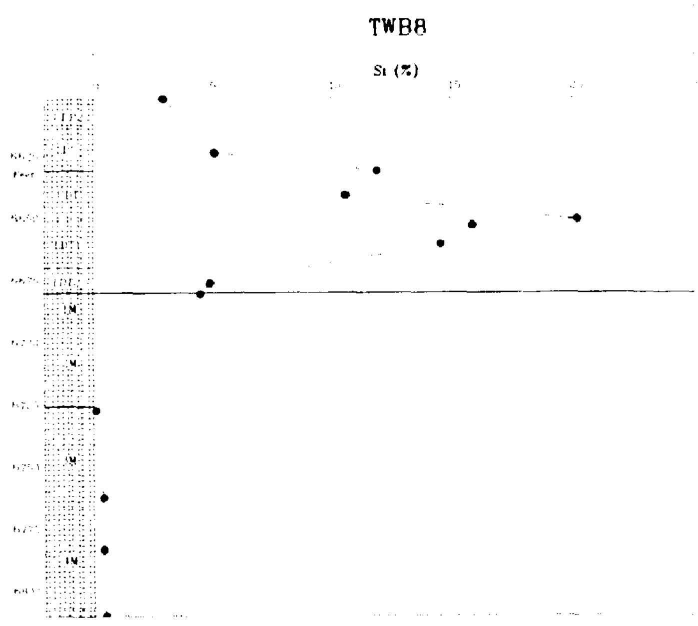

Fig. 43. Si distribution along drill core TWB-8 showing elevated contents in Danian strata.

Average Si data for the reservoir units of wells TWB-8 and E-lx are plotted vs. porosity and permeability in Fig. 44. It appears from the figure that most of the high-porosity reservoir units are characterized by Si contents below about 6% (about 13% SiO_2). If we exclude the E-lx Maastrichtian data, we deduce the following empirical equation:

$$\text{Porosity (\%)} = -1.35 \times \text{Si (weight \%)} + 44.2$$

i.e. a Si content of 1% in the Tyra chalk decreases porosity by a relative amount of about 3%.

While porosity and Si values consider the uppermost 2 reservoir units of E-lx as of good reservoir quality, permeability figures are significant lower than the comparable ones of TWB-8; generally, permeability values of E-lx are low, even at widely varying Si. This suggests that reservoir quality is influenced not only by the altitude of some geochemical indicators (e.g. Si, Al, Fe), but also by physical parameters (e.g. texture).

5.4.2.3 Mn Diagenesis

The most pronounced geochemical feature of the Tyra structure (and the Upper Cretaceous and Lower Paleocene chalk deposits in general) is the distribution of manganese. The distributions with depths in drill cores TWB-8 and E-lx are quite similar (Figs. 7 and 26) although the analytical results for both cores were obtained by two different analytical methods.

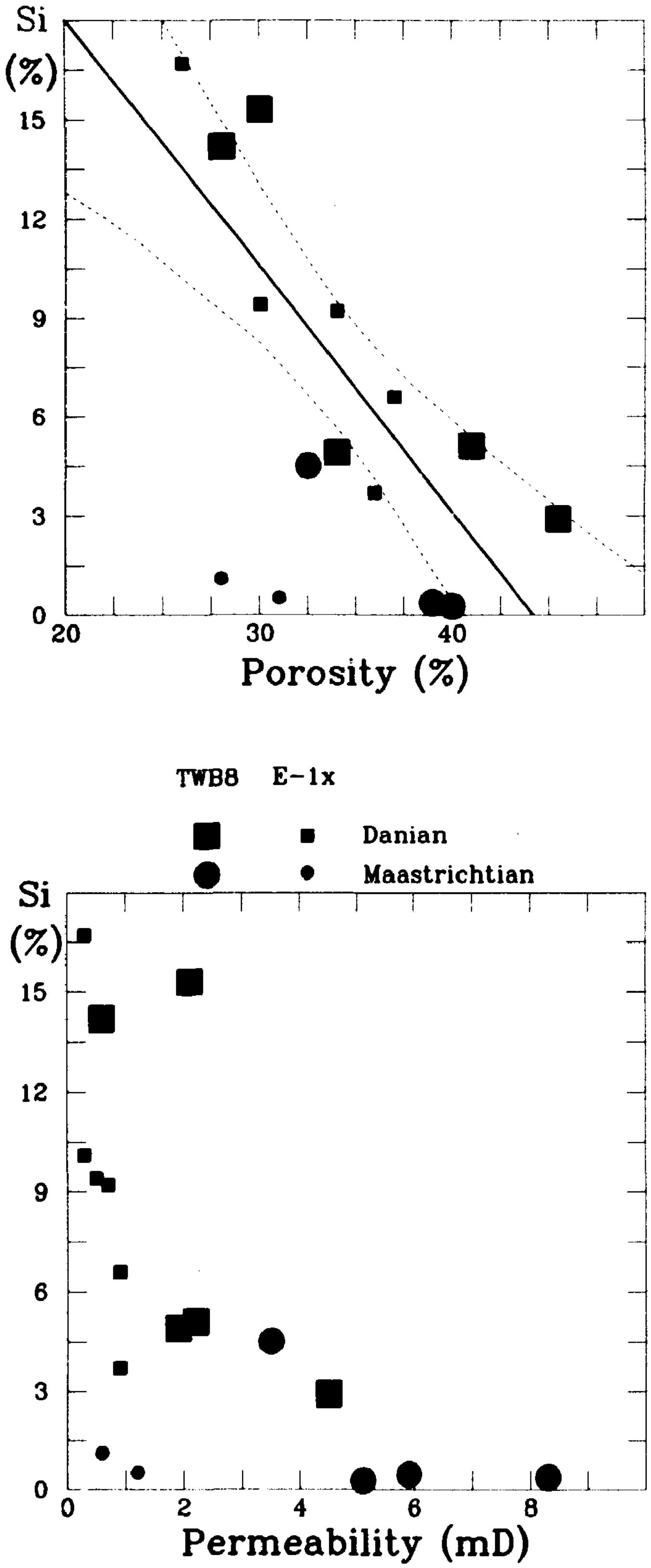

Fig. 44. Average Si data plotted vs. porosity and permeability.

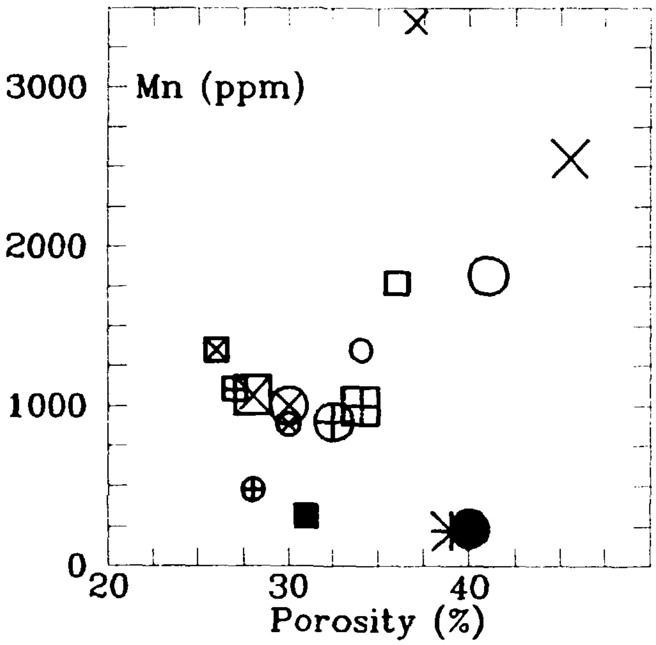

Fig. 45. Average Mn contents plotted vs. porosity.

A number of possible mechanisms explaining the Mn behaviour in the chalk samples has been discussed by *Kunzendorf* et al. (1985). However, as this behaviour is unique for Upper Cretaceous and Danian chalk, it is very likely that Mn occurrences in the chalk deposits are an important expression for the paleoenvironment. Because there is little correlation of Mn content with reservoir quality parameters, e.g. porosity (Fig. 45), Mn behaviour with depth is discussed only briefly within the present investigation.

Plots of detailed and smoothed data in Fig. 46 from drill core TWB-8 show the following trend:

- reservoir units 5M, 4M and 3M are characterized by relatively low Mn (< 200 ppm);
- from the lowermost portion of 2M onwards, Mn values increase linearly to about 400 ppm at the transition to 1M; there is no further Mn increase in 1M;
- Dania chalks all have higher Mn contents than the Maastrichtian strata;
- from the bottom of unit LDT2 there is an upwards increase of Mn contents (from about 600 to 750 ppm) until unit LDP;
- in unit LDP, Mn contents increase from about 750 to about 1500 ppm;
- There is a further linear upwards increase of Mn contents through the uppermost Danian chalks.

The upwards increase of Mn contents has also been found mainly in drilling muds and some drill core material from other wells (e.g., *Jørgensen*, 1986). Besides the possibility of paleoenvironmental influences, such features in general could also be an expression of hydrocarbon invasion and hence be important for the development and retention of reservoir pressure. Because the behaviour of Mn is unique for Danian-Maastrichtian strata of the entire Danish Subbasin, more detailed studies are required to explain, on a fine scale, the geochemical observation.

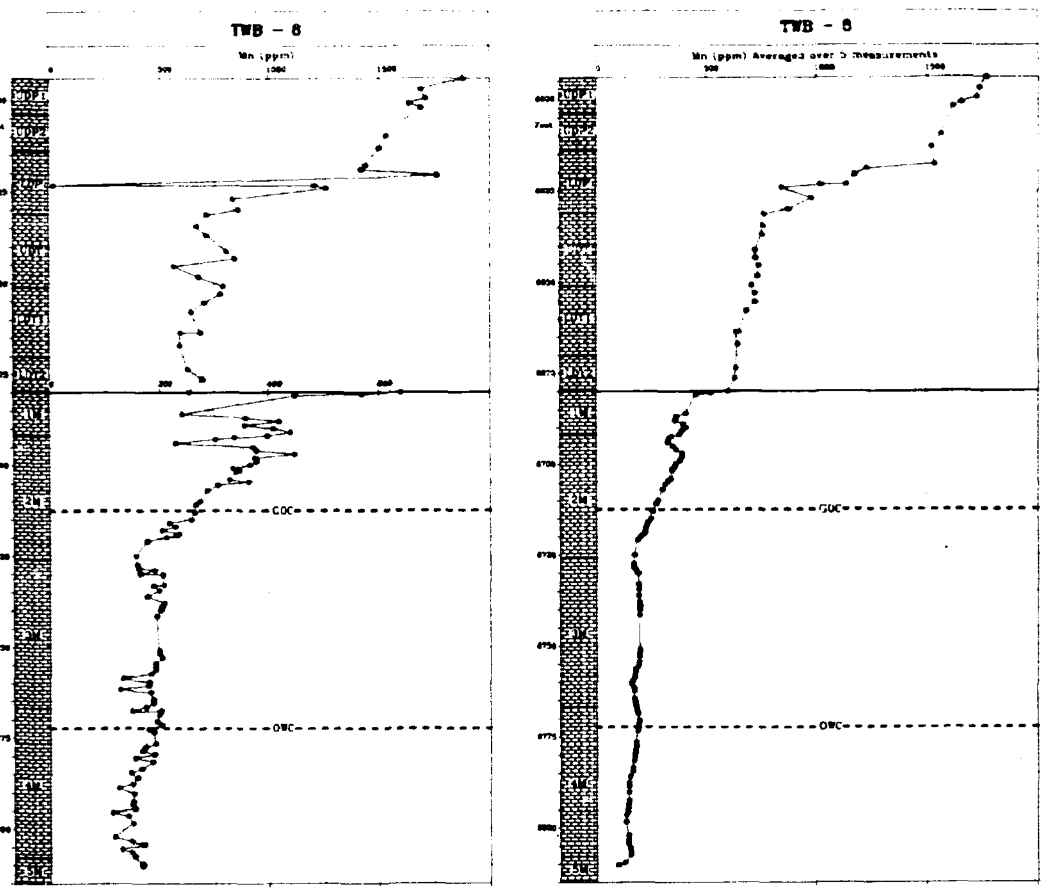

Fig. 46. Manganese distribution with depth in TWB-8. Left part of the figure shows raw data while the right part gives 5-point averages.

5.4.2.4 Regional Geochemical Interpolations

The geochemical data for both drill core may be used in geochemical contouring within the Tyra structure. The most appropriate software to use is the UNIRAS system. The chemical data for the two drill cores were used in the computer manipulations. Because of the relatively large extension between the two drill holes (about 7 km), such efforts are not very meaningful, especially in the absence of any limiting constraint. They are shown here, however, to draw attention to the possibilities of 3-D geochemical mapping.

By introducing fault lines such as, e.g., unit boundaries Top Danian 1, Top Maastrichtian 1 and Top Maastrichtian 2, Fig. 47 shows 2-D plots for elements Ca, Al, Na and Mn. Including another well between TWB-8 and E-1x in the investigations, interpolations of geochemical data sets would be more meaningful.

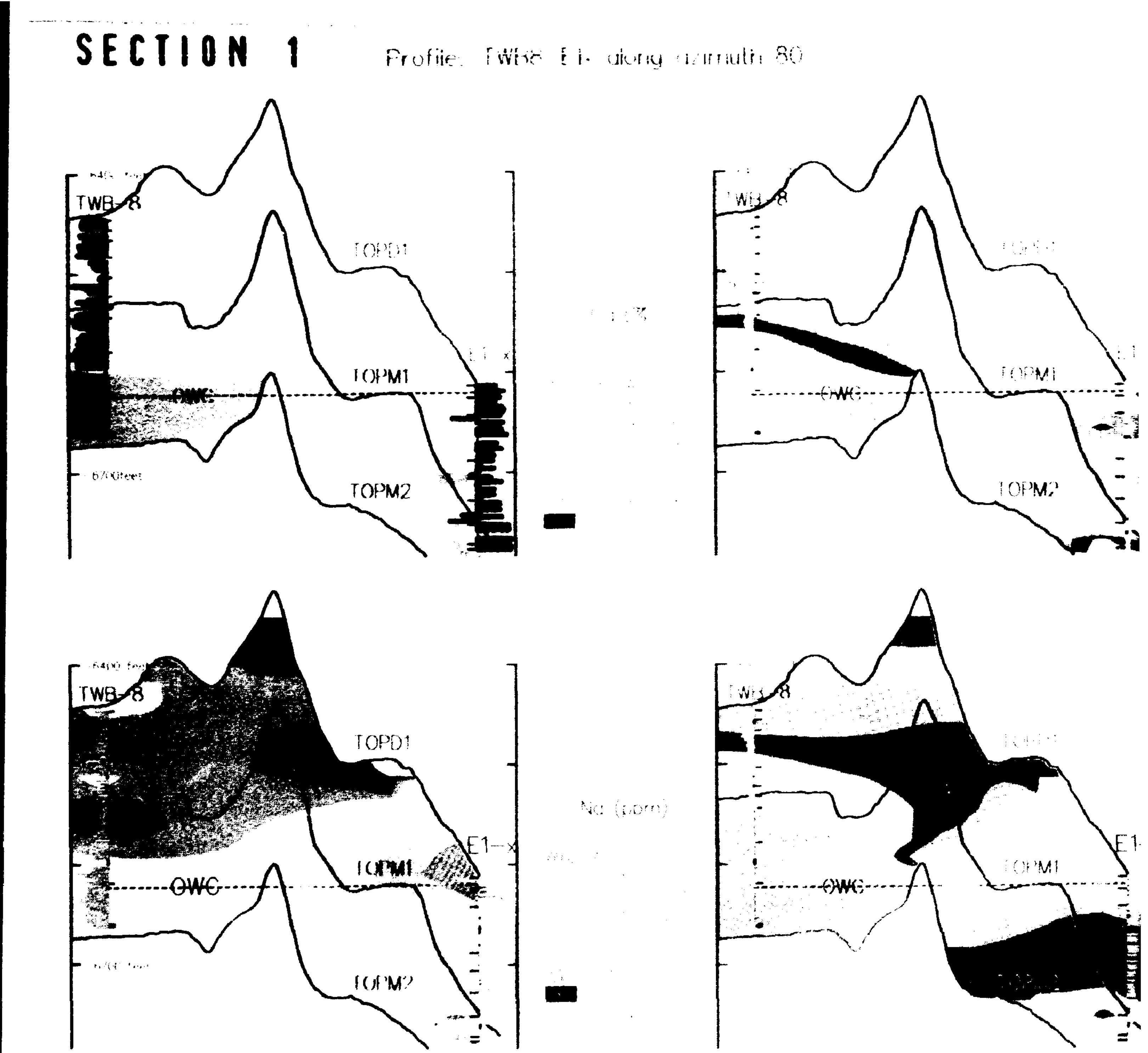

Fig. 47. UNIRAS contouring of geochemical data for Ca, Al, Na and Mn
two wells using stratigraphical borders as contouring fault lines.

SECTION 2

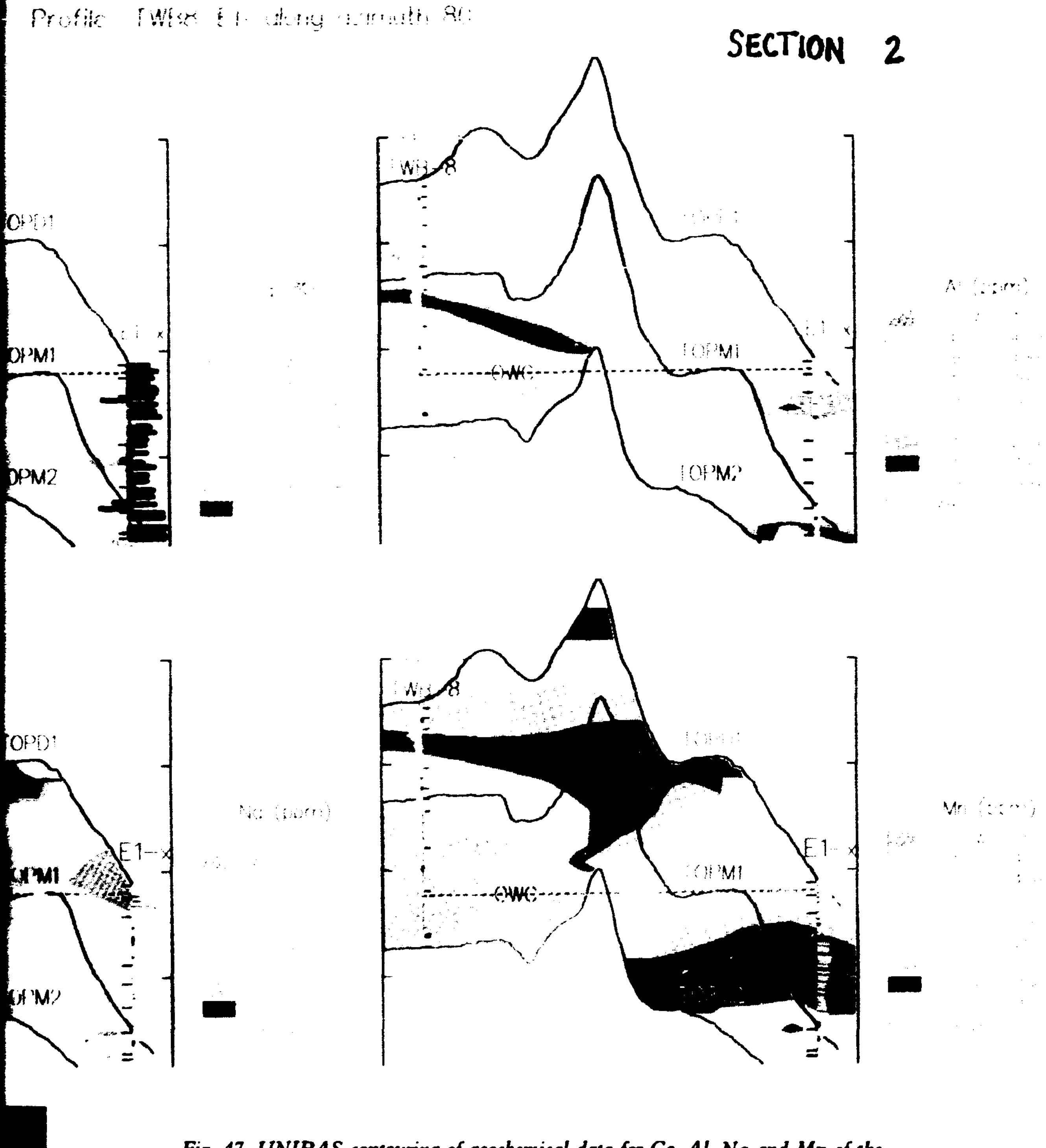

Fig. 47. UNIRAS contouring of geochemical data for Ca, Al, Na and Mn of the two wells using stratigraphical borders as contouring fault lines.

6. Conclusions

Detailed analytical investigations on drill core samples from two wells of the gas-producing Tyra structure, combined with evaluation of geophysical data in the form of well-logs leads us to conclude the following in connection with reservoir quality variations.

Well logging predicts high porosity chalks for both the central (TWB-8) and marginal parts (E-lx) of the Tyra structure. Permeability values are significantly reduced in the marginal well. The Danian section of TWB-8, in its middle part (units LDP and UDT), shows core porosity reduction down to less than 20% but increases again in the Maastrichtian strata. A similar reduction (start at unit UDT) is observed in the respective section of E-lx, but high porosity is not achieved again in the uppermost Maastrichtian section (1M and 2M). Such features are registered by the geophysical tools but difficult to explain by logging data alone.

The distribution of the major element Ca with depth in both drill cores is similar: contents are generally between 30 and 35%, the higher figures being generally connected with the Maastrichtian strata. The reduced-porosity section of core TWB-8 accordingly shows reduced Ca content.

Important for outlining reservoir quality variations regionally and on a local scale are chemical changes (diagensis) in the chalk induced by minor elements Si, Al, Na and Mn.

Silicon diagenesis is the most important chemical alteration process of the Tyra field reservoir rocks. Visible on a macro scale by chert formation (nodules and layers), it is also observed to act on a smaller scale. In the form of coatings and impregnations, Si diagensis initiates pore space reduction (porosity loss) and permeability is also altered due to different flow characteristics of Si-coated grains.

The Danian Tyra reservoir chalks from the central part of the structure (TWB-8) through the analytical data (up to 16% Si) show that silicification in units LDP and UDT must be responsible for a reduction of core porosity. Other chemical data also suggest that this diagenetical stage goes along with Al and Fe enrichment in the chalks, probably through the emplacement of smectite. Chalk reservoir degradation caused by Si diagenesis can therefore also be monitored through Al and to some extent also through Fe distributions. Locally, secondary Fe may also be generated by carbonate mineral diagenesis leading to pyrite formation.

Sodium and chlorine contents in the reservoir chalks are generally connected with formation waters and could be an indication of water saturation figures. In this respect, oil-bearing drill core sections are outlined through their lowered Na and Cl contents. However, care has to be taken in the interpretation because of possible contamination through drill fluids.

The most significant geochemical feature of the Tyra reservoir rocks is the distribution of Mn with depth overprinting all other observed chemical distributions, i.e. Mn is not connected with any of the other major, minor or trace elements in the chalks. The phenomenon is unique, and viewing the Mn analyses on a relatively large scale (tens of cm) leads to a steadily upwards increasing Mn distribution for both investigated drill core sections. In this respect, the Mn distribution could be related to the paleoenvironment or to a large-scale diagenetic feature, but other, yet unknown explanations could be introduced. Detailed studies are necessar, to outline the behaviour of Mn in the Tyra chalks and the chalks of the Danish subbasin.

Trace elements in chalk can be clearly coupled to appropriate major and minor elements, minerals, or mineral phases. In this respect, some of the trace element distributions could be used instead of major and minor elements to outline changes in the reservoir rocks. For instance, the trace element Sc usually follows closely the distribution observed for Si and Al. For carbonate rocks some of the traces indicate that environmental changes have taken place such as metals connected with residual minerals (heavy mineral horizons).

A special group to be investigated in chalk samples are the rare earth elements, which through their distribution pattern and distribution with depth may outline changes in redox conditions within the sediments (e.g. through the ratio Ce/La) and/or fractionation trends during their precipitation from seawater (ratio of light to heavy REE).

A detailed outline of the inorganic geochemistry and the estabishment of 3-D geochemical maps of the Tyra structure requires a more detailed sampling and analysis program from more than only two wells. By taking into account the recent availability of quick analytical methods, this could be facilitated within a reasonable time span.

7. Acknowledgements

During the initial stages of this investigation we profitted very much from the suggestions and the work offered by R. Gwozdz and H.J. Hansen, University of Copenhagen. Discussions during project meetings with N.O. Jørgensen, University of Copenhagen, are greatly appreciated. Invaluable help during this study was offered by E. Nygaard, DGU, L.N. Jørgensen and N. Klem, Mærsk Olie og Gas A/S. We thank the staff of the Isotope Laboratory of Risø for help and assistance during irradiations, and P.I. Jensen for analytical work at our laboratory.

8. References

Achauer C.W. 1985. Facies, morphology, and major reservoir controls in the Lower Cretaceous James Reef, Fairway field,east Texas. In: P.O. Roehl and P.W. Choquette, (eds.) Carbonate petroleum reservoirs, Springer, pp. 487-494.

Anikouchine W.A. 1967. Dissolved chemical substances in compacting marine sediments. J. Geophys. Res. 72: 505-509.

Bath A.H. and Edmunds W.M. 1981. Identification of connate water in interstitial solution of chalk sediment. Geochim. Cosmochim. Acta 45: 1449-1461.

Bathurst R.G.C. 1980. Lithification of carbonate sediments. Sci. Prog., Oxf 66: 451-471.

Bathurst R.G.C. 1975. Carbonate sediments and their diagenesis. Elsevier, 613 pp.

Bencini A. and Turi A. 1974. Mn distribution in the Mesozoic carbonate rocks from Lima valley, northern Appenines. J. Sed. Petrol. 44: 774-782.

Berner R.A. 1980. Early diagenesis: A theoretical approach. Princeton University Press, 241 pp.

Berner R.A. 1971. Principle of chemical sedimentology. McGraw-Hill, 240 pp.

Berner R.A. 1964. An idealized model of dissolved sulfate distribution in recent sediments. Geochim. Cosmochim. Acta 28: 1497-1503.

Billings G.K. and Ragland P.C. 1968. Geochemistry and mineralogy of the recent reef and lagoonal sediments south of Belize (British Honduras). Chem. Geol. 3: 135-153.

Birkelund T., Kegel-Christensen W. and Bromley R.G. 1979. Cretaceous-Tertiary boundary events. Rept. University of Copenhagen, 219 pp.

Bjørlykke K., Mo. A. and Palm E. 1988. Modelling of thermal convection in sedimentary basins and its relevance to diagenetic reactions. Marine and Petroleum Geology 5: 338-350.

Bjørlykke K., Ramm M. and Saigal G.C. 1989. Sandstone diagenesis and porosity modification during basin evolution. Geologische Rundschau. vol. 78 no 1: 243-269

Bo P. 1981. In situ determination of permeability and solute retention. European Appl. Res. Rept.-Nucl. Sci. Technol. 3: 1413-1464.

Boles J.R. and Ramseyer K. 1987. Diagenetic carbonate in Miocene sandstone reservoir. Am. Ass. Petr. Geol. Bull. 71: 1475-1487.

Brand U. and Veizer J. 1980. Chemical diagensis of a multicomponent carbonate system - 1: Trace elements. J. Sedim. Petrol. 50: 1219-1236.

Brown B.J. and Farrow G.E. 1978. Recent dolomitic concretions of crustacean burrow origin from Loch Sunart, west coast of Scotland. J. Sedim. Petrol. 48: 825-834.

Buckley D.E. and Cranston R.E. 1988. Early diagenesis in deep sea turbidites: The imprint of paleo-oxidation zones. Geochim. Cosmochim. Acta 52: 2925-2939.

Burruss R.C., Cercone K.R. and Harris P.M. 1985. Timing of hydrocarbon migration: Evidence from fluid inclusions in calcite cements, tectonics and burial history. In: N. Schneidermann and P.M. Harris (eds.), Carbonate cements, Society of economic paleontologists and mineralogists, Tulsa, pp. 277-289.

Calvert S.E. 1974. Deposition and diagenesis of silica in marine sediments. Spec. Publs int. Ass. Sediment. 1: 273-299.

Chapman S., Colson J.F., Flaum C., Hertzog R.C., Pirie G., Scott H., Everett B., Herron, M.M., Schweitzer J.S., La Vigne J., Quirein J. and Wendtlandt R. 1987. The emergence of geochemical well logging. Schlumberger Technical Review **35**: 27-35.

Carlsen L., Batsberg W., Jensen B.S. and Bo P. 1981. Permeability, porosity, dispersion-, diffusion- and sorption characteristics of chalk samples from Erslev, Mors, Denmark. Risø-R-451, 47 pp.

Carozzi A.V. and Falkenstein F.U.H. 1985 . Depositional and diagenetic evolution of Cretaceous oncolitic packstone reservoirs, Macae Formation, Campos Basin, offshore Brazil. In: P.O. Roehl and P.W. Choquette (eds.), Carbonate petroleum reservoirs, Springer, pp. 473-484.

Chilingarian G.V. and Wolf K.H. 1976. Developments in sedimentology 18B: Compaction of coarse-grained sediments, II. Elsevier, 808 pp.

Chilingar G.V., Bissell H.J. and Fairbridge R.W. 1967. Developments in Sedimentology 9B: Carbonate rocks. Elsevier, 413 pp.

Chilingar G.V. 1956. Relationship between Ca/Mg ratio and geologic age. Bull. Amer. Assoc. Petroleum Geologists **40**: 2256-2266.

Clayton C.R.I. and Mathews M.C. 1987. Deformation, diagenesis and the mechanical behaviour of chalk. Geol. Soc. London Spec. Publ. **29**: 55-62.

Cody R.D. 1971. Adsorption and the reliabaility of trace elements as environment indicators for shales. J. Sedim. Petrol. **41**: 461-471.

D'Heur M. 1977. Chalk reservoir of the west Ekofisk field. Proceed. Norwegian Petroleum Society. Geilo.

Davis J.A., Fuller C.C. and Cook A.D. 1987. A model for trace metal sorption at the calcite surface: Adsorption of Cd^{2+} and subsequent solid solution formation. Geochim. Cosmochim. Acta **51**: 1477-1490.

Dic 1962. Dictionary of geological termes. Dolphin, 545 pp.

Dittmar H. and Vogel K. 1968. Die Spurenelemente Mangan und Vanadium in Brachiopoden-Schalen in Abhängigkeit vom Biotop. Chem. Geol. **3**: 95-110.

DOE 1987. Deep burial diagenesis of carbonate reservoirs. DOE/ER/13322--T1, 90 pp.

Drever J.I. 1971. Magnesium-iron replacement in clay minerals in anoxic marine sediments. Science **172**: 1334-1336.

Dravis J. 1981. Porosity evolution in Upper Cretaceous Austin chalk formation, south-central Texas. AAPG Bull. **65**: 922.

Dunham J.B. and Larter S. 1981. Association of stylolytic carbonates, organic matter: Implications for temperature control on stylolite formation. AAPG Bull. **65**: 922.

Dunn W.W., Eha S. and Heikkila H.H. 1973. North Sea is a tough theater for the oil-hungry industry to explore. Oil & Gas J. Jan. 8, pp. 122-128 and Jan. 15, pp. 90-93.

Durney D.W. 1972. Solution-transfer, an important geological deformation mechanism. Nature **235**: 315-317.

Ellis D., Grau J., Schweitzer and Hertzog R. 1988. Basics of nuclear logging. The Technical Review (Schlumberger) 35, **3**: 5-18.

Engelhardt W.v. and Gaida K.H 1963. Concentration changes of pore solutions during the compaction of clay sediments. J. Sedim. Petr. **33**: 919-930.

Engell-Jensen M., Korsbech U. and Madsen F.E. 1984. U, Th and K in Upper Cretaceous and Tertiary sediments in Denmark. Bull. geol. Soc. Denmark vol 32. part 3-4: 107-120

Enos P. 1985. Cretaceous debris reservoirs, Poza Rica field, Veracruz, Mexico. In: P.O. Roehl and P.W. Choquette (eds.), Carbonate petroleum reservoirs, Springer, pp. 457-469.

Ernst H. 1982. The marl layer M100 in the Maastrichtian of Hemmoor - An example of selective $CaCO_3$ dissolution. Geol. Jb. **A61**: 109-127.

Feazel C.T. and Schatzinger R.A. 1985. Prevention of carbonate in petroleum reservoirs. In: N. Schneidermann and P.M. Harris (eds.), Carbonate cements, Society of economic paleontologists and mineralogists, Tulsa, pp. 97-106.

Feazel C.T., Keany J. and Peterson R.M. 1985. Cretaceous and Tertiary chalk of the Ekofisk field area, Central North Sea. In: P.O. Roehl and P.W. Choquette (eds), Carbonate petroleum reservoirs, Springer, pp. 497-507.

Friedman G.M. 1969. Trace elements as possible environmental indicators in carbonate sediments. Soc. Econ. Paleont. Mineralogists, Spec. Publ. No. **14**: 193-198.

Frykman P., Lieberkind K. and Nygaard E. 1983. Oil- and gas containing chalk reservoir in the Danish part of the Central Graben. Geol. Survey of Denmark, EFP-81 project. 158 pp.

Girardi F., Guzzi G. and Pauly J. 1965. Reactor neutron activation analysis by the single comparator method. Anal. Chem. **37**: 1085-1092.

Hancock N.J. and Taylor A.M. 1978. Clay mineral diagenesis and oil migration in the Middle Jurassic Brent Sand Formation. J. geol. Soc. London **135**: 69-72.

Halley R.B. 1985. Setting and geological summary of the Lower Cretaceous, Sunniland Field, Southern Florida. In: P.O. Roehl and P.W. Choquette (eds.), Carbonate petroleum reservoirs, Springer, pp. 445-454.

Hansen J.M. and Mikkelsen N. 1983. Hydrocarbon geological aspects of subsidence curves: Interpretations based on released wells in the Danish Central Graben. Bull. geol. Soc. Denmark **31**: 159-169.

Harbaugh J.W. 1962. Carbonate oil reservoir rocks. In: G.V. Chilingar et al. (eds.), Carbonate rocks. Elsevier, pp. 349-398

Hardman R.F.P. 1982. Chalk reservoirs of the North Sea. Bull. geol. Soc. Denmark **30**: 119-137.

Hardman R.F.P. 1981. Chalk reservoirs of the North Sea. Bull. geol. Soc. Denmark, arsskrift 1981, pp.171.

Hardman R.F.P. and Kennedy W.J. 1977. Chalk reservoirs of the Hod fields, Norway. Proceed. Norwegian Petroleum Society. Geilo.

Harris P.M., Moore C.H. and Wilson J.L. 1986. Carbonate platforms. Colorado School of Mines, Golden. 60 pp.

Harris P.M., Kendall C.G.S.C. and Lerche I. 1985. Carbonate cementation - A brief review. In: N. Schneidermann and P.M. Harris (eds.), Carbonate cements, Society of economic paleontologists and mineralogists, Tulsa, pp. 79-95.

Hartmann M. 1964. Zur Geochemie von Mangan und Eisen in der Ostsee. Meyniana **14**: 3-20.

Hays J.D. and Pitman W.C. 1973. Lithospheric plate motion, sea level changes and ecological consequences. Nature **246**: 18-22.

Håkansson E., Bromley R. and Perch-Nielsen K. 1974. Maastrichtian chalk of north-west Europe - a pelagic shelf sediment. Spec. Publs int. Ass. Sediment. **1**: 211-233.

Helander D.P. 1983. Fundamentals of formation evaluation. OGCI Publications, 332 pp.

Herron M.M. 1987. Estimating the intrinsic permeability of clastic sediments from geochemical data. The Log Analyst, Jan.-Febr., pp. 49.

Herron M.M. 1986. Mineralogy from geochemical well logging. Clays and clay Minerals **34**: 204-213.

Hitchon B. and Filby R.H. 1984. Use of trace elements for classification of crude oils into families - Example from Alberta, Canada. Amer. Assoc. Petroleum Geologists Bull. **68**: 838-849.

Hirst D.M. 1962. The geochemistry of modern sediments from the Gulf of Paria - II: The location and sitribution of trace elements. Geochim. Cosmochim. Acta **26**: 1147-1187.

Holland H.D., Holland H.J. and Munoz J.L. 1964. The coprecipitation of cations with $CaCO_3$ - II: The coprecipitation of Sr^{2+} with calcite between 90° and 100° C. Geochom. Cosmochim. Acta **28**: 1287-1301.

Honjo S. and Tabuchi H. 1970. Distribution of some minor elements in carbonate rocks, I. Pacific Geology **2**: 41-79.

Ichikuni M. 1973. Partitition of strontium between calcite and solution: Effect of substitution by manganese. Chem. Geol. **11**: 315-319.

Indelicato G.J. and Tipton G.A. 1988. Identifying potential petroleum accumulations. Oil & Gas J. Mar **28**: 73-76.

Jarvis I. 1984. Rare earth element geochemistry of Late Cretaceous chalks and phosphorites from northern France. Geological Survey of India Spec. Publ. **17**: 179-190.

Jensen B.S. 1979. Critical review of available information on migration phenomena of radionuclides into the geosphere. EC contract no. 066-78-1 WASDK. Internal reports, 142 pp.

Jordan C.F., Conally T.C. and Vest H.A. 1985. Middle Creataceous carbonates of the Mishrif Formation, Fateh Field, offshore Dubai, U.A.E. In: P.O. Roehl and P.W. Choquette (eds.), Carbonate petroleum reservoirs, Springer, pp. 427-442.

Jorgensen N.O. 1986. Chemostratigraphy of Upper Cretaceous chalk in the Danish subbasin. AAPG Bull. **70**: 309-317.

Jorgensen N.O. 1986. Geochemistry, diagenesis and nannofacies of chalk in the North Sea Central Graben. Sedim. Geol. **48**: 267-294.

Jorgensen N.O. 1983. Dolomitization in chalk from the North Sea Central graben. J. sedim. petrol. 53: 557-564.

Jorgensen N.O. 1981. Mg and Sr distribution in carbonate rocks from the Maastrichtian/Danian boundary of the Danish subbasin and the North Sea Central graben. Sedim. Geol. **30**: 311-325.

Jorgensen N.O. 1975. Mg/Sr distribution and diagenesis of Maastrichtian white chalk and Danian bryozoan limestone from Jylland, Denmark. Bull. geol. Soc. Denmark, **24**: 299-325.

Kaiser W.R. 1984. Predicting reservoir quality and diagenetic history in the Frio Formation (Oligocene) of Texas. In: D.A. McDonald and R.C Surdam (eds.) AAPG Memoir **37**: 195-215.

Kennedy W.J. 1980. Aspects of chalk sedimentation in the southern Norwegian offshore. Procced. Norwegian Petroleum Soc. The sedimentation of the North Sea reservoir rocks., Geilo, Norway May 11-14 1980. 29 pp.

Kennedy W.J. and Garrison R.E. 1975. Morphology and genesis of nodular chalks and hardgrounds in the Upper Cretaceous of southern England. Sedimentology **22**: 311-386.

Kharaka Y.K. and Carothers W.W. 1986. Oxygen and hydrogen isotope geochemistry of deep basin brines. In: P. Fritz and J.C. Fontes (eds.) Handbook of environmental isotope geochemistry, The terrestrial environment, pp. 305-360.

Kinsman D.J.J. 1969. Interpretation of Sr^{2+} concentrations in carbonate minerals and rocks. J. sedim. Petrol. **39**: 486-503.

Koczy F.F. 1951. Factors determining the element concentration in sediments. Geochim. Cosmochim. Acta, 1: 73-85.

Krouse H.R., Viau C.A., Eliuk L.S., Ueda A. and Halas S. 1988. Chemical and isotopic evidence of thermochemical sulphate reduction by light hydrocarbon gases in deep carbonate reservoirs. Nature 333: 415-419.

Kunzendorf H., Gwozdz R. and Hansen H.J. 1989. Uranium at the Cretaceous-Tertiary boundary in Denmark. Terra, in press.

Kunzendorf H., Gwozdz R., Hansen H.J. and Svendsen N. 1986. Trace elements in a North Sea drill core. Applied Geochemistry 1: 383-394.

Kunzendorf H., Gwozdz R., Hansen H.J., Nygaard E. and Svendsen N. 1985. Trace element analysis of North Sea chalk. Internal report, project EM-22510-8, 49 pp.

Kunzendorf H., Løvborg L. and Christiansen E.M. 1980. Automated uranium analysis by delayed-neutron counting. Risø-Report Nr. 429, 38 pp.

Lasaga A.C. 1984. Chemical kinetics of water-rock interactions. J. Geophys. Res. 89: 4009-4025.

Leeder M.R. 1982. Sedimentology. Allen & Unwin, 337 pp.

Lind I. 1988. Stylolite formation. Unpubl. Ph.D. thesis, Institute for Applied Geology, Technical University of Denmark, 250 pp.

Lloyd R.M. 1981. Porosity reduction by chemical compaction-stable isotope model. AAPG Bull. 65: 809.

Lock G.A. and Hoyer W.A. 1971. Natural gamma-ray spectral logging. The Log Analyst Sept.-Oct., pp. 3-9.

Lonnie T.P. 1982. Mineralogical and chemical comparison of marine, nonmarine, and transitional clay beds on south shore of Long Island, New York. J. Sedim. Petrol. 52: 529-536.

Lovering T.G. and Patten L.E. 1962. The effect of CO_2 at low temperature and pressure on solutions supersaturated with silica in the presence of limestone and dolomite. Geochim. Cosmochim. Acta 26: 787-796.

Lynn D.C. and Bonatti E. 1965. Mobility of manganese in diagenesis of deep-sea sediments. Mar. Geol. 1: 459-474.

Madirazza I. 1981. Geology and structure of the North Sea Basin. Dept. of Geology, Univ. Aarhus, Geokompendier No. 18, 100 pp.

Majid A.H. and Veizer J. 1986. Deposition and chemical diagenesis of Tertiary carbonates, Kirkuk Oil Field, Iraq. Bull. AAPG, 70: 898-913.

Mapstone N.B. 1975. Diagenetic history of a North Sea chalk. Sedimentology 22: 601-614.

Margolis S.V., Mount F.F., Doehne E., Showers W. and Ward P. 1987. The Cretaceous/Tertary boundary carbon and oxygen isotope stratigraphy, diagenesis, and paleoceanography at Zumaya, Spain. Paleoceanography 2: 361-377.

Michard G. 1971. Theoretical model for manganese distribution in calcareous sediment cores. J. Geophys. Res. 76: 2179-2186.

Michelsen O. (Edit.) 1982. Geology of the Danish Central Graben. Geological Survey of Denmark, Series B, No. 8, 133 pp.

Milliman J.D. 1966. Submarine lithification of carbonate sediments. Science 153: 994-997.

Mimram Y. 1977. Chalk deformation and large-scale migration of calcium carbonate. Sedimentology 24: 333-360.

Mucci A. 1988. Manganese uptake during calcite precipitation from seawater: Conditions leading to the formation of pseudokutnahorite. Geochim. Cosmochim. Acta 52: 1859-1868.

Müller G., Irion G. and Förstner U. 1972. Formation and diagenesis of inorganic Ca-Mg carbonates in the lacustrine environment. Naturwissenschaften 59: 158-164.

Mærsk 1987. Tyra field chalk stratigraphy. Internal Report, Mærsk Olie & Gas.

Neugebauer J. 1974. Some aspects of cementation in chalk. Spec. Publs int. Ass. Sediment. 1: 149-176.

Neugebauer J. 1973. The diagenetic problem of chalk. N. Jb. Geol. Paläont. Abh. 143: 223-245.

Nielsen B.L., Løvborg L., Sørensen P. and Mose E. 1987. Gamma-ray analsysis for U, Th and K on bulk cutting samples from deep wells in the Danish subbasin and the North German Basin. Risø-M-2646, 80 pp.

Nielsen O.J., Bo P. and Carlsen L. 1985. COLUMN2- A computer program for simulating migration. Risø-R-514, 85 pp.

Nyberg Y., Lien K., Lindberg P.A. and Smistad J.K. 1978. Mineral composition, and aid in classical log analysis used in Jurassic sandstone of the northern North Sea. SPWLA 19. Annual Meeting, pp. 1-35.

Okita P.M., Maynard J.B., Spiker E.C. and E.R. Force 1988. Isotopic evidence for organic matter oxidation by manganese reduction in the formation of stratiform manganese carbonate ore. Geochim. Cosmochim. Acta 52: 2679-2685.

Park W.C. and Schot E.H. 1968. Stylolites: Their nature and origin. J. Sedim. Petrol. 38: 175-191.

Pevear D.R. and Grabowski G.J. 1985. Geology and geochemistry of the Toolebuc Formation, an organic-rich chalk from the Lower Cretaceous of Queensland, Australia. SEPM Core Workshop, Vol. 6: 303-341.

Pollastro R.M. and Scholle P.A. 1986. Diagenetic relationships in a hydrocarbon-productive chalk: The Creataceous Niobrara Formation. U.S. Geological Survey Bulletin, P 1578: 219-236.

Porthault B. and Sauvan P. 1979. Quelques applications de la geochimie des elements en traces en exploration petroliere et miniere. Phys. Chem. Earth 11: 703-716.

Pingitore N.E. 1978. The behaviour of Zn^{2+} and Mn^{2+} during carbonate diagenesis: Theory and applications. J. Sedim. Petrol. 48: 799-814.

Rao M.V. and Fontenot J.E. 1988. MWD gains as formation-evaluation tool. Oil & Gas J., Feb 8: 44-48.

Reeder R.J. (edit.) 1983. Carbonates: Mineralogy and chemistry. Reviews in Mineralogy, Vol. 11, 394 pp.

Reijers T.J.A. and Bartok P. 1985. Porosity characteristics and evolution in fractured Cretaceous carbonate reservoirs, La Paz field area, Maracaibo Basin, Venezuela. In: P.O. Roehl and P.W. Choquette (eds.), Carbonate petroleum reservoirs, Springer, pp. 409-423.

Roberts H.H., Sassen R. and Aharon P. 1988. Petroleum-derived authigenic carbonates of the Louisiana continetal slope. Proceed. Oceans 88, pp. 101-105.

Runnels D.D. 1969. Diagenesis, chemical sediments, and the mixing of natural waters. J. Sedim. Petrol. 39: 1188-1201.

Sayles F.L. and Manheim F.T. 1975. Interstitial solutions and diagenesis in deeply buried marine sediments: Results from the Deep Sea Drilling Project. Geochim. Cosmochim. Acta 39: 103-127.

Scholle P.A. and Halley R.B. 1985. Burial diagenesis: Out of sight, out of mind. In: N. Schneidermann and P.M. Harris (editors), Carbonate cements, Society of economic paleontologists and mineralogists, Tulsa, pp. 309-334.

Scholle P.A. 1977. Chalk diagenesis and its relation to petroleum exploration: Oil from chalk, a modern miracle? Amer. Assoc. Petroleum Geologists Bull. **61**: 982-1009.

Scholle P.A. 1974. Diagenesis of Upper Cretaceous chalks from England, Northern Ireland, and the North Sea. Spec. Publs int. Ass. Sediment. **1**: 177-210.

Showers W.J., Lent R.M. and Margolis S.V. 1987. BSEM evaluation of carbonate diagenesis: Benthic foraminifera from the Miocene Pungo River Formation, North Carolina. Geology **15**: 731-734.

Scott H.D. and Smith M.P. 1973. The aluminum activation log. The Log Analyst Sept.-Oct., pp. 3-12.

Sippel R.F. and Glover E.V. 1964. The solution alteration of carbonate rocks, the effects of temperature and pressure. Geochim. Cosmochim. Acta **28**: 1401-1417.

Suau J. and Spurlin J. 1982. Interpretation of micaceous sandstones in the North Sea. SPWLA 23. Logging Symp., 37 pp.

Svendsen N. 1979. The Tertiary/Cretaceous chalk in the Dan Field of the Danish North Sea. In: T. Birkelund and A.G. Bromley (eds), Createceous-Tertiary boundary events, Univ. Copenhagen, 8 pp.

Szatmari P. 1986. Plate tectonic control of synthetic oil formation. Oil & Gas J. Sept., pp. 67-69.

Tourtelot H.A. 1964. Minor-element composition and organic carbon content of marine and nonmarine shales of Late Cretaceous age in the western interior of the United States. Geochim. Cosmochim. Acta **28**: 1579-1604.

v. Rad U. and Rosch H. 1974. Petrography and diagenesis of deep-sea cherts from the central Atlantic. Spec. Publs int. Ass. Sediment. **1**: 327-347.

Veizer J. 1983. Trace elements and isotopes in sedimentary carbonates. In: R.j. Reeder (edit.), Carbonates: Mineralogy and chemistry. Reviews in Mineralogy, Vol. 11, pp. 265-299.

Veizer J. 1977. Diagenesis of pre-Quaternary carbonates as indicated by tracer studies. J. Sedim. Petrol. **47**: 565-581.

Veizer J. and Demovic R. 1974. Strontium as a tool in facies analysis. J. Sedim. Petrol. **44**: 93-115.

Veizer J. 1979. Secular variations in chemical composition of sediments: A review. In: L.H. Ahrens (edit.) Second symposium on the origin and distribution of the elements, Paris, France, May, 1977. Phys. Chem. Earth **11**: 269-278

Wangersky P.J. and Joensuu O. 1964. Strontium, magnesium, and manganese in fossil foraminiferal carbonates. J. Geol. **72**: 477-483.

Watts N.L., Lapre J.F., van Schijndel-Goester F.S. and Ford A. 1980. Upper Cretaceous and lower Tertiary chalks of the Albuskjell area, North Sea: Deposition in a slope and a base-of-slope environment. Geology **8**: 217-221.

Weber J.N. 1964. Trace element composition of dolostones and dolomites and its bearing on the dolomite problem. Geochim. Cosmochim. Acta **28**: 1817-1868.

Weyl P.K. 1959. Pressure solution and force of crystallization - A phenomenological theory. J. Geophys. Res. **64**: 2001-2025.

Whitten D.G.A. and Brooks J.R.V. 1976. The Penguin dictionary of geology. Penguin, 495 pp.

Wise S.W. and Weaver F.M. 1974. Chertification of oceanic sediments. Spec. Publs int. Ass. Sediment. **1**: 301-326.

Woo K.S. 1986. Coordinated textural-isotopic-chemical investigation of Mid-Cretaceous rudist limestones, Texas and Mexico: implications for diagenetic histories. J. Geol. Soc. Korea **22**: 381.
Zachos J.C. and Arthur M.A. 1986. Paleoceanography of the Cretaceous/Tertiary boundary event: Inferences from stable isotopic and other data. Paleoceanography **1**: 5-26.

APPENDIX I

Brief Description of Samples from TWB-8

Depth	Unit	Remarks
6592'2''	UDP1	No comments
6594'	UDP1	Very porous; 6'' beneath the contact; arenitic? glauconitedraped skeletal clasts/tracks; relatively arenitic; graduational decrease of the sand fraction with depth in the core.
6597'	UDP1	No visible strucures; porous.
6599'-6600'		Similar to above
6601'	UDP1	Top section of the core shows dense anastomosed, healed small fractures which in almost all cases are vertical to the marl laminae; sample is relatively homogeneous with shows of pattern chalk structures.
6602'	UDP1	Relatively homogeneous pattern chalk structure sample; coarse, homogeneous matrix with few healed small fractures; soft chalk (gas?).
6609'9''	UDP1	Relatively homogeneous sample (wackestone?); single stylolite; few pattern chalk structures; just above the sample, dense system of anastomised and crossing healed fractures
6613'	UDP2	Pure coccolith micrite, otherwise similar to above; some large crushed echinides.
6617'10''	LDP	Sample contains marl laminae and micro-stylolites; some healed microfractures.
6619'	LDP	Sample from an area with prominent glide/"criss cross" healed fractures; from this depth, the rocks are more layered/laminated with oriented open pattern-chalk structures, just above one flint layer is a hard and dense chalk *with micro stylolites, at a depth of 6623' occurrence of thick* flint layer with inclusions of soft chalk.
6623'23''	LDP	Flint sample.
6624'	LDP	Beneath the flint; chalk is dense, relatively homogeneous and hard with homogeneously occuring pattern-chalk structures in several generations; the pattern-chalk structure is partly concentrated around bright vertical tracks and some (white) <u>zoophycos</u>.
6627'	LDP	Hard, single unit with graduations (pattern graduation) showing <u>bathichnus</u> corona and some central tracks; the pattern-chalk structure is relatively homogeneous.
6630'	LDP	Section with pattern chalk structure; relatively homogeneous, but with layered orientation; relatively soft rock.
6631'6''	LDT1	Dark, silicified chalk (dark grey), presumably marly with very dark pattern-chalk structures, numerous trace fossils, preferentially <u>zoophycos</u>.
6634'6''	LDT1	Strongly silicified section which may be divided into several 10 cm thick units; some about 3 cm thick marly bands occur.
6637'	LDT1	Dispersed chert; core box appears generally darker with more well-defined layering; dark, silicified bands, one visible platy-chert band.
6641'3''	LDT1	Very pronounced pattern-chalk structures in several grey varieties; 5 to 10 cm bedding; top of the core box similar above.
6643-44'	LDT1	At least 40 units with isometrical 1 to 2 cm pattern-chalk structures with some isolated light points; it looks as if the laminated pattern-chalk structure rocks above was produced by compaction.
6645'6''	LDT1	Silicified, dark and weak pattern-chalk structure.
6648'4''	LDT1	Few <u>zoophycos</u> occurrences; relatively sharp layering on a 40-cm scale which in general shows weak pattern-chalk structure.
6650'10''	LDT1	Similar as above but really weakly visible structures.
6653'	LDT2	Silicified chalk showing significant bedding on a 40-cm scale; <u>zoophycos</u> occurrences suggest bedding on a 3 to 5 cm scale, relatively few pattern-chalk structures, essentially only in one 10 cm thick band; the whole core section shows a crenulated micro-Steinich lamination.
6655'6''	LDT2	Core box contains grey chert layers.
6657'10''	LDT2	The top of the core box contains homogeneous chalk with bedding characteristics as described above; below this are there strong track (40 cm long) that crosses three silicified marly bands pattern-chalk structures which partly occur close to a vertical
6660'6''	LDT2	Hard, silicified (disseminated) chalk with pattern-chalk structure; weak 20-cm bedding with very low marl content.
6663'7''	LDT2	Core box with 3 silica-rich marly layers (60 to 40 cm distance between layers); Very strong pattern-chalk structure, especially in the bottom of the core; here, there is a grey platy chert layer (R7) which cuts the pattern-chalk structure, the sample was collected from a section between the marly layers.
6665'8''	LDT2	Core shows a gradual transition from marl (bluish-grey, with 3-mm <u>zoophycos</u>) to whittish patched pattern-chalk structured, track-like light rock.
6667'	LDT2	Similar sections; finely, whittish-spotted pattern-chalk structure rock (10-cm layering) in a more orless marly-looking rock.
6673'8''	LDT2	Bluish core with some few white spots; <u>zoophycos</u>.
6676'5''	LDT2	Hard silicified chalk with occurrences of disseminated pyrite; R-7.
6680'	IM	White pattern-chalk structure which appears open and relatively open with few 0.5 to 1 cm thick layers. Weak pattern-chalk structure.
6680'6''	IM	Chert sample.

APPENDIX II

Brief Sampling Section Description of E-1x.

Depth (feet)	Unit	Description
6732 - 6735	UDP1	Chalk with light and greenish marl occurring at a depth of about 6733', some small glauconite concretions, white chalk-like intraclasts
6735 - 6737.5	UDP1	Chalk with some marly horizons; thin glauconitic spar; chalk percentage is increasing with depth; pyrite occurs in the form of disseminations and concretions, stylolites in the form of lumps
6738 - 6740	UDP1	Homogenous chalk showing increasing hardening with depth
6740 - 6743	UDP1	Little sample material available from the core; homogeneous laminated chalk, micro- stylolites occur
6743 - 6746	UDP1	Little sample material left in core box; chalk is white and homogeneous; micro-stylolites occur.
6746 - 6748	UDP1	White chalk with some brownish horizons
6748 - 6751	UDP2	Homogeneous chalk with horizontal shear zones, patterned chalk
6751 - 6752	UDP2	Patterned chalk.
6752 - 6755	UDP2	Homogeneous chalk with mm-size-and micro-stylolites, bluish appearance, micro Chondrite
6755 - 6758	UDP2	White to bluish chalk, micro Chondrite
6758 - 6761	UDP2	Slightly bluish chalk, micro Chondrite. Healed fractures.
6761 - 6763	UDP2	Slightly brownish hardened chalk; stylolite horizon
6763 - 6766	UDP2	Homogeneous chalk.
6766 - 6768	LDP	Homogeneous chalk with micro-stylolites.
6768 - 6771	LDP	Greyish-to brownish chalk with some chert horizons
6771 - 6774	LDP	Hard homogeneous chalk, healed fractures occur.
6774 - 6776	LDP	Homogeneous white chalk; stylolite horizon at 6774'.
6776 - 6780	LDP	Homogeneous white chalk.
6780 - 6783	LDP	Homogeneous white chalk with micro-stylolites, healed fractures
6783 - 6786	LDP	Mostly homogeneous white chalk; micro-stylolites and healed fractures; light-colored chert
6786 - 6793	LDP	Very little core material available, some chert
6793 - 6794	LDP	Slightly brownish white chalk
6794 - 6797	LDP	Dense white chalk with skeletal remains
6797 - 6799	LDP	Weakly whittish-spotted chalk, light chert horizon
6799 - 6802	LDP	White chalk with whittish chert in the upper section.
6802 - 6804	LDP	No change.
6804 - 6807	LDP	No change
6807 - 6809	LDP	No change
6809 - 6811	LDP	Dense chalk.
6811 - 6814	UDT	Chalk with some clasts
6814 - 6816	UDT	Chalk with some marly horizon in the lower part
6816 - 6819	UDT	No change
6819 - 6821	UDT	Occurrences of dissiminneret spar
6821 - 6824	UDT	No change
6824 - 6826	UDT	No change.
6826 - 6829	UDT	No change
6829 - 6831	LDT1	No change
6831 - 6834	LDT1	Chalk with some greenish marl horizons
6834 - 6836	LDT1	Dark chalk with light specks, bluish flint
6836 - 6838	LDT1	Whittish-spotted chalk with a generally bluish appearance
6838 - 6841	LDT1	Chalk with some brownish margins probably caused by probably oil-staining
6841 - 6843	LDT1	White chalk with some brownish staining (oil?) in the upper parts.
6843 - 6845	LDT1	Chalk with flint layer showing oil-staining, core box contains many loose pieces
6845 - 6848	LDT1	Chalk core shows divisions of dark and light parts, flint with thick whittish margins
6848 - 6850	LDT1	Chalk with greenish intraclast at the bottom (glauconite?)
6850 - 6853	LDT2	Chalk with greenish nodular clasts
6853 - 6855	LDT2	Chalk with greenish intraclasts
6855 - 6858	LDT2	Homogeneous chalk with skeletal intraclasts
6858 - 6860	LDT2	Hard white chalk
6860 - 6863	LDT2	Similar
6863 - 6865	LDT2	Chalk with pyrite, both as concretions and dissiminated, healed fractures
6865 - 6868	LDT2	Similar
6868 - 6870	LDT2	Similar
6870 - 6872	LDT2	No change
6872 - 6875	LDT2	No change
6875 - 6878	1M	Greyish, relatively hard chalk, vertical stylolites
6878 - 6881	1M	Chalk with some microfossils, healed fratures
6881 - 6884	1M	Greyish chalk with horizontal stylolites
6884 - 6886	1M	Chalk with many horizontal parallel stylolites
6886 - 6889	1M	No change
6889 - 6891	1M	No change
6891 - 6894	1M	Chalk with many stylolites, maximum stylolite hight is 10 mm.
6894 - 5897	2M	Greyish hard chalk with still relatively high stylolite bands
5987 - 6900	2M	Mud-coloured chalk, strongly fragmented
6900 - 6902	2M	No change

APPENDIX III

Analytical Results from Short-Lived INAA of Samples from TWB-8. Depth Is in Feet and All Analytical Data Are in ppm, Except Ca (in %) and U (in ppb). If Depth Is Greater than 4 Digits, Then the Last Digit(s) Refer to Inches.

Depth	Na	Mg	Al	Cl	Ca	V	Mn	Sr	Eu	Dy	U
UDP1:											
65922	11200	25400	86200	655	-	222	186	361	2.1	6.2	2080
6594	1390	10800	3810	1030	33.90	23.4	1880	-	-	3.0	984
6597	711	5760	2930	807	34.60	11.1	1690	-	-	2.5	325
65996	839	-	4470	1020	35.00	10.0	1710	1140	-	2.8	398
6601	788	-	2040	1880	34.80	4.6	1640	-	-	2.8	163
6602	819	4990	2600	1820	33.90	8.7	1690	1750	-	-	230
UDP2:											
66099	733	-	1760	2000	35.80	-	1530	892	-	-	178
6613	695	-	1600	1960	33.80	5.0	1500	-	-	1.6	132
LDP:											
661710	997	-	3410	1880	33.50	8.7	1440	1050	-	3.6	257
6619	947	-	3550	1910	33.50	9.0	1420	1030	-	1.5	285
66207	773	-	3010	2220	36.20	15.6	1760	-	-	2.4	315
66233	571	-	2000	707	30.30	13.5	1210	841	-	1.5	183
6624	783	-	1560	-	35.80	10.2	1260	1010	-	1.9	226
6627	1250	-	1760	2870	35.20	8.1	835	987	-	2.3	123
6630	898	-	2250	1500	36.90	7.0	864	717	-	1.6	187
UDT:											
66313	1410	-	4780	2840	27.50	8.1	720	853	-	2.2	251
66346	1200	-	2520	1970	28.80	5.3	674	717	-	1.5	117
6637	1260	-	5580	2450	31.40	6.9	718	714	0.8	3.1	256
66413	755	-	4410	894	29.90	6.1	803	836	0.8	2.2	154
66434	744	-	2380	954	28.70	5.8	844	617	-	1.6	116
66456	2190	-	9580	2720	24.60	15.9	566	554	1.2	4.0	358
66484	1040	-	5090	1120	25.80	8.9	683	816	1.2	1.8	182
665010	1230	-	4400	1230	26.50	9.4	790	1160	-	2.1	162
LDT1:											
6653	1470	3430	6500	2140	27.40	10.8	776	926	1.1	2.9	214
66556	1100	-	3250	885	26.30	7.2	710	858	0.8	1.5	125
665710	959	-	4440	1070	26.30	6.4	650	717	0.9	2.2	136
66008	-	-	3130	-	39.10	7.1	-	-	-	-	111
65637	1210	-	2920	-	33.00	7.0	692	736	-	2.9	113
66638	1170	-	4010	3230	29.20	7.7	597	913	-	2.4	183
6667	915	3910	3180	1660	31.60	7.1	593	889	-	1.5	137
LDT2.											
66738	1660	-	2710	1910	32.30	8.7	632	685	-	2.1	198
66755	1030	-	2590	1790	36.90	7.3	700	928	0.6	1.4	185
1M:											
6680	1010	-	2670	1180	33.30	8.2	640	1200	0.9	2.1	190
66806	621	4280	1960	1030	33.90	7.4	569	847	0.7	1.7	154
668011	1020	3640	2740	1600	22.20	6.9	449	603	0.6	1.7	290
6686	566	-	966	1390	30.90	-	242	363	0.3	0.6	217
6687	940	-	774	2310	30.50	-	359	836	-	0.9	100
6688	769	-	917	2050	34.00	-	418	707	0.5	1.3	189
6689	444	3320	486	464	36.30	3.9	357	613	-	0.8	74
6690	757	-	920	1480	37.00	-	408	849	0.5	0.7	282
6691	713	-	980	1050	32.90	-	440	721	0.5	1.2	310
2M:											
6692	917	-	1100	1700	34.80	-	297	826	0.4	1.1	374
66925	971	-	1000	1120	32.30	4.2	337	934	0.5	1.7	487
6693	870	-	626	2850	31.50	4.1	301	918	-	1.2	889
6694	775	3090	1130	2310	32.80	4.9	299	950	0.4	1.5	990
6695	865	-	632	2300	39.70	3.6	372	947	0.4	1.2	973
6696	1160	-	1350	2900	31.50	5.2	378	893	0.4	1.7	396
6697	736	-	66	1590	33.40	4.9	448	1170	0.3	1.8	467
6698	933	2280	1710	2130	34.30	6.5	375	995	0.3	1.4	448
6699	916	-	857	2740	32.90	3.8	378	1170	-	1.0	619
6700	1120	-	827	2420	39.10	-	366	1100	0.3	1.5	830
6701	941	-	1420	2770	34.70	5.5	334	1170	0.4	1.5	725
67015	1380	-	1440	4440	35.90	-	347	1200	0.4	1.7	859
6702	853	-	1270	2300	33.60	-	340	1160	0.4	1.5	600
6704	854	-	813	2700	31.90	-	327	1080	0.4	1.4	499
67045	716	-	454	2500	31.20	-	364	1050	0.3	1.6	449
67055	852	-	425	2620	31.20	-	305	1150	-	1.4	487
6707	754	-	428	2250	31.60	-	287	1270	-	1.0	555
6710	897	-	642	2490	34.70	2.7	275	1040	-	1.0	668
6711	652	-	276	1630	35.20	-	267	1110	-	1.0	513
6713	725	-	386	1750	36.20	-	266	1110	-	0.9	490
6714	-	-	331	-	35.50	-	-	-	-	-	466
6715	870	-	878	2110	-	-	259	1210	0.3	1.2	614
6716	1240	-	730	3430	33.20	-	216	1440	0.5	1.9	1090
6717	994	-	876	2620	-	-	228	1330		0.9	438
6718	1230	-	900	2950	-	-	202	1310	0.5	1.6	958
6719	880	-	674	1610	36.70	-	235	1290	0.3	1.2	712
67195	1240	-	499	2420	35.50	-	229	1300	0.3	1.2	467
6720	1430	-	475	3690	35.20	-	210	1320	0.3	1.1	481
6721	1360	-	214	3920	32.80	-	176	1360	-	0.9	494
6725	1220	-	325	4610	37.30	-	157	1200	-	0.8	454
3M:											
67275	1490	-	268	4410	38.10	-	159	1110	-	0.5	342
67285	1660	-	232	3450	36.70	-	152	1140	-	0.3	354
6729	1110	-	272	1390	37.80	-	198	1200	0.4	1.6	252
6730	901	-	1094	1330	39.50	[illegible]	[illegible]	1140	-	0.6	441
67302	1030	-	862	1770	37.60	2.1	203	1200	0.2	1.0	332
6733	732	1955	598	945	39.50	3.1	206	1180	-	0.8	282
67332	986	2430	712	966	33.80	1.8	187	983	0.2	0.7	287
67345	1170	-	587	1690	32.50	2.3	197	1010	-	0.9	348
6736	-	-	584	-	31.10	-	-	-	-	-	337
67361	2130	-	450	3420	33.90	-	176	1210	-	1.1	505
6738	1170	-	605	1690	36.60	-	207	1150	0.4	0.8	285
6739	1270	-	513	1880	35.20	-	201	1070	-	0.9	227
67392	1130	-	765	1580	32.50	-	203	1120	0.3	1.2	286
5740	1610	-	855	2470	30.60	-	199	1070	0.3	1.0	429
67415	1480	-	903	2040	36.60	2.6	192	1180	-	1.0	308
6751	1640	-	689	3050	35.20	-	196	1020	-	1.0	257
6752	1790	-	490	3060	36.10	3.6	197	922	-	0.7	200
6753	1370	-	1380	1950	36.70	3.6	202	1060	0.5	1.7	505
67546	1400	2079	559	2180	39.40	2.9	189	997	-	0.8	368
67558	1960	3810	804	2910	36.50	3.6	189	1030	0.2	0.8	411
67565	1310	2180	999	1780	37.80	3.3	189	1130	0.3	-	341
67576	3530	-	892	5580	39.40	-	181	896	-	0.9	194
67587	759	1640	674	418	35.70	2.4	132	737	0.2	0.7	292
67597	1370	1910	662	1800	37.90	2.0	179	951	0.3	1.1	262
67607	2590	-	504	3920	37.30	1.7	178	1030	-	0.8	174
67617	1800	3111	597	951	39.40	-	127	688	-	0.5	220
67620	990	-	667	1360	36.00	2.7	181	1080	-	1.0	318
67646	2340	2450	750	3750	-	-	186	1000	0.2	1.2	367
67656	1140	-	654	1870	37.90	1.9	186	1070	0.3	1.0	247
67666	2420	3060	756	4010	37.60	3.2	173	927	0.3	1.0	184

Continued

Depth	Na	Mg	Al	Cl	Ca	V	Mn	Sr	Eu	Dy	U
4M:											
67677	1680	-	562	2960	36.90	2.3	150	1070	-	0.7	197
67678	1820	6090	1200	2850	37.10	2.3	200	1050	0.4	1.7	-
67686	1040	1781	884	1730	39.40	2.0	196	1010	0.3	1.2	180
67705	2290	-	600	3980	37.50	-	192	996	0.2	1.0	222
67716	1930	2489	933	2980	39.20	1.7	201	1080	-	0.9	167
67726	2040	-	758	3370	38.30	2.2	178	878	-	1.2	184
67735	2570	2360	769	4870	35.80	-	186	1010	0.3	1.0	147
67767	2390	-	947	4250	36.70	2.3	189	1060	0.4	1.0	316
67775	2360	2330	543	4110	36.40	2.3	172	1020	-	0.7	165
67786	2150	2190	647	3570	36.30	-	167	1180	-	0.9	208
67796	1760	-	1280	2690	38.10	2.7	187	1260	0.5	1.3	452
67805	2540	-	663	4600	36.80	-	155	1120	-	1.0	162
67817	1150	-	902	1800	39.60	4.2	184	1230	0.5	1.0	486
67836	2200	-	642	4460	36.80	3.4	165	1080	-	1.1	392
67846	3110	-	657	5710	37.30	2.3	147	1250	0.3	1.4	539
67857	2110	-	610	4020	37.60	2.3	159	1120	0.2	0.8	383
67876	2020	3988	602	3250	39.20	1.8	151	1090	-	0.7	292
67886	2580	-	-	1630	-	-	124	874	-	0.5	380
5790	2010	-	679	3070	-	4.1	153	1130	-	1.3	205
67925	2330	-	-	4230	-	-	152	1180	-	1.0	372
67934	2340	2004	704	4060	39.30	-	150	1240	0.3	1.0	281
67944	2270	-	663	3630	36.40	-	155	1290	0.3	1.0	303
67956	1110	-	641	665	35.60	3.4	111	882	0.2	0.7	281
67964	1500	2210	805	1980	35.40	4.0	142	1110	-	0.8	256
67983	2710	-	-	4830	38.80	-	151	1150	0.3	0.9	286
68021	1450	3050	585	693	37.20	-	115	1100	0.4	1.1	671
68034	2340	-	738	3490	38.70	-	148	1340	0.5	1.2	393
68043	2350	-	365	10900	38.00	2.1	169	1640	0.3	1.0	398
68055	2170	1820	225	3440	-	-	130	1360	-	0.7	375
68064	-	2016	450	123	35.90	2.1	148	1340	0.2	1.1	452
68076	516	2250	630	984	37.80	2.5	154	1093	-	0.8	170
5M:											
68096	1640	3590	693	2810	-	1.6	166	1030	0.4	1.0	269
68104	1720	3060	757	3020	37.30	3.2	167	927	-	0.9	154

APPENDIX IV

Analytical Results of Selected Drill Core Samples from TWB-8

Depth	Na	Ca	Fe	Sc	Cr	Co	Zn	As	Br	Rb	Sr	Sb	Cs	Ba	Hf	Th	La	Ce	Nd	Sm	Eu	Tb	Yb	Lu	Ce/La	La/Yb
UDP1:																										
6601	0.10	32.40	2170	1.1	6.0	1.7	23	-	8.3	-	983	-	0.1	171	0.1	0.5	8.8	6.6	9.0	1.9	0.3	0.3	0.7	0.1	0.75	13.3
UDP2:																										
66099	0.09	33.60	936	1.2	5.7	1.7	28	-	8.2	-	987	-	0.1	142	0.1	0.4	10.6	8.4	9.2	2.4	0.4	0.4	0.7	0.1	0.79	10.0
LDP:																										
661710	0.11	33.20	1280	2.1	6.5	3.4	42	-	9.9	-	1020	-	0.2	167	0.2	1.0	15.2	14.1	15.1	3.8	0.7	0.6	0.9	0.2	0.93	16.5
66207	0.10	33.10	1620	1.9	8.8	3.7	42	-	8.7	-	1120	6.4	0.2	134	0.2	0.9	15.1	13.3	13.4	3.7	0.7	0.4	1.0	0.2	0.88	15.4
6630	0.12	33.50	1920	1.8	4.2	2.7	39	-	11.1	-	986	0.2	0.1	172	0.1	0.9	14.6	13.0	14.2	3.9	0.6	0.4	1.0	0.2	0.89	15.2
UDT:																										
66413	0.10	29.60	3260	2.8	8.5	15.7	19	3.9	6.5	-	1110	0.8	0.3	2120	0.3	1.6	15.4	18.4	12.5	3.6	0.6	0.5	1.3	0.2	1.19	12.0
LDT:																										
6653	0.19	26.80	5230	4.1	10.3	9.2	45	-	13.5	-	921	0.6	0.3	673	0.4	2.3	22.5	29.0	20.3	5.7	1.0	0.6	1.5	0.2	1.29	15.2
6667	0.12	28.90	3230	2.1	5.8	6.6	29	2.5	10.7	-	1120	4.7	0.2	635	0.2	1.4	19.4	17.3	15.2	4.2	0.6	0.5	0.9	0.1	1.12	16.4
1W:																										
668011	0.13	20.70	3000	1.9	7.0	3.5	54	-	8.1	-	891	0.5	0.1	1370	0.2	1.1	13.3	14.9	11.1	3.7	0.6	0.4	0.9	0.1	1.12	14.5
2W:																										
6692	0.11	34.40	1800	1.0	3.6	2.6	28	-	10.9	-	875	0.2	0.1	595	0.1	0.4	9.5	7.4	6.7	2.1	0.4	0.3	0.5	0.1	0.78	17.9
6700	0.11	34.00	1790	1.1	4.0	5.9	25	-	13.5	3	1240	0.4	0.1	90	0.1	0.3	10.6	7.9	8.0	2.3	0.4	0.3	0.7	0.1	0.75	15.8
6717	0.13	36.20	480	0.6	4.0	0.8	17	-	9.2	-	1350	-	-	81	0.0	0.1	7.5	4.1	5.0	1.4	0.2	0.2	0.6	0.1	0.55	12.9
3W:																										
6751	0.21	35.50	551	0.8	5.4	0.8	15	-	22.7	-	1030	-	0.1	144	0.1	0.2	7.8	5.6	4.7	1.6	0.3	0.2	0.6	0.1	0.72	13.5
4W:																										
67817	0.14	37.40	375	0.8	4.8	7.9	23	-	17.2	-	1300	-	-	40	0.1	0.2	7.8	5.2	7.8	1.6	0.3	0.2	0.6	0.1	0.67	14.2
67956	0.15	36.60	253	0.4	3.1	0.6	20	-	19.5	-	1260	-	-	101	0.0	0.1	5.8	3.4	4.6	1.7	0.2	0.2	0.4	0.1	0.59	13.8
68050	0.26	35.20	237	0.4	2.6	1.9	21	-	37.0	-	1360	-	-	245	0.0	-	5.0	2.6	3.6	1.4	0.2	0.1	0.4	0.1	0.52	12.8
Other samples:																										
Bryozoan chalk, onshore (Stevns)																										
	0.07	38.20	803	0.7	1.6	1.7	38	-	4.0	-	70*	0.3	-	-	0.1	0.4	7.7	4.4	6.3	1.6	0.3	0.2	0.6	0.1	0.57	14.0
Grey chalk, onshore (Stevns)																										
	0.02	37.40	294	0.6	1.6	1.0	23	-	1.0	-	860	-	0.1	-	0.1	0.2	8.2	3.8	5.9	1.4	0.2	0.2	0.5	0.1	0.61	12.1
White chalk, onshore (Stevns)																										
	0.03	37.00	330	0.7	2.4	1.2	37	-	1.1	-	1100	-	0.1	-	0.1	0.2	7.3	4.6	6.1	1.5	0.3	0.2	0.6	0.1	0.63	12.6
Stylolite																										
	0.47	23.10	10700	5.0	25.2	27.5	220	12.7	40.1	38	1260	2.2	1.9	1420	2.0	12.5	116	103	150	34.1	5.9	3.8	5.8	0.9	0.89	20.0

APPENDIX V

Analytical Results for Samples from Drill Core E-1x Obtained by INAA. Some Data Are by XRF.

Element	Depth (feet) 6734 UDP1	6737	6738-5	6742-5	6744-5	6749 UDP2
Na(%)	0.45	0.26	0.25	0.32	0.29	0.20
K (%)	0.57	0.15	-	-	-	-
Ca(%)	17.20	32.50	31.30	36.10	33.50	34.30
Fe(%)	1.08	1.41	0.26	0.19	0.29	0.22
Al(%)XRF	0.51	0.38	0.26	0.18	0.26	0.16
Ti(ppm)XRF	1370	170	130	80	120	78
Mn(ppm)XRF	2050	4390	3590	3170	3050	1610
Fe(%)XRF	1.08	0.53	0.18	0.12	0.18	0.15
Si(%)XRF	18.9	7.7	9.9	3.7	5.1	2.9
Rb(ppm)XRF	19	3	3	3	3	2
Zr(ppm)XRF	30	6	5	3	4	3
Zn(ppm)XRF	51	32	24	36	27	33
Cu(ppm)XRF	12	10	8	9	11	12
V(ppm)XRF	35	-	-	-	-	-
Sc(ppm)	5.1	2.3	1.7	2.0	2.9	1.5
Cr(ppm)	25.0	7.0	5.6	6.5	7.4	4.8
Co(ppm)	3.6	1.5	1.2	8.2	2.4	2.9
Zn(ppm)	30.6	24.6	22.8	16.2	18.1	34.6
As(ppm)	6.6	7.3	-	2.7	0.8	1.5
Br(ppm)	17.2	26.8	34.9	41.1	35.1	29.5
Rb(ppm)	25.5	5.3	4.8	3.6	4.4	3.0
Sr(ppm)	897	1290	1260	1570	1580	1510
Sb(ppm)	0.3	0.2	0.1	0.2	0.1	0.1
Cs(ppm)	1.4	0.3	0.2	0.1	0.2	0.1
Ba(ppm)	300	184	644	164	182	128
Hf(ppm)	1.1	0.3	0.2	0.1	0.2	0.1
Ta(ppm)	0.2	-	-	-	-	-
Au(ppb)	-	-	-	-	-	-
Th(ppm)	3.4	0.9	0.8	0.6	0.8	0.5
U (ppm)	3.1	1.1	2.7	2.1	1.7	1.5
U DNC	0.80	0.43	0.39	0.21	0.24	0.20
La(ppm)	22.9	12.7	10.8	9.6	12.9	10.0
Ce(ppm)	37.3	21.8	14.3	15.4	19.6	13.3
Nd(ppm)	20.4	8.7	10.6	10.8	12.1	10.2
Sm(ppm)	4.4	2.4	2.2	2.4	2.9	2.3
Eu(ppm)	0.9	0.5	0.4	0.5	0.6	0.5
Tb(ppm)	0.6	0.4	0.3	0.4	0.4	0.4
Yb(ppm)	1.4	1.0	0.9	1.0	1.4	1.0
Lu(ppm)	0.2	0.2	0.1	0.1	0.1	0.1

Element	Depth (feet) 6753-5 UDP2	6758	6760-5	6763	6767 LDP	6770
Na(%)	0.24	0.21	0.19	0.22	0.17	0.25
K (%)	-	-	-	-	-	-
Ca(%)	32.10	35.00	36.10	35.90	34.20	13.90
Fe(%)	0.36	0.26	0.22	0.15	0.13	0.12
Al(%)XRF	0.37	0.23	0.17	0.10	0.13	0.09
Ti(ppm)XRF	193	120	79	55	60	70
Mn(ppm)XRF	2290	1770	1670	1520	1560	1040
Fe(%)XRF	0.24	0.20	0.18	0.10	0.11	0.10
Si(%)XRF	7.2	3.5	2.8	2.1	2.3	21.2
Rb(ppm)XRF	4	2	-	-	-	1
Zr(ppm)XRF	5	4	3	3	3	5
Zn(ppm)XRF	29	27	53	40	33	29
Cu(ppm)XRF	14	12	10	11	9	9
V(ppm) XRF	6	-	-	-	-	-
Sc(ppm)	2.7	2.4	2.3	1.1	1.7	0.7
Cr(ppm)	9.4	4.6	5.3	3.6	4.3	2.8
Co(ppm)	3.0	3.0	2.4	2.0	8.5	2.4
Zn(ppm)	-	21.4	87.4	47.5	9.3	10.4
As(ppm)	1.9	2.1	1.9	1.2	2.3	1.8
Br(ppm)	28.1	35.2	26.0	35.5	31.0	26.5
Rb(ppm)	6.6	3.4	2.3	-	-	1.3
Sr(ppm)	1360	1500	1600	1490	1400	645
Sb(ppm)	0.1	0.1	0.2	0.2	0.1	0.1
Cs(ppm)	0.3	0.2	0.1	0.1	0.1	0.1
Ba(ppm)	154	145	150	136	139	214
Hf(ppm)	0.3	0.1	0.1	0.1	0.1	0.1
Ta(ppm)	-	-	-	-	-	-
Au(ppb)	-	-	-	-	-	-
Th(ppm)	0.9	0.7	0.6	0.4	0.5	0.5
U (ppm)	1.1	0.7	1.6	0.3	2.6	2.4
U DNC	0.35	0.23	0.21	0.14	0.24	0.11
La(ppm)	12.5	11.7	14.8	7.2	10.1	5.1
Ce(ppm)	20.9	16.3	16.2	9.3	13.0	7.0
Nd(ppm)	14.4	12.6	14.7	8.6	9.7	3.9
Sm(ppm)	2.9	2.7	2.9	2.0	2.7	1.5
Eu(ppm)	0.6	0.5	0.6	0.3	0.5	0.3
Tb(ppm)	0.5	0.5	0.5	0.3	0.4	0.2
Yb(ppm)	1.2	1.3	1.3	0.7	1.1	0.4
Lu(ppm)	0.1	0.1	0.1	0.1	0.1	0.1

Element	Depth (feet) 6774 LDP	6780-5	6783	6795	6798-5	6800-4
Na(%)	0.18	0.22	0.15	0.13	0.18	0.19
K (%)	-	-	-	-	-	-
Ca(%)	35.50	34.70	35.10	32.90	32.30	34.90
Fe(%)	0.19	0.25	0.18	0.27	0.22	0.24
Al(%)XRF	0.12	0.20	0.14	0.33	0.28	0.25
Ti(ppm)XRF	57	105	78	140	137	105
Mn(ppm)XRF	1340	1170	1180	1410	1250	1420
Fe(%)XRF	0.12	0.15	0.12	0.20	0.15	0.17
Si(%)XRF	2.6	4.7	4.3	8.7	10.0	5.6
Rb(ppm)XRF	-	2	-	2	3	2
Zr(ppm)XRF	2	4	3	5	6	4
Zn(ppm)XRF	26	39	34	26	24	21
Cu(ppm)XRF	[illegible]	7	9	6	8	6
V(ppm)XRF	-	2	1	3	-	-
Sc(ppm)	1.3	2.1	1.9	2.8	2.5	3.1
Cr(ppm)	3.3	3.8	4.2	5.5	6.3	4.4
Co(ppm)	3.9	13.5	4.2	4.6	3.8	3.6
Zn(ppm)	22.2	40.0	34.5	-	-	-
As(ppm)	1.8	2.8	1.2	1.1	1.4	1.4
Br(ppm)	35.3	33.3	31.0	16.7	30.5	26.3
Rb(ppm)	1.3	5.3	2.9	4.1	4.7	3.5
Sr(ppm)	1590	1430	1420	1300	1260	1340
Sb(ppm)	[illegible]	0.2	0.2	0.2	0.2	0.2
Cs(ppm)	0.1	0.2	0.1	0.2	0.2	0.2
Ba(ppm)	130	144	157	202	[illegible]82	139
Hf(ppm)	0.1	0.2	0.1	0.2	0.2	0.2
Ta(ppm)	-	-	-	-	-	-
Au(ppb)	-	-	-	-	-	2.4
Th(ppm)	0.6	1.3	1.1	1.8	1.7	1.2
U (ppm)	2.0	2.0	1.9	0.9	0.8	0.8
U DNC	0.12	0.16	0.20	0.14	0.13	0.12
La(ppm)	9.0	11.7	11.5	15.3	13.6	16.4
Ce(ppm)	11.1	15.6	14.4	23.2	22.1	23.5
Nd(ppm)	8.9	12.2	8.9	18.6	15.5	16.9
Sm(ppm)	2.2	3.0	3.0	4.3	4.2	4.8
Eu(ppm)	0.4	0.6	0.5	0.7	0.7	0.8
Tb(ppm)	0.3	0.4	0.4	0.6	0.5	0.6
Yb(ppm)	0.8	0.1	1.0	1.5	1.2	1.6
Lu(ppm)	0.1	0.1	0.1	0.2	0.1	0.2

Element	Depth (feet) 6802 LDP	6807-5	6810	6812-5 UDT	6816	6820
Na(%)	0.19	0.13	0.14	0.18	0.21	0.16
K (%)	-	-	-	-	-	-
Ca(%)	31.00	31.50	27.30	31.00	25.80	31.50
Fe(%)	0.22	0.44	0.28	0.36	0.35	0.36
Al(%)XRF	0.30	0.30	0.28	0.42	0.40	0.56
Ti(ppm)XRF	170	150	136	194	247	-
Mn(ppm)XRF	1215	1680	1610	1540	1230	-
Fe(%)XRF	0.16	0.24	0.20	0.26	0.29	0.28
Si(%)XRF	11.6	11.4	18.3	13.8	22.1	10.7
Rb(ppm)XRF	2	3	2	4	3	4
Zr(ppm)XRF	7	4	4	6	8	6
Zn(ppm)XRF	27	37	22	37	33	19
Cu(ppm)XRF	10	11	6	14	16	9
V(ppm)XRF	-	4	-	3	4	10
Sc(ppm)	2.8	3.5	2.5	4.0	3.8	3.8
Cr(ppm)	5.9	5.4	5.9	5.5	6.0	5.8
Co(ppm)	10.8	5.8	4.5	6.9	12.7	6.7
Zn(ppm)	-	-	-	-	-	-
As(ppm)	-	3.4	3.1	1.3	1.9	-
Br(ppm)	19.7	11.4	16.1	15.3	13.2	12.8
Rb(ppm)	5.4	4.7	4.2	5.5	6.6	6.5
Sr(ppm)	1180	1410	1210	1280	1180	1430
Sb(ppm)	0.2	0.4	0.7	0.4	0.6	0.3
Cs(ppm)	0.2	0.2	0.2	0.3	0.2	0.3
Ba(ppm)	197	208	283	241	336	198
Hf(ppm)	0.3	0.3	0.2	0.3	0.4	0.3
Ta(ppm)	-	-	-	-	-	-
Au(ppb)	-	-	-	-	-	-
Th(ppm)	1.7	1.7	1.4	2.4	2.8	2.6
U (ppm)	0.6	0.9	0.8	0.9	0.8	0.8
U DNC	0.13	0.14	0.12	0.15	0.25	0.17
La(ppm)	15.5	15.8	13.1	16.3	18.7	17.6
Ce(ppm)	25.4	27.7	21.5	31.4	37.0	32.3
Nd(ppm)	20.0	18.4	15.8	18.3	19.0	19.4
Sm(ppm)	4.9	4.8	3.9	4.9	5.9	5.3
Eu(ppm)	0.8	0.8	0.7	0.8	1.0	0.9
Tb(ppm)	0.5	0.7	0.5	0.5	0.7	0.7
Yb(ppm)	1.4	1.6	1.3	1.6	1.7	1.6
Lu(ppm)	0.2	0.2	0.2	0.2	0.2	0.2

Element	Depth (feet) 6822 UDT	6826-3	6829	6833-5 LDT1	6836-5	6841
Na(%)	0.22	0.24	0.19	0.26	0.22	0.21
K (%)	-	-	-	-	-	-
Ca(%)	25.60	21.90	30.30	34.70	24.60	31.50
Fe(%)	1.19	0.25	0.27	0.19	0.60	0.39
Al(%)XRF	0.32	0.50	0.36	0.17	0.35	0.34
Ti(ppm)XRF	158	237	140	88	151	155
Mn(ppm)XRF	1440	1290	1250	1050	910	870
Fe(%)XRF	0.29	0.25	0.20	0.13	0.34	0.28
Si(%)XRF	22.2	16.4	14.8	5.8	9.4	12.2
Rb(ppm)XRF	2	4	3	1	2	3
Zr(ppm)XRF	5	7	4	3	4	4
Zn(ppm)XRF	30	31	21	25	36	29
Cu(ppm)XRF	8	8	8	12	8	10
V(ppm)XRF	-	6	-	-	6	5
Sc(ppm)	3.2	4.8	2.3	2.2	3.0	3.5
Cr(ppm)	4.0	4.7	10.4	16.4	9.7	9.5
Co(ppm)	25.5	7.1	3.5	2.1	38.7	2.5
Zn(ppm)	-	-	-	-	-	-
As(ppm)	46.0	-	-	1.0	9.9	1.1
Br(ppm)	18.3	21.4	16.6	26.6	26.4	24.6
Rb(ppm)	7.1	5.0	3.7	3.3	4.0	4.5
Sr(ppm)	1160	1120	1420	1590	1530	1340
Sb(ppm)	0.9	0.3	0.3	0.2	0.6	0.3
Cs(ppm)	0.2	0.2	0.2	0.1	0.2	0.3
Ba(ppm)	302	216	202	159	165	166
Hf(ppm)	0.2	0.3	0.2	0.2	0.2	0.2
Ta(ppm)	-	-	-	-	-	-
Au(ppb)	-	-	-		-	-
Th(ppm)	2.1	2.7	1.6	1.3	2.2	1.6
U (ppm)	0.4	0.5	0.7	0.8	0.5	0.7
U DNC	0.11	0.17	0.13	0.10	0.16	0.15
La(ppm)	12.5	19.8	13.1	14.2	16.5	17.6
Ce(ppm)	25.3	29.1	25.2	19.9	28.5	28.7
Nd(ppm)	16.6	21.0	15.7	15.1	16.6	18.9
Sm(ppm)	3.8	6.2	3.8	4.0	4.6	5.4
Eu(ppm)	0.6	0.9	0.7	0.7	0.9	0.9
Tb(ppm)	0.4	0.7	0.5	0.5	0.7	0.7
Yb(ppm)	1.3	1.5	1.2	1.3	1.3	1.8
Lu(ppm)	0.2	0.2	0.1	0.1	0.2	0.2

Element	Depth (feet) 6846 LDT1	6848-5	6852 LDT2	6855	6857	6861
Na(%)	0.15	0.19	0.25	0.12	0.19	0.19
K (%)	-	-	-	-	-	-
Ca(%)	31.50	26.10	26.20	34.20	27.30	33.90
Fe(%)	0.29	0.35	0.32	0.23	0.21	0.23
Al(%)XRF	0.28	0.76	0.37	0.19	0.33	0.25
Ti(ppm)XRF	119	266	139	58	129	107
Mn(ppm)XRF	710	880	870	990	1030	1250
Fe(%)XRF	0.20	0.30	0.20	0.13	0.13	0.16
Si(%)XRF	12.5	[illegible]	7.8	8.3	13.6	8.3
Rb(ppm)XRF	2	3	2	1	2	2
Zr(ppm)XRF	4	8	5	2	4	2
Zn(ppm)XRF	32	53	37	26	27	28
Cu(ppm)XRF	10	30	16	10	9	15
V(ppm)XRF	3	11	-	-	-	-
Sc(ppm)	2.5	4.0	2.3	1.7	2.6	2.4
Cr(ppm)	9.8	10.2	11.5	11.7	10.8	11.4
Co(ppm)	15.2	3.1	27.1	2.5	7.6	3.9
Zn(ppm)	-	-	-	-	-	-
As(ppm)	3.1	1.1	4.5	1.4	1.2	1.5
Br(ppm)	27.0	9.4	22.5	15.7	14.2	15.4
Rb(ppm)	2.9	7.0	3.7	2.0	3.4	3.0
Sr(ppm)	1540	1490	1760	1560	1290	1060
Sb(ppm)	0.4	0.4	0.4	0.2	0.3	0.2
Cs(ppm)	0.2	0.2	0.2	0.1	0.1	0.1
Ba(ppm)	201	146	149	174	190	204
Hf(ppm)	0.2	0.4	0.3	0.1	0.2	0.2
Ta(ppm)	-	-	-	-	-	-
Au(ppb)	-	-	-	-	-	-
Th(ppm)	1.8	2.3	2.4	1.0	1.4	1.5
U (ppm)	0.4	0.5	0.6	0.7	0.7	0.6
U DNC	0.11	0.23	0.15	0.12	0.13	0.13
La(ppm)	14.5	22.6	17.2	12.1	13.9	15.3
Ce(ppm)	20.7	35.2	30.4	17.3	23.2	21.2
Nd(ppm)	15.0	23.1	17.9	14.2	14.6	16.5
Sm(ppm)	4.2	6.4	4.8	3.5	4.1	4.3
Eu(ppm)	0.7	1.0	0.9	0.6	0.7	0.7
Tb(ppm)	0.6	0.8	0.6	0.5	0.5	0.5
Yb(ppm)	1.3	1.8	1.3	1.1	1.2	1.5
Lu(ppm)	0.2	0.2	0.2	0.1	0.1	0.2

Element	Depth (feet) 6064-5 LD72	6066	6068-4	6072	6076-4 3M	6079-6
Na(%)	0.16	0.23	0.14	0.78	0.12	0.10
K (%)	-	-	-	0.57	-	-
Ca(%)	25.90	18.00	35.00	12.63	38.13	38.20
Fe(%)	0.27	0.57	0.80	2.02	0.09	0.10
Al(%)XRF	0.26	0.74	0.46	-	0.29	0.08
Ti(ppm)XRF	134	306	186	31	38	36
Mn(ppm)XRF	1280	1150	1160	570	540	490
Fe(%)XRF	0.72	0.44	0.31	-	0.06	0.07
Si(%)XRF	12.3	15.3	5.2	-	1.3	1.3
Rb(ppm)XRF	1	5	3	-	-	2
Zr(ppm)XRF	-	7	3	-	1	3
Zn(ppm)XRF	26	50	49	-	17	24
Cu(ppm)XRF	8	16	9	-	4	10
V(ppm)XRF	-	12	5	-	-	-
Sc(ppm)	2.4	4.6	4.2	12.7	1.5	1.9
Cr(ppm)	9.3	15.8	11.4	34.3	12.0	11.9
Co(ppm)	2.2	12.2	15.9	34.0	0.6	1.1
Zn(ppm)	-	-	-	-	-	-
As(ppm)	-	1.2	24.0	4.8	-	0.5
Br(ppm)	12.1	31.4	13.4	21.2	17.2	11.5
Rb(ppm)	2.9	7.3	3.9	36.7	1.6	1.7
Sr(ppm)	1630	1590	1060	1280	1450	1530
Sb(ppm)	0.2	0.6	0.7	2.6	0.1	0.1
Cs(ppm)	0.1	0.3	0.2	1.5	0.1	0.1
Ba(ppm)	125	246	124	260	76	89
Hf(ppm)	0.2	5.4	0.3	2.2	0.1	0.1
Ta(ppm)	-	0.1	-	-	-	-
Au(ppb)	-	-	-	-	-	-
Th(ppm)	1.5	3.7	2.4	12.1	0.3	0.4
U (ppm)	0.4	1.2	0.9	3.3	0.5	1.2
U DNC	0.13	0.37	0.23	1.03	0.41	0.63
La(ppm)	10.7	25.5	18.3	82.6	8.6	10.2
Ce(ppm)	18.9	52.4	34.4	155	9.8	11.7
Nd(ppm)	12.5	42.0	23.3	95.2	6.1	9.8
Sm(ppm)	3.3	7.1	5.1	25.1	2.3	2.7
Eu(ppm)	0.5	1.5	1.0	4.5	0.4	0.5
Tb(ppm)	0.4	1.1	0.8	3.3	0.3	0.4
Yb(ppm)	1.1	2.2	1.6	4.8	1.0	1.1
Lu(ppm)	0.1	0.2	0.2	0.7	0.1	0.1

Element	Depth (feet) 6081-6 1M	6090	6092-3	6096 2M	6098	6101
Na(%)	0.11	0.07	0.14	0.11	0.17	0.14
K (%)	-	-	-	-	-	-
Ca(%)	38.00	39.40	38.30	38.10	39.00	38.60
Fe(%)	0.13	0.37	0.07	0.07	0.08	0.06
Al(%)XRF	0.11	0.34	0.38	0.05	0.36	0.04
Ti(ppm)XRF	36	16	33	20	21	14
Mn(ppm)XRF	490	400	393	349	340	250
Fe(%)XRF	0.07	0.04	0.05	0.04	0.05	0.03
Si(%)XRF	1.2	0.6	0.9	0.6	0.6	0.4
Rb(ppm)XRF	2	-	-	-	-	-
Zr(ppm)XRF	-	-	-	-	-	-
Zn(ppm)XRF	40	21	19	27	20	22
Cu(ppm)XRF	10	11	8	6	7	10
V(ppm)XRF	-	-	-	-	-	-
Sc(ppm)	1.0	0.8	1.0	0.9	1.1	0.5
Cr(ppm)	8.9	9.4	8.7	9.3	10.9	9.6
Co(ppm)	3.8	0.5	0.7	3.5	0.7	0.6
Zn(ppm)	-	-	-	35	-	10
As(ppm)	0.6	1.6	-	-	-	-
Br(ppm)	19.0	10.3	21.3	24.6	22.1	23.7
Rb(ppm)	-	-	1.5	-	1.2	-
Sr(ppm)	1050	1630	1600	1710	1800	1050
Sb(ppm)	0.3	0.1	0.1	0.1	0.2	0.1
Cs(ppm)	0.1	-	-	-	0.1	-
Ba(ppm)	84	106	82	84	135	93
Hf(ppm)	0.1	-	0.1	-	0.1	-
Ta(ppm)	-	-	-	-	-	-
Au(ppb)	-	-	-	2.5	-	-
Th(ppm)	0.4	0.2	0.3	0.2	0.2	0.2
U (ppm)	1.5	0.7	-	1.2	-	0.8
U DNC	1.02	0.35	0.49	0.63	0.76	0.40
La(ppm)	10.7	6.2	8.8	7.9	8.9	5.7
Ce(ppm)	11.8	6.2	9.2	7.5	8.3	5.2
Nd(ppm)	7.4	8.3	9.3	9.4	10.7	6.7
Sm(ppm)	2.9	1.7	2.4	2.0	2.4	1.3
Eu(ppm)	0.4	0.2	0.4	0.3	0.4	0.2
Tb(ppm)	0.3	0.2	0.3	0.2	0.3	0.2
Yb(ppm)	1.1	0.7	0.9	0.9	1.9	0.6
Lu(ppm)	0.1	0.1	0.1	0.1	0.1	0.1

APPENDIX VI

Well-Logging Data for TWB-8. Depth Is in Feet, Asterix (*) Gives the Average Value of Two Neighbouring Values, and Values in Parenthesis Suggest Overflow.

Depth	GR (GAPI)	SP (mV)	NPHI (%)	ILM (Ohm m)	ILD (Ohm m)	CILD (m mho)	SFLA (Ohm m)
UOP1							
6594.00	6.63	254	0.315	110	(2000)	-7.29	8.00
6597.00	7.71	744	0.291	19.6	26.2	38.2	7.00
6599.50	8.04	231	0.261	32.2	24.2	41.3	7.27
6601.00	6.35	222	0.283	31.7	30.6	32.6	7.28
6602.00	6.61	233	0.288	33.4	23.5	42.5	7.48
UOP2							
6609.75*	7.48	230	0.262	11.8	13.8	73.4	4.76
6612.00	6.33	211	0.305	14.9	20.7	34.8	4.96
LSP							
6617.83*	5.92	215	0.284	9.14	9.37	107	2.00
6619.00	6.64	208	0.293	8.90	10.6	93.9	2.75
6620.50*	7.05	199	0.307	8.90	9.67	104	2.60
6623.25*	7.45	201	0.303	7.14	6.74	149	2.35
6623.75*	7.45	201	0.303	7.14	6.72	149	2.35
6624.00	9.13	196	0.313	7.07	6.44	155	2.31
6627.00	10.5	104	0.202	11.5	12.9	77.6	2.29
6630.00	8.80	207	0.293	8.91	7.56	132	2.16
UOT							
6631.25*	9.29	223	0.272	6.27	6.27	160	2.12
6634.50	8.83	170	0.289	6.79	6.90	145	2.09
6637.00	8.00	180	0.261	6.41	5.13	195	1.97
6641.25*	8.32	182	0.272	10.3	7.45	135	2.03
6643.33*	8.10	208	0.285	9.20	5.83	172	2.24
6645.50	9.94	210	0.244	8.99	6.64	151	2.25
6648.33*	9.21	209	0.272	6.33	5.53	181	2.26
6650.83*	9.87	193	0.266	6.92	5.29	190	2.24
LOT1							
6653.00	6.91	192	0.293	8.87	6.61	151	2.31
6655.50	8.03	199	0.308	10.5	7.14	140	2.38
6657.83*	7.45	213	0.267	9.43	7.18	140	2.46
6660.67*	9.03	199	0.281	8.32	6.53	157	2.46
6663.50*	9.69	195	0.259	10.3	13.60	75.9	2.62
6663.57*	9.69	195	0.259	10.3	13.60	75.0	2.62
6667.00	9.43	234	0.270	7.35	8.05	124	2.39
LOT2							
6673.67*	8.74	184	0.244	(2000)	12.9	77.0	3.01
6676.42*	8.33	259	0.321	27.3	27.2	37.4	5.25
1W							
6680.30	7.98	230	0.220	12.6	13.2	75.9	4.76
6680.50	7.99	227	0.229	12.2	10.7	93.2	4.06
6680.92*	7.72	226	0.227	11.7	10.7	93.4	4.02
6686.00	8.60	241	0.259	20.0	18.7	53.4	4.95
6687.00	9.17	241	0.258	18.5	16.6	60.0	4.96
6688.00	9.98	240	0.243	16.1	12.5	80.0	5.10
6689.00	8.56	240	0.259	17.3	15.4	65.0	5.09
6690.00	6.90	236	0.231	20.8	13.6	73.7	5.01
6691.00	8.50	233	0.232	23.8	16.3	61.3	5.16
2W							
6692.00	10.8	234	0.243	37.5	14.8	67.4	5.21
6692.50	9.72	238	0.234	49.2	15.9	63.2	5.43
6693.00	9.17	241	0.233	45.2	15.4	64.8	5.52
6694.00	8.87	244	0.251	36.7	20.8	48.1	5.85
6695.00	9.12	249	0.273	24.7	17.4	57.5	6.22
6696.00	8.84	253	0.259	20.3	20.1	49.8	6.47
6697.00	8.31	251	0.255	25.9	20.0	50.0	6.39
6698.00	9.41	246	0.230	28.2	66.9	14.9	5.39
6699.00	7.73	238	0.248	34.3	(2000)	-15.5	6.09
6700.00	7.99	241	0.261	28.1	73.6	13.6	5.60
6701.00	8.54	244	0.215	14.6	20.1	49.8	4.98
6701.50	9.66	245	0.211	11.2	18.9	52.9	4.72
6702.30	8.32	242	0.206	11.3	14.6	68.3	4.52
6704.30	7.20	236	0.267	9.86	11.3	88.3	4.13
6704.50	8.05	221	0.245	12.3	8.53	116.3	3.96
6705.50	8.57	215	0.234	11.2	8.77	114.2	3.75
6707.30	7.46	211	0.266	13.5	11.8	84.4	3.71
6710.30	9.92	224	0.373	13.7	15.5	65.2	3.53
6711.00	9.66	219	0.390	13.9	30.6	32.7	3.36
6713.30	6.39	226	0.437	11.0	166	6.01	2.93
6714.30	7.77	228	0.412	9.41	17.2	58.1	2.59
6715.00	8.07	227	0.438	7.08	8.36	124	2.39
6716.00	9.42	224	0.443	7.33	10.1	99.3	2.17
6717.00	5.55	214	0.446	6.65	19.9	50.2	2.08
6718.00	5.29	199	0.445	5.22	107	9.31	1.96
6719.00	7.21	197	0.442	4.94	23.2	43.1	1.72
6719.50	7.75	194	0.455	4.43	10.4	96.6	1.59
6720.00	6.64	191	0.476	4.32	5.73	175	1.47
6721.00	5.51	178	0.467	3.56	4.12	242	1.32
6725.00	8.80	116	0.454	3.42	3.57	280	1.11
3W							
6727.50	5.83	134	0.398	2.64	2.73	366	0.984
6728.50	7.70	110	0.380	2.57	2.82	357	0.974
6729.00	8.80	103	0.400	2.44	2.84	347	0.947
6730.00	8.30	90	0.402	2.47	3.25	327	0.930
6730.20*	7.80	89	0.400	2.52	3.37	299	0.919
6733.50	9.70	73.7	0.454	2.22	2.47	404	0.797
6733.20*	9.29	76.3	0.467	2.16	2.31	435	0.786
6734.50	7.21	75.4	0.437	1.96	1.85	542	0.747
6736.00	7.73	54.4	0.379	1.93	1.84	533	0.727
6736.20*	8.15	49.9	0.390	2.31	1.85	543	0.727
6738.00	8.59	21.3	0.453	2.45	1.94	515	0.722
6739.00	9.04	21.4	0.433	2.41	2.12	471	0.722
6739.20*	7.90	28.1	0.419	2.33	2.29	478	0.724
6740.00	8.33	56.3	0.402	2.39	1.94	515	0.725
6741.50	7.15	71.2	0.403	2.21	2.17	460	0.738
6751.00	7.47	14.3	0.426	1.83	2.54	394	0.536
6752.00	6.35	1.8	0.400	1.92	2.34	426	0.520
6753.00	7.45	3.3	0.37[illegible]	1.94	2.35	423	0.538
6754.50	4.99	19.8	0.370	1.81	2.10	476	0.497
6755.63*	6.66	17.1	0.374	1.73	1.73	580	0.488
6756.46*	7.35	10.1	0.394	1.53	1.67	605	0.486
6757.50	5.54	4.9	0.440	1.60	1.80	556	0.486
6758.58*	6.65	-1.34	0.416	1.72	1.75	572	0.490
6759.58*	6.94	-9.65	0.411	1.71	1.78	562	0.490
6760.58*	6.03	-6.50	0.397	1.61	1.84	545	0.488
6761.63*	6.08	-2.23	0.427	1.54	1.73	579	0.485
6762.50	6.35	-4.46	0.399	1.49	1.62	618	0.482
6764.50	9.13	-29.5	0.457	1.44	1.63	615	0.474
6765.50	6.94	-42.0	0.459	1.40	1.70	588	0.471
6766.58*	6.70	-41.7	0.424	1.38	1.77	566	0.463
4W							
6767.58*	6.91	-51.9	0.384	1.39	1.73	578	0.454
6767.59*	6.51	-51.9	0.384	1.38	1.73	578	0.444
6768.58*	7.18	-60.4	0.384	1.37	1.54	609	0.444
6770.50	7.74	-65.3	0.396	1.17	1.33	755	0.429
6771.50	6.89	-71.6	0.361	1.17	1.28	784	0.422
6772.63*	7.30	-97.1	0.431	1.22	1.31	763	0.418
6773.50	5.77	-117	0.424	1.25	1.35	740	0.416
6776.67*	7.91	-98.2	0.434	1.18	1.45	694	0.406
6777.46*	7.35	-97.1	0.461	1.17	1.42	707	0.404
6778.54*	6.35	-113	0.410	1.12	1.41	712	0.397
6779.50	7.46	-116	0.441	1.10	1.44	595	0.395

Continued

Depth	GR (GAPI)	SP (mV)	NPHI (%)	ILM (Ohm m)	ILD (Ohm m)	CILD (m mho)	SFLA (Ohm m)
6700.46"	7.94	-126	0.447	1.11	1.46	686	0.391
6701.50"	6.64	-137	0.440	1.11	1.33	754	0.382
6703.54"	8.13	-140	0.431	1.13	1.29	781	0.372
6704.54"	8.96	-142	0.407	1.12	1.28	781	0.371
6706.00	6.39	-142	0.398	1.20	1.26	795	0.371
6707.50"	8.30	-134	0.410	1.13	1.41	708	0.380
6708.50"	7.19	-145	0.407	1.17	1.33	756	0.367
6790.25"	8.45	-143	0.425	1.12	1.01	990	0.364
6792.46"	5.95	-116	0.423	1.12	0.92	1080	0.376
6793.33"	7.90	-132	0.405	1.20	1.11	907	0.380
6794.33"	7.90	-151	0.420	1.45	1.36	739	0.401
6795.50	8.02	-127	0.443	1.49	1.49	680	0.400
6796.42"	8.33	-92.6	0.427	1.41	1.37	733	0.411
6798.33"	7.63	-35.0	0.426	1.17	1.02	980	0.419
6802.17"	7.91	-120	0.413	1.54	1.22	824	0.452
6803.33"	6.92	-99.0	0.416	1.45	1.24	802	0.462
6804.29"	6.40	-65.2	0.443	1.40	1.39	725	0.472
6805.50	8.06	-30.2	0.462	1.41	3.02	331	0.402
6806.42"	7.00	-33.6	0.400	1.42	3.47	290	0.475
6807.54"	9.07	-53.1	0.363	1.60	4.10	244	0.440
SW:							
6809.50"	7.30	-45.7	0.414	1.92	2.26	459	0.403
6810.33"	8.26	-47.2	0.427	1.70	1.83	546	0.402

Depth	RHOB (g/cm^3)	PEF	DT (us/f)	LITH (cps)	AMPL (mV)	RHGX (g/cm^3)
UDP1:						
6594.00	1.77	6.39	147	165	2.75	2.47
6597.00	1.74	5.86	140	179	3.68	2.43
6599.50	1.74	5.59	147	184	2.37	2.41
6601.00	1.75	5.59	149	181	2.46	2.44
6602.00	1.77	5.70	149	172	2.97	2.45
UDP2:						
6609.75*	1.79	7.36	120	149	0.878	2.46
6613.00	1.78	6.46	133	164	2.59	2.47
LDP:						
6617.83*	1.89	6.25	121	135	1.77	2.50
6619.00	1.90	6.60	122	129	1.92	2.54
6620.58*	1.88	6.82	133	130	2.06	2.54
6623.25*	1.95	7.61	123	107	1.15	2.58
6623.26*	1.95	7.61	123	107	1.15	2.58
6624.00	1.98	6.71	119	99.8	0.971	2.60
6627.00	1.92	6.55	105	123	1.07	2.54
6630.00	2.00	6.70	94.8	108	1.39	2.60
UDT:						
6631.25*	2.05	6.71	99.8	96.7	1.41	2.61
6634.50	2.17	7.26	93.0	76.8	1.65	2.69
6637.00	2.23	6.44	95.6	68.3	1.36	2.69
6641.25*	2.20	6.32	87.0	74.7	0.550	2.69
6643.33*	2.17	6.28	96.9	83.3	0.930	2.68
6645.50	2.22	6.21	107	69.4	1.59	2.67
6648.33*	2.24	7.22	112	68.0	1.65	2.71
6650.83*	2.11	6.47	118	79.7	2.03	2.64
LDT1:						
6653.00	2.02	6.36	120	106	2.68	2.61
6655.50	2.01	6.28	120	104	2.01	2.61
6657.83	1.99	6.31	113	114	2.02	2.57
6660.67	1.97	6.46	122	117	1.29	2.57
6663.58	2.02	6.59	115	104	1.68	2.56
6663.67*	2.02	6.59	115	104	1.68	2.56
6667.00	1.92	6.30	121	121	1.20	2.54
LDT2:						
6673.67*	1.96	6.71	109	119	1.86	2.53
6676.42*	2.02	7.00	121	103	3.52	2.63
1M:						
6680.00	2.13	7.25	129	79.9	2.65	2.60
6680.50	2.06	7.41	129	88.8	2.46	2.58
6680.92	2.05	7.47	128	91.8	2.88	2.57
6685.00	1.91	6.79	122	117	1.01	2.52
6687.00	1.88	6.05	141	126	4.06	2.50
6688.00	1.90	6.72	135	132	2.18	2.49
6689.00	1.88	6.11	135	132	3.09	2.49
6690.00	1.88	6.59	135	136	2.68	2.47
6691.00	1.88	6.89	135	131	1.86	2.48
2M:						
6692.00	1.89	6.33	138	129	2.42	2.49
6692.50	1.88	6.30	141	133	3.51	2.47
6693.00	1.85	6.58	142	144	3.54	2.46
6694.00	1.82	6.59	143	148	2.97	2.46
6695.00	1.82	6.67	144	147	2.64	2.47
6696.00	1.81	6.62	147	148	1.74	2.46
6697.00	1.82	6.60	145	150	2.75	2.45
6698.00	1.80	6.73	144	150	0.379	2.42
6699.00	1.78	6.51	142	156	0.786	2.42
6700.00	1.75	6.43	143	166	1.28	2.42
6701.00	1.76	6.11	146	166	1.29	2.38
6701.50	1.77	5.93	145	165	2.97	2.38
6702.00	1.78	5.90	144	165	2.13	2.28
6704.00	1.76	6.27	143	166	2.10	2.43
6704.50	1.75	6.51	142	170	2.68	2.40
6705.50	1.77	6.30	139	161	3.41	2.41
6707.00	1.81	6.48	134	153	2.10	2.46
6710.00	1.86	6.19	144	144	3.54	2.57
6711.00	1.87	6.15	141	141	3.54	2.59
6713.00	1.88	6.91	142	136	3.10	2.65
6714.00	1.88	6.75	138	130	2.51	2.62
6715.00	1.89	6.21	133	131	3.61	2.65
6716.00	1.86	6.27	133	144	4.10	2.63
6717.00	1.85	6.43	134	145	3.90	2.63
6718.00	1.86	6.39	136	140	4.14	2.64
6719.00	1.87	6.41	133	139	3.77	2.64
6719.50	1.86	6.36	132	139	3.78	2.65
6720.00	1.85	6.19	130	139	3.55	2.67
6721.00	1.89	6.45	122	134	1.25	2.69
6725.00	1.90	6.79	124	126	4.84	2.70
3M:						
6727.50	1.96	6.57	123	113	3.59	2.66
6728.50	1.97	6.23	126	112	3.66	2.65
6729.00	1.98	6.16	127	113	3.78	2.68
6730.00	1.96	6.41	130	118	4.21	2.67
6730.20*	1.96	6.50	131	118	4.36	2.67
6733.00	1.99	6.68	130	108	4.21	2.77
6733.20*	1.99	6.65	136	109	4.21	2.76
6734.50	1.99	6.96	130	109	3.74	2.73
6736.00	1.99	6.58	123	110	3.28	2.66
6736.20*	1.99	6.54	122	111	3.40	2.67
6738.00	1.96	6.61	119	116	4.29	2.74
6739.00	1.95	6.44	120	117	3.98	2.70
6739.20*	1.95	6.54	120	120	3.60	2.68
6740.00	1.94	6.55	120	120	4.05	2.65
6741.50	1.98	7.15	117	110	4.03	2.68
6751.00	2.02	6.80	124	102	4.74	2.75
6752.00	2.06	7.31	125	95.6	5.29	2.74
6753.00	2.06	7.21	123	91.4	4.63	2.71
6754.50	2.04	6.68	121	99.3	5.45	2.68
6755.63*	2.03	7.01	120	100	5.34	2.69
6756.46*	2.04	7.33	120	99.1	5.39	2.72
6757.50	2.04	7.36	118	97.0	5.32	2.80
6758.58*	2.01	6.79	118	103	3.89	2.72
6759.58*	2.03	7.57	116	101	4.69	2.74
6760.58*	2.04	7.10	117	96.3	4.57	2.71
6761.63*	2.03	7.04	118	99.3	4.55	2.78
6762.50	2.03	7.02	116	99.7	4.12	2.71
6764.50	2.03	6.90	120	103	5.18	2.83
6765.50	2.02	7.22	120	99.4	4.71	2.83
6766.58*	2.07	7.73	123	90.5	4.73	2.80
4M						
6767.58*	2.06	6.91	121	89.5	5.03	2.72
6767.59*	2.06	6.91	121	89.5	5.03	2.72
6768.58*	2.08	7.34	123	92.2	4.79	2.73
6770.50*	2.02	6.80	124	100	4.63	2.70
6771.50	2.03	6.54	125	102	4.68	2.67
6772.63*	2.02	6.86	124	105	4.75	2.75
6773.50	1.99	6.90	124	107	4.36	2.72
6776.67*	2.00	6.85	126	109	4.95	2.69
6777.46*	2.00	6.90	126	107	5.07	2.81
6778.54*	2.01	6.98	127	106	5.23	2.71
6779.50	2.01	6.88	127	102	4.94	2.78
6780.46*	2.01	6.67	127	105	5.01	2.78

Depth	RHOB (g/cm^3)	PEF	DT (us/f)	LITH (cps)	AMPL (mV)	RHGX (g/cm^3)
6781.58*	1.99	6.65	128	112	5.15	2.74
6783.54*	2.00	6.63	127	109	5.16	2.74
6784.54*	2.01	6.60	127	107	5.75	2.71
6786.00	1.98	6.63	128	111	5.36	2.68
6787.58*	1.99	6.66	128	112	5.77	2.70
6788.58*	1.98	7.13	128	112	5.17	2.69
6790.25*	1.97	6.75	128	110	5.11	2.70
6792.46*	1.97	6.82	129	113	5.58	2.70
6793.33*	1.96	6.78	125	113	5.40	2.74
6794.33*	1.98	7.14	122	110	4.06	2.76
6795.50	1.99	7.04	117	106	4.56	2.75
6796.42*	1.98	7.03	119	109	4.27	2.69
6798.33*	1.97	6.76	124	113	5.27	2.70
6802.17*	2.06	7.01	115	94.6	4.97	2.77
6803.33*	2.01	6.62	115	103	5.17	2.72
6804.29*	1.99	6.68	119	109	5.18	2.75
6805.50	1.96	7.75	116	109	5.54	2.67
6806.42*	2.01	7.99	114	104	5.39	2.69
6807.54*	2.06	8.31	115	87.9	4.73	2.69
SH:						
6809.58*	2.06	9.35	115	88.9	5.23	2.77
6810.33*	2.06	10.4	116	88.6	5.51	2.79

APPENDIX VII

Well-Logging Data for E-1x. Depth in Feet.

Depth	GR (GAPI)	CALI (inch)	DT (us/f)	RHOB (g/cm^3)	SNP (PU)	SP (mV)	SN (Ohm m)	IL (Ohm m)	LL (Ohm m)	MLL (Ohm m)	MINV (Ohm m)	MNOR (Ohm m)
UDP1:												
6734.00	14.7	11.8	100	2.27	26.3	29.2	1.96	1.79	1.76	3.03	1.39	1.76
6737.00	12.8	11.9	112	2.09	34.5	12.3	1.55	1.09	1.24	2.90	1.03	1.24
6738.42*	11.3	11.9	109	2.05	36.7	0.881	1.34	0.885	1.14	2.35	0.972	1.08
6742.42*	11.7	11.9	108	2.10	35.6	0.861	1.10	0.689	0.922	1.98	0.967	0.922
6744.42*	12.0	12.0	106	2.07	38.7	0.764	1.07	0.715	0.854	1.76	1.00	0.854
UDP2:												
6749.00	13.3	11.8	108	2.08	37.8	8.91	1.05	0.714	0.830	1.75	1.08	0.830
6753.42*	11.3	11.8	107	2.09	37.0	0.827	1.04	0.710	0.862	1.74	1.15	0.862
6758.00	12.0	11.9	111	2.06	37.9	7.21	0.988	0.664	0.839	1.83	1.12	0.839
6760.42*	10.1	11.8	108	2.08	38.7	0.803	0.996	0.681	0.805	1.53	1.15	0.805
6763.00	10.6	11.8	107	2.09	36.6	7.27	1.06	0.782	0.850	1.80	1.09	0.850
LDP:												
6767.00	8.81	11.8	108	2.08	33.6	7.33	1.11	0.762	1.07	2.33	1.18	1.07
6770.00	11.3	12.0	106	2.07	36.0	9.04	1.09	0.753	0.858	1.91	1.01	0.858
6774.00	11.1	11.7	102	2.13	33.5	8.96	1.27	0.908	1.09	1.05	0.936	1.09
6780.42*	11.4	11.9	103	2.08	37.7	0.692	1.61	1.16	1.26	2.41	0.917	1.26
6783.00	12.9	11.9	112	2.12	34.2	8.33	1.37	0.919	1.32	2.48	0.850	1.32
6795.00	13.4	11.9	96.2	2.16	33.0	11.4	1.49	1.05	1.10	2.25	0.952	1.10
6798.42*	12.0	11.9	98.5	2.21	31.9	16.3	1.53	1.15	1.42	2.76	0.978	1.42
6800.33*	11.2	11.9	104	2.10	36.9	12.4	1.32	0.897	1.13	2.11	0.886	1.13
6802.00	11.6	11.9	99.0	2.08	36.4	11.8	1.34	0.877	1.10	1.78	0.780	1.10
6807.42*	12.1	12.2	98.9	2.18	33.6	13.3	1.54	1.08	1.22	2.57	1.01	1.22
6810.00	13.0	12.0	86.7	2.22	29.0	16.2	1.98	1.38	1.45	2.47	0.994	1.45
UDT:												
6812.42*	13.4	12.1	85.2	2.24	30.6	17.0	2.28	1.80	1.84	3.35	1.16	1.84
6816.00	12.6	12.0	78.0	2.36	22.5	25.0	3.11	2.88	2.45	6.12	1.86	2.45
6820.00	13.2	12.1	84.0	2.33	19.3	25.8	2.90	2.44	2.70	3.96	1.62	2.70
6822.00	11.7	12.1	80.1	2.33	23.7	25.3	2.90	2.32	2.33	6.09	1.80	2.33
6826.25*	12.9	12.0	81.1	2.33	21.9	24.3	2.75	2.43	2.36	4.07	1.75	2.36
6829.00	13.5	11.9	87.6	2.34	22.5	22.9	2.47	1.95	2.43	5.31	1.46	2.43
LDT1:												
6833.42*	11.3	11.9	95.7	2.19	32.0	16.7	1.94	1.31	1.66	3.32	1.17	1.66
6836.42*	11.9	11.9	93.8	2.18	33.8	12.0	1.99	1.30	1.69	7.86	1.01	1.59
6841.00	10.0	11.9	88.1	2.19	33.7	11.0	2.10	1.42	1.31	2.17	1.03	1.31
6846.00	10.1	11.9	94.4	2.15	31.0	11.9	1.81	1.11	1.37	3.17	1.41	1.37
6848.42*	11.1	12.1	96.5	2.16	30.8	13.2	1.86	1.21	1.43	2.34	1.47	1.43
LDT2:												
6852.00	12.2	11.8	85.4	2.42	21.4	25.9	2.34	1.98	2.08	3.34	1.64	2.08
6855.00	13.3	11.8	96.9	2.20	28.1	21.4	1.85	1.34	1.85	2.42	1.08	1.85
6857.00	11.3	12.1	98.0	2.20	32.0	22.1	1.61	1.15	1.38	2.81	1.08	1.38
6861.00	14.1	12.0	95.0	2.19	29.6	19.3	1.81	1.22	1.79	2.83	1.06	1.79
6864.42*	10.6	11.7	90.2	2.24	28.8	15.1	1.85	1.27	1.40	2.50	0.922	1.46
6866.00	12.4	11.6	83.1	2.30	24.5	20.2	2.23	1.72	1.67	1.99	1.07	1.67
6868.33*	14.7	12.0	96.2	2.31	20.8	21.3	2.76	2.14	2.36	2.89	1.24	2.36
6872.00	12.6	11.9	90.3	2.28	29.2	17.9	2.52	1.82	1.87	2.66	1.12	1.87
1M:												
6876.25*	8.39	12.0	77.8	2.42	21.0	14.3	3.24	2.16	2.69	5.20	1.06	2.69
6879.50	10.7	11.8	86.4	2.31	26.5	9.93	2.49	1.59	2.34	26.2	1.14	2.34
6881.50	11.5	11.8	88.9	2.28	27.7	9.00	2.12	1.39	1.83	2.76	0.946	1.83
6890.00	12.4	12.8	92.9	2.19	28.9	7.63	1.73	1.20	1.39	3.10	0.936	1.39
6892.25*	10.8	13.0	86.0	2.20	31.6	7.75	1.82	1.27	1.34	3.10	0.868	1.34
2M:												
6896.00	11.4	12.6	90.0	2.21	31.7	7.10	1.60	1.02	1.38	2.83	0.711	1.38
6898.00	9.08	12.6	96.4	2.14	34.2	7.17	1.42	0.959	1.22	2.81	0.551	1.22
6901.00	10.8	12.8	97.4	2.13	30.9	5.74	1.29	0.890	1.09	2.67	0.601	1.09

APPENDIX VIII

Selection of Abbreviations Used in Well-Logging.

A	Amount of oil/gas in unit volume of reservoir rock A = porosity * hydrocarbon saturation
AMPL	Sonic log Amplitude from E2
BHC	Borehole Compensated Sonic Log porosity increases Dt values
CALI	Caliper
CBL	Sonic log E1 amplitude for CBL
CGR	Corrected Gamma Ray Total GR minus Uranium
CIL	Induction tool conductivity
CILD	Induction log Deep conductivity
CNL	Compensated neutron log (porosity determinations) dual spacing thermal neutrons ratio of counting rates from two detectors 16 Curie source (little statistical fluctuation) radial depth of investigation not good in gas-filled holes often run in combination with FDC
CORIBAND	Combined program
CS	Cable speed
Ct	Total conductivity
DIL	Dual Induction Log includes: Deep Induction log: ILd Medium Iinduction Log: ILD Laterolog 8, LL8 Log: ILM SP SFL (SFLU) gives the R of the flushed zone IM indicates R of flushed and invaded zones ID gives the R of the uncontaminated zone (R_t)
DRHO	Bulk density correction determined from FDC
Dt=DT DT	Delta t = travel time of an acoustic wave in SONIC log
Dt_f	Transit time in pore fluid
Dt_{ma}	Transit time in rock matrix
ES	Electrical Survey (resistivity logs) SP 16" Normal: shallowest penetration 64" Normal 18'8" Lateral: deepest penetration
F	Formation resistivity factor $F = a / Phi^m$ a = determined empirically m = cementation factor Sands: $F = 0.81 / Phi^2$ Compacted formation: $F = 1 / Phi^2$
FACIOLOG	Interpretation method using electrofacies
FCNL	CNL log Far detector
FDC	Formation Density Compensated log medium-energy gamma rays (Compton scattering) two detectors oil does not change the Rho value significantly presence of gas will lower the apparent Rho
GLOBAL	A statistical interpretation method
GNT	Neutron log detector sensitive to both high-energy capture gamma rays and to thermal neutrons uncertainties in cased holes run eccentric to minimize borehole effects
GR	Gamma ray log gross count rate API units
GRS	Gamma ray log spectrometry for U,Th,K
Hh	Hydrogen index of hydrocarbons
h_{mc}	Thickness of mud cake
H_w	Hydrogen index of salt water $H_w = 1 - 0.4*P$ P= NaCl concentration in ppm*10^{-6}
IES	Induction Electrical Survey Induction log
IL	Induction Log conductivity measured
ILd	Deep-reading induction device
ILm	Medium induction device
ISF/SONIC	Combination log includes: ILd SFL SP BHCsonic GR
IT	Sonic log Internal transit time
K	absolute permeability
K_o	effective permeability for oil
K_{ro}	relative permeability $K_{ro} = K_o / K$
K_{rw}	relative permeability for oil-water system $K_{rw} = K_w / K$
K_w	effective permeability for water

Laterolog 3	Focusing-electrode tool (electrical log) LL3 large electrodes are used better resolution and more detail than LL7 often recorded with GR
Laterolog 7	Focusing electrode tool (electrical log) Center electrode plus 3 pairs of electrodes LL7
Laterolog 8	Focusing-electrode tool (electrical log) similar to LL7 shallow recorded with small electrodes on the Dual Induction Laterolog
LDT	Litho Density Tool Mainly measuring Pe
LITH	Lithology window count rate
LL	Long lower window count rate
LS	Long-spacing computed count rate LL+LLU/2
LSRH	Long-spacing RHOB uncorrected
LU	Long upper 1-2 window count rate LU1+LU2
LU1	Long upper 1 window count rate
LU2	Long upper 2 window count rate
LURH	Long upper RHOB
Microlaterolog	Microresistivity device to measure R_{x0} influence of mud cake depressed well working in salt-base muds if $h_{mc} > (3/8)''$ Proximity log and MICROSFL are better determination of R_{x0}
Microlog	Resistivity measurements accurate delineation of permeable beds readily detection of mud cakes not quantitatively interpretable satisfactorily R_{x0} and porosity if $R_{x0}/R_{mc} < 15$ $h_{mc} < 0.5''$ depth of invasion > 4"
MICROSFL MSFL	Microresistivity device to estimate R_{x0} spherically focused logging
MID	Matrix Identification Plot
MINV	Micro inverse resistivity, ohms
MLL	MLL resistivity, ohms
MNOR	Micro normal resistivity, ohms
n	Saturation exponent usually n = 2
NCNL	CNL log Near detector
NGS	Natural Gamma Spectrometry log

NPHI	Neutron porosity determined by CNL
NRAT	Neutron ratio from CNL NCNL/FCNL
P	NaCl concentration
PEF	Photo-electric factor
Pe	Photo electric cross section index per unit of mass
Phi	porosity Phi = fraction of total volume occupied by pores $Phi = (Dt - Dt_{ma}) / (Dt_f - Dt_{ma})$ Dt = reading on the sonic log Dtma = from an empirical table Dt_f = 189 usec/ft $Phi = (Rho_{ma} - Rhob) / (Rho_{ma} - Rho_{liq})$ $Phi = R_0 / R$ $Phi = R_{x0} / R_{mf}$
Phi_a	apparent matrix porosity from density-neutron crossplot
Porosity overlay	quick visual interpretation
Proximity log	Log to determine R_{x0} similar to the Microlaterolog
R	resistivity
R_0	Resistivity of a non-shaly formation
R_{mc}	Resistivity of mud cake
R_{mf}	Resistivity of mud filtrate
RHGX	Grain density from cross-plot porosity
Rhob RHOB	Bulk density (g/cm^3) $Rhob = Phi * Rho_f + (1-Phi) * Rho_{ma}$
Rho_f	Fluid density (g/cm^3)
Rho_h	Hydrocarbon density
Rho_{ma}	Matrix density (g/cm^3) from density-neutron crossplot
Rho_{liq}	Liquid density (g/cm^3)
R_t	True resistivity determined by Laterolog 7 Laterolog 3 LLd Dual Laterolog
R_w	Formation water resistivity 100% saturated brine From SP curve
R_{x0}	Resistivity of the flushed zone $R_{x0} = F * R_{mf} / S_{x0}^2$
S1RH	Short-spacing 1 density
Sand line	Set by the logger in the SP log
SARABAND	Combination program
SFL	Spherically-focused Log part of the ISF/Sonic combination

SFLA	Spherically-focused log Averaged over 2.5"
SFLU	Spherically-focused log Unaveraged
Sigma	Thermal neutron capture cross section
S_h	Hydrocarbon saturation S_h = fraction of pore volume filled with hydrocarbons $S_h = 1 - S_w$
Shale base line	Shale line in SP log, set by the logger
S_{hr}	Residual hydrocarbon saturation in the flushed zone $S_{hr} = 1 - S_{xo}$
SN	Short normal from IEL, in ohms
SNP	Neutron log (porosity determinations) neutron source and detector mounted on a skid proportional counter measurement of epithermal neutrons (effects of strong neutron absorbers such as Cl and B are minimized) automatically corrected for salinity Too low reading if gas is present
SONIC	Sonic Log travel time Δt is determined
SP	Spontaneous potential log - detect permeable beds - determine R_w - qualitative impression of shaliness mud cake present if caliper reading depressed
SRAT	Sonic log ratio Near-to-far amplitude
SS1	Short-spacing 1 window count rate
SS2	Short-spacing 2 window count rate
SSP	Static SP
S_{xo}	S_{xo} = sqrt $(F * R_{mf} / R_{xo})$
S_w	Fraction of pore volume occupied by formation water Water saturation $S_w^n = F * R_w / R_t$ S_w = sqrt $(F * R_w / R_t)$ S_w = sqrt (R_0 / R_t) for clean formations $S_w = ((R_{xo}/R_t)/(R_{mf}/R_w))^{5/8}$ if R_{xo} and R_{mf} are known
S_{wirr}	Irreducible water saturation
S_{xo}	Mud filtrate saturation $S_{xo} = 1 - S_{hr}$
TENS	Tension
TDT	Thermal decay time
U	Photo electric cross section per unit of volume product Pe * density
U_{fl}	U fluid
U_{log}	$U_{log} = (1-Phi_e)*U_{ma} + Phi_e*U_{fl}$
U_{ma}	U matrix

Bibliographic Data Sheet **Risø-M-2779**

Title and authors

Geochemical Criteria for Reservoir Quality Variations in Chalk from The North Sea

H. Kunzendorf and P. Sørensen

ISBN			ISSN
87-550-1511-5			0418-6435
Dept. or group			**Date**
Chemistry Department			December 1989
Groups own reg. number(s)			**Project/contract no.**
			EM-Journal no. 1313/86-5
Pages	**Tables**	**Illustrations**	**References**
100	14	49	147

Abstract (Max. 2000 characters)

The research project (EFP-86) systematically investigates the influence of chalk geochemistry on petrophysical parameters determining hydrocarbon reservoir quality, i.e. porosity and permeability. Two wells of the North Sea Tyra gas field were chosen for the present investigation: the central well TWB-8 and eastern marginal well E-1x. Geophysical logging data with interpretations exist for both wells. Drill core sections of Upper Maastrichtian and Danian chalk were selected for the geochemical investigations. Chemical data on chalk samples were gathered by using both conventional (X-ray fluorescence) and special instrumental analytical techniques (instrumental neutron activation). The geochemical data are compared with the well-logging results. Geophysical logging suggests that there is reduced porosity in the Danian reservoir units LDP and UDT in both the central and marginal wells. The chalk drill core samples from the section with reduced porosity also show a lower Ca content. At the same time, a high Si content is observed in these samples and a number of trace elements in chalk show a similar distribution with depth. Silicon diagenesis is therefore regarded as being responsible for reservoir quality variations in Tyra rocks. A linear dependence is observed between chalk porosity and silicon content of chalk, i.e. reservoir porosity may be estimated from the Si content of chalk. Chalk permeability may also be determined by Si content but the linear dependency is less significant. Geochemically, depth distributions of elements Al, Fe and Sc show the same trends as that for Si. Therefore, diagenetic changes in chalk also include clay minerals. Other features of the Tyra gas reservoir are displayed through the chemical data. The gas zone in TWB-8 is characterized by low contents of Na and Cl, i.e. lower water saturation is indicated. Low concentrations of rare earths in all chalk samples show a shale-normalized pattern that is characteristic of marine sediments laid down under oxic conditions. Some changes that occur with depth in the Ce anomaly probably indicates a slight change in the depositional environment. A most pronounced feature of the Tyra chalk is the depth distribution of manganese: the content continuously decreases with depth, i.e. from Danian (about 2000 ppm) to Maastrichtian strata (less than 200 ppm). In this respect, no other chemical element in chalk correlates with Mn. At present, there is no indication as to which mineral or mineral phase one is likely to find the element.

Descriptors INIS/EDB

ALUMINIUM; CALCIUM; CLAYS; DEPTH; DIAGENESIS; DRILL CORES; ELEMENTS; EXPERIMENTAL DATA; GEOCHEMISTRY; GEOLOGIC DEPOSITS; GEOPHYSICS; IRON; LIMESTONE; MANGANESE; NATURAL GAS; NEUTRON ACTIVATION ANALYSIS; NORTH SEA; PERMEABILITY; POROSITY; RARE EARTHS; SILICON; SPATIAL DISTRIBUTION; TRACE AMOUNTS; WELL LOGGING; X-RAY FLUORESCENSE ANALYSIS

Available on request from Risø Library, Risø National Laboratory, (Risø Bibliotek, Forskningscenter Risø), P.O.Box 49, DK-4000 Roskilde, Denmark. Telephone 42 37 12 12, ext. 2268/2269 Telex 43 116. Telefax 46 75 56 27.

Available on exchange from:
Risø Library,
Risø National Laboratory,
P.O. Box 49, DK-4000 Roskilde, Denmark
Phone + 45 42 37 12 12, ext. 2268/2269,
Telex 43116, Telefax + 45 46 75 56 27

ISBN 87-550-1511-5
ISSN 0418-6435